SANDIA REPORT

SAND87—2039 • UC—60
Unlimited Release
Printed November 1987

Fatigue Crack Growth Due to Random Loading

Paul S. Veers

Prepared by
Sandia National Laboratories
Albuquerque, New Mexico 87185 and Livermore, California 94550
for the United States Department of Energy
under Contract DE-AC04-76DP00789

Issued by Sandia National Laboratories, operated for the United States Department of Energy by Sandia Corporation.

Printed in the United States of America
Available from
National Technical Information Service
U.S. Department of Commerce
5285 Port Royal Road
Springfield, VA 22161

NTIS price codes
Printed copy: A08
Microfiche copy: A01

SAND87-2039

November 1987

Fatigue Crack Growth due to Random Loading

Paul S. Veers

Sandia National Laboratories
Albuquerque, New Mexico 87185-5800

ABSTRACT

Fatigue crack growth due to random loading is investigated, showing a variety of approaches that are tailored to the level of complexity required for the application at hand. The emphasis is on creating the simplest models, of both the crack growth process and the random loading, that maintain the desired level of accuracy.

A new crack growth model, which combines some of the features of existing models, is introduced and shown to predict several sets of published test results. The model provides a means of approximating load sequence effects by continuously updating the crack opening stress, accounting for both acceleration and retardation effects in a simplified manner. This model is used as the standard crack growth model that includes sequence effects.

Random load models, which describe the relevant events in the loading necessary to implement the above crack growth model, are outlined. These models range from simple random variable descriptions, which are useful in sequenceless applications, to random process simulations, which include the relative likelihood of various load sequences. Existing random variable descriptions of narrow-band loadings are shown to be useful approximations for any Gaussian loading. New results that account for the overall peaks and ranges in wide-band loadings are obtained through *racetrack filtering*. An efficient sequential simulation method uses the random variable results to simulate only the most significant events in a random process by breaking the loading into slow (mean variations) and fast (amplitude variations) parts.

Practical methods for calculating crack growth life are presented by applying the load models to the above crack growth model, and to an alternative model that neglects sequence effects. Inherent difficulties in the traditional, sample-block, load model can be eliminated with a continuously defined loading, which can be obtained by the sequential simulation method. This simulation method is used in

studies that illustrate the relative importance of including load sequence effects in crack growth analysis. For stationary Gaussian loadings, sequence effects can often be neglected. Nonstationary random loadings are also simulated and shown to produce greater sequence effects. When distinct overloads are present, the regularity of the spacing is important; assuming uniform spacing can be nonconservative.

As an alternative to simulation, analytical estimates of crack growth life, including sequence effects, are examined using diffusion models. The emphasis is on simplifying the problem (i.e., scalar diffusion models) so that solutions can be obtained with limited computational resources. Solutions for mean and variance of the time to failure due to constant amplitude loading with distinct tensile overloads are presented. The mean time to failure due to stationary Gaussian loading is also estimated. More complete, but computationally expensive, solution methods using vector diffusion models are outlined.

Table of Contents

List of Tables

List of Illustrations

Acknowledgments

The author wishes to recognize the helpful comments and editorial suggestions of Professor Drew V. Nelson, Stanford University Mechanical Engineering Department. The direction of Professor C. Allin Cornell, Stanford University Civil Engineering Department, who gave generously of his time and provided valuable insight, is also acknowledged. The author thanks Professor Steven R. Winterstein, also of the Stanford Civil Engineering Department, a tireless co-worker and constant source of ideas and encouragement. Without the interest of Professor Winterstein, this work would have been much more limited in scope and application. Thanks are also due to Larry Ellis, Gayle Shipp, Jerry O'Brien, and the rest of the Sandia National Laboratories Satellite Data Division, who unselfishly provided me access to their equipment and support in using it to complete the document typesetting in Albuquerque. Herb Sutherland, of Sandia's Wind Energy Research Division, and Keith Miller of Sandia's Applied Mechanics Division, are to be commended for their perseverance as reviewers.

CHAPTER 1

INTRODUCTION

1.1 History

Structures and machines have been designed and used for centuries without any reference to the phenomenon which we now call fatigue. The concept that a structure able to withstand a given load level will always be able to withstand that load was a sufficient guide for design. A gradual change in this attitude began at the time of the industrial revolution, when structures and machines were expected to withstand more and more dynamic loading. In addition, traditional construction materials, such as wood and stone, were replaced with metals.

The first suspicion that the strength of metals can degrade due to repeated loadings was reported in 1829 when Albert noted the failure of welded link hoist chains in German mines [Moore and Kommers, 1927]. The chains appeared to fail due to loadings that were no greater than had been applied repeatedly over months of use. This same phenomenon was noticed in other industries where metals were being used under cyclic loadings, but was especially troubling to the fledgling railroad industry. Axle failures were expensive and far too frequent. The location of the failures at abrupt changes in diameter was observed early on and soon led to the good design practice of minimizing stress concentrations; but no explanation of the cause of failure was found. Failure due to repeated loading below the static strength of the material was given the name of fatigue in 1839 by Poncelet [Timoshenko, 1953].

In 1842, Hood interpreted the crystalline appearance of fatigue fracture surfaces as an indication that the material microstructure had changed due to cyclic loading [Hood, 1842]. Perhaps, he reasoned, the material becomes crystalline and brittle, which leads to failure under reduced load. This, of course, is entirely false. It was refuted in the following year by Rankine [1843] (who is better known for his work in thermodynamics). Rankine's view of the process as the formulation and growth of cracks until the stress in the remaining material exceeds the material strength is remarkably accurate. The objective evidence that Rankine's view was the correct one was not obtained until 1903, when

Ewing and Humphrey published metallographic observations of fatigue cracks. This delay allowed ample time for the crystallization theory to become embedded in engineering thinking. In fact, the 1939 ASM Handbook still included a refutation of the crystallization theory [Fine, 1980].

Fatigue was first studied in a systematic manner by the German railroad engineer, Wöhler, beginning in the 1850's [Wöhler, 1867]. He conducted tests in which rotating axles were subjected to bending stresses in a fixed direction, subjecting each point on the axle surface to a sinusoidally varying stress. The results of these tests were plotted with stress amplitude, S, on the vertical axis and number of cycles to failure, N, on the horizontal axis. The resulting $S-N$ curve is still the basis for most estimates of fatigue life [Fuchs and Stephens, 1980].

Wöhler observed that when the cyclic stress amplitude is below a certain level, the axle seemed to have infinite life. The existence of a cyclic stress amplitude below which fatigue failures will not occur (known as the fatigue limit, or endurance limit) is valuable to the design engineer. With the knowledge that it is possible that the part may fail at stress levels below the static strength, but never below the fatigue limit, it is possible to once again choose adequate sizes for structural components. But because the fatigue limit is often one tenth to one fifth of the yield strength, a significant cost in additional material is required. When the loading is nearly constant amplitude, as might be expected for rolling axles, pressure vessels, or rotating machinery, this additional cost may be necessary.

With the birth of the automotive and aircraft industries, it became much more common to have loadings in which the highest stresses are relatively rare events. This is true of heavy equipment used in construction, mining and farming as well as cars and trucks. Aircraft, including passenger, cargo and military planes, experience rare high stress events. These irregular loadings are also common in energy extraction applications including well drilling for oil and geothermal energy, in offshore structures and in wind turbines. The need to reduce cost, weight, or overall size makes it increasingly unacceptable to base a design on criteria sufficiently conservative to keep the highest stresses below the fatigue limit. Because high stress events are rare, it should be possible to achieve a sufficient life with some stress peaks above the fatigue limit. The difficulty lies in how high the stresses should be allowed to go and how many stress cycles above the fatigue limit can be tolerated.

1.2 Cumulative Damage Estimation

A simple solution to estimating the life of a material experiencing variable amplitude fatigue loading was suggested by Miner [1945]. He assumed that the *damage* suffered by the material in any given number of cycles at a given cyclic stress amplitude is equal to the ratio of the number of cycles applied to the total number of cycles to failure at that amplitude. The damage, D, due to an irregular loading is then the sum of the damages due to each cyclic stress amplitude:

$$D = \sum_i \frac{n_i}{N_i} \tag{1.1}$$

where n_i is the number of applied cycles at cyclic stress amplitude S_i and N_i is the total number of cycles to failure at the same amplitude. Failure is predicted when the total damage is equal to one. The term *damage* does not have any inherent physical meaning; it is a fictitious quantity that is useful in summing the *damaging* effects of loading at different stress levels.

In addition to changes in the cyclic stress amplitude, the mean stress may also vary. The *Goodman diagram,* which plots the stress amplitude for a given fatigue life as a linear function of mean stress, was introduced for the purpose of estimating the mean stress effect. For a given fatigue life, the allowable cyclic stress amplitude decreases from that allowable at zero mean stress to zero when the tensile mean stress equals the ultimate strength. Gerber suggested an improvement to this estimate of mean stress effect with a quadratic relationship [Forrest, 1962]. The test data for most materials lie between the Goodman and Gerber estimates [Sandor, 1972].

The use of constant amplitude, zero mean-stress test data with Miner's rule and a Goodman diagram makes it fairly simple to estimate fatigue life for irregular loadings (as long as all of the stress cycles have been defined). Unfortunately, the simple procedure is not always accurate; at times Miner's rule over estimates life, while at other times it under estimates life.

Miner's rule was first systematically investigated by conducting fatigue tests of smooth (unnotched) specimens with two step loading, low level constant amplitude followed by high level constant amplitude and vice versa. These two loadings produced markedly different results. It was initially thought that the difference was due to a nonlinearity in the accumulation of fatigue damage, which was not modeled correctly with Miner's rule. Freudenthal was careful to note that a nonlinearity is only a problem when the sequence of loads is

specified, and that for random loading, the nonlinear damage accumulation may produce no sequence effects [Freudenthal and Gumbel, 1956]. Many alternate cumulative damage rules were subsequently suggested [Corten and Dolan, 1956; Freudenthal and Heller, 1959; Manson, et.al., 1967]. These more complicated rules did a better job of predicting the results of the two step loading tests, but were unable to produce more accurate results for the wide variety of loadings found in real applications.

Another interesting effect is that smooth specimens subjected to constant amplitude cycles and occasional overloads have fatigue lives reduced far below what Miner's rule would predict [Freudenthal and Gumbel, 1956]. It is even possible to have a finite life when almost all the loading is below the fatigue limit. The implication is that once the limit has been exceeded, it no longer exists, so no cycles with stress amplitudes above the fatigue limit are totally *safe*.

It is difficult to sort out the progress of damage in a fatigued material because damage is a fictitious quantity that cannot be measured during a test. By shifting emphasis to fatigue crack growth, a physical measure of the current state of damage (i.e., crack length) is available.

Many relationships between crack growth rate, da/dN, applied stress, ΔS, and crack length, a, were postulated in the 1950's and early 1960's. Most of them took the form

$$\frac{da}{dN} = C\, a^n\, \Delta S^m \tag{1.2}$$

where C, n, and m are material constants [Hoeppner and Krupp, 1974].

Paris and Erdogan [1963] suggested that the crack growth rate should be related to the stress intensity factor by the following relation:

$$\frac{da}{dN} = C\, \Delta K^b \tag{1.3}$$

where $\Delta K = \sqrt{\pi a}\, Y(a) \Delta S$, and $Y(a)$ is a function of crack geometry. Eq. 1.3, called Paris' law, is still the fundamental method of predicting fatigue crack growth.

An improvement that accounts for the stress ratio, R (minimum stress divided by the maximum stress), as well as improving the prediction of unstable crack growth as the stress intensity approaches the critical stress intensity, K_c, is given by [Forman, et.al., 1967]

$$\frac{da}{dN} = \frac{C \Delta K^b}{(1-R) K_c - \Delta K} \tag{1.4}$$

and is known as Forman's equation.

The total amount of crack growth due to an irregular loading is usually calculated by simply adding up the increments in crack growth due to each stress cycle, which is analogous to Miner's rule for adding up the damage due to each stress cycle in a total life calculation. No *memory* or *sequence effects* are considered (i.e., the increment in crack growth depends only on the current applied stress range and crack length, and not on past loading).

One advantage of crack growth analysis over the fictitious damage estimates of Miner's rule lies in the ability to monitor the damage level during the material lifetime with crack-detection procedures. The residual lifetime of a structural member can be estimated by measurements on the member without analysis of the prior loading, which is especially important in life critical applications (e.g., aircraft). An inspection can insure that there are no cracks present below the minimal detectable size and a crack growth analysis can then insure that the largest possible crack will not grow to a critical size before the next inspection.

Besides this very practical advantage, it is possible to monitor the development of damage, in the form of a crack, during fatigue testing, which led to the discovery of sequence effects in crack growth rates. Schijve was one of the earliest researchers to identify the differences in fatigue crack growth rates between irregular loadings and both short and long blocks of constant amplitude loadings at different levels [Schijve, 1960]. A significant difference in time to failure was observed in block type loadings when the order of the blocks was changed (decreasing amplitude blocks versus increasing amplitude blocks) [Schijve, 1973]. Even a single tensile overload inserted in a constant amplitude loading was shown to produce a retardation in subsequent fatigue crack growth and to extend the life of the member [von Euw, et.al., 1972; Trebules, et.al., 1973; Vargas and Stephans, 1973; Watson, et.al., 1973]. This life extension is exactly opposite to the effect of overloads on smooth specimen fatigue life, which is dominated by crack initiation, where initiation is taken as the appearance of a crack of several millimeters in size. The explanation for this different behavior lies in the different mechanisms responsible for fatigue crack initiation and fatigue crack growth.

1.3 Fatigue Mechanisms

1.3.1 Fracture

The basic question which gave birth to the field of fatigue analysis is: How can a piece of metal end up in two pieces without ever experiencing a load large enough to exceed the initial strength of the piece? The answer was suggested by Rankine [1843] and formalized by Griffith [1920] through his study of the strength of brittle materials. The answer is that the strength of a piece of material depends on the size of cracks present in the material.

Griffith used an energy balance to explain the fracture of brittle materials. He suggested that when the release of internal strain energy due to a small extension of a preexisting crack is greater than the increase in surface energy due to the creation of new crack surfaces, the crack will extend in an unstable manner. By setting the rate of change of total energy with respect to crack length equal to zero, and separating the material constants from the loading and geometric parameters, Griffith showed that the criterion for brittle failure is reached when the applied stress intensity, K, is greater than the critical value, K_c, which is a material property known as the fracture toughness:

$$K_c = \sqrt{2 E \gamma_s} \tag{1.5}$$

where γ_s is the surface energy per unit area, and E is Young's modulus. Equating the applied stress intensity at fracture to K_c in Eq. 1.5 assumes that all of the strain energy at fracture is taken up in surface energy.

In ductile materials there is a great deal of energy absorbed by plastic deformation during fracture. Orowan [1950] expanded Griffith's result to ductile materials by adding this plastic strain energy to the surface energy in the fracture toughness. For most structural materials (steel, aluminum, etc...) the plastic strain energy dominates the fracture toughness. Orowan defined K_c as

$$K_c = \sqrt{2 E (\gamma_s + \gamma_p)} \tag{1.6}$$

where γ_p is the plastic strain energy.

Initial flaws and cracks are often present in materials, produced by inclusions, machining flaws, thermal cracking, forging, or welding during the manufacturing process. These small flaws can grow under cyclic loading, increasing the stress intensity due to a given stress level. Eventually the strength of the part is exceeded, not by increasing the load level, but by

decreasing the strength of the material.

Even initially crack free materials are susceptible to fatigue. Metals are polycrystalline materials with stacking faults in the crystal lattice. These misalignments between atoms in the crystal structure are called *dislocations.* Dislocations move along slip planes in the crystal when shear stresses are applied in the slip plane directions. Dislocation motion is responsible for almost all plastic strain. Under cyclic loading, the dislocations form tangles that make further motion more difficult. The tangles tend to form vein-like structures, with veins of tangles alternating with veins of dislocation free material [Brown, 1981]. After some time, the dislocation motion will be restricted to the tangle free regions known as *persistent slip bands* [Forsythe, 1969]. Slip on parallel planes within a persistent slip band is not homogeneous or equal in both direction. This causes planes of atoms to ratchet in different directions, creating surface discontinuities by extruding some planes out of the surface and intruding others into the surface. Flaws can also develop within the material, especially at grain boundaries. These surface irregularities and internal flaws are the nucleation points for cracks that continue to grow under cyclic loading until the critical stress intensity is exceeded and the material fractures.

1.3.2 Sequence Effects in Crack Initiation

Local plastic strain is a necessary component of progressive fatigue damage in a metal because without plastic strain there can be no relative motion of atoms leading to crack initiating flaws. Dislocation motion is responsible for almost all plastic strain; locking of dislocations makes fatigue damage impossible.

One way dislocations are commonly locked in structural steel is by *Cotrell atmospheres* [Cotrell, 1969]. The state of stress around a dislocation is tensile on one side, where there is a missing plane of atoms, and compressive on the other, where there is an extra plane of atoms. When small substitutional atoms diffuse into the region of compressive stress and large substitutional, or small interstitial, atoms diffuse into the region of tensile stress, these stresses are relieved. Movement of the dislocation out of this local atmosphere of solute atoms increases the strain energy in the material. Because the atoms seek the lowest energy configuration, the dislocations are effectively locked in place until an applied stress large enough to overcome the Cotrell atmosphere moves the dislocation. Once it has been moved out of the Cotrell atmosphere, much smaller

loads can continue the dislocation motion. This is the phenomenon responsible for the yield point in mild steel.

Another locking mechanism is present in two phase, or precipitation hardened, alloys where dislocation motion is blocked by phase boundaries and precipitate particles. Again, when an applied stress large enough to shear the blocking particle has removed the obstacle, further dislocation motion, and therefore plastic strain, is possible under smaller loads.

In constant amplitude fatigue testing, any barrier to dislocation motion for one of the load cycles will be effective for all of the load cycles; plastic straining can be locally eliminated. In carbon steels, where dislocations are locked by Cotrell atmospheres of carbon atoms, this results in a fatigue, or endurance, limit. Stress amplitudes below this limit cannot cause plastic strain and the material then exhibits an *infinite* life. If, however, the loading is irregular with some stress amplitudes above and some below the fatigue limit, the high loads will remove the barriers to dislocation motion and the low amplitude loading will be able to cause plastic strain and continue the process of fatigue damage. This is a source of *sequence effects* in crack initiation. It has been suggested that under irregular loading, the $S-N$ curve should be treated as though the fatigue limit does not exist and finite lives are expected at all stress amplitudes [Fuchs and Stephens, 1980]. It is possible that the misapplication of the fatigue limit in analysis of irregular loadings has been a great source of error in applying Miner's rule and may have led to some of the suggestions that Miner's rule is inadequate.

1.3.3 Sequence Effects in Crack Growth

The nonlinear nature of crack growth is caused by the dependence of the crack growth rate on crack length. Paris' law relates crack growth rate to crack length through the stress intensity factor, as shown in Eq. 1.3. The crack growth rate increases nonlinearly with crack length because, typically, $2<b<4$. It is important to notice that for stress intensity ranges, which can be written as separable functions of stress range and crack length (as in Eq. 1.3), the sequence of application of any set of loads has no effect on the calculated crack growth [Freudenthal and Gumbel, 1956; Orringer, 1984]. This can be demonstrated by separating the load dependent and crack length dependent variables in Eq. 1.3 and integrating:

$$\int_{a_o}^{a_f} \frac{da}{C(\sqrt{\pi a}\,Y(a))^b} = \sum_{i=1}^{N} \Delta S_i^b \tag{1.7}$$

The number of cycles (N) to grow from initial (a_o) to final (a_f) crack lengths depends on the summation over the applied stress ranges, and not on the order of application. The nonlinearity in the crack growth equation is not responsible for sequence effects in crack growth.

The sequence effects that were observed by Schijve and many other investigators involve a change in the effective stress intensity range due to *crack closure,* which is qualitatively described as follows: The predicted *elastic* stress at a crack tip is infinite. In reality, there is always a zone of plastic strain at the crack tip. A tensile load opens the crack and plastically deforms the material at the tip. As the load is released, the material at the crack tip is compressed and the crack actually closes, for two reasons. First, the material at the crack tip is plastically deformed in tension while the bulk of the material remains elastic. When the rest of the material seeks its original shape upon unloading, it acts as a clamp on the crack tip. Second, the crack grows by stretching and tearing material at the crack tip. This failed material in the wake of the crack tip has a residual tensile strain that acts as a wedge behind the crack tip. Both of these factors produce a compressive stress at the crack tip that depends on the past loadings. A large tensile load produces a large plastic zone and a large residual compressive stress, which does not allow the crack to reopen until a sufficient tensile load has counteracted the compression at the crack tip. The part of the stress range that is taken up in overcoming the residual compression does not contribute to crack growth. The effective stress range is the difference between the maximum stress and the stress at which the crack tip opens [Elber, 1971].

The crack growth rate following a large tensile overload is therefore reduced, or *retarded.* The retardation usually reaches its maximum after the crack has grown a small distance into the plastic zone [Trebules, et.al., 1973; von Euw, et.al., 1972], and then gradually dies out as the crack grows beyond the influence of this overload induced plastic zone.

Compressive loads can also influence crack growth by changing the state of residual stress at the crack tip. A compressive load large enough to yield the closed crack tip will reduce the compressive residual stresses and accelerate the subsequent crack growth [Stephens, et.al., 1974]. This acceleration effect is not as great as the retardation effect [Trebules, et.al., 1973] and is often neglected in crack growth modeling [Chang and Hudson, eds., 1981].

1.4 Models for Crack Growth due to Irregular Loading

In this section, several approaches to calculating crack growth life in an irregular loading environment are presented and compared. Equations necessary for comprehension are included, but are not intended to supply a sufficient description to implement each model. The symbols used in the descriptions have been changed to be consistent with those used in the following chapters.

1.4.1 The Wheeler Model

Wheeler obtains an empirical approach to estimating the retardation effect by multiplying the crack growth rate by an exponential shaping function while the crack tip is in the overload induced crack-tip plastic zone [Wheeler, 1972]. The retarded crack growth rate is defined by

$$\frac{da}{dN} = C_p \left[C \Delta K^b\right] \tag{1.8a}$$

where

$$C_p = \left(\frac{r_y}{a_z - a}\right)^m \tag{1.8b}$$

and a is current crack length, a_z is the maximum extent of the crack-tip plastic zone, r_y is the crack-tip plastic zone radius due to the current applied stress, and m is an empirical shaping exponent.

Thus, the retardation is assumed to be greatest immediately following the overload and decreases to zero when the crack tip grows beyond the overload plastic zone. The shaping exponent depends on both material and type of loading, and is determined by crack growth testing with a specified irregular load block; m must be reevaluated for each new type of irregular loading. Reported values of m range from 1.3 to 3.4. Although this method can be quite accurate when m is tailored to a specific load block with sufficient test data [Broek, 1984], it can not predict sequence effects without this *load specific* testing.

1.4.2 The Willenborg Model

This approach assumes that the compressive residual stress at the crack tip due to the crack-tip plastic zone is responsible for crack growth retardation [Willenborg, et.al., 1971]. Like the Wheeler model, the compressive residual stress is assumed to be maximum immediately following the overload, and to decrease as the crack grows through the crack-tip plastic zone. The reduction in the crack

growth rate is governed by the the stress, S_r, necessary to create a plastic zone that extends beyond its current limits:

$$S_r = \frac{S_y}{Y(a)} \left(\frac{2(a_z - a)}{a} \right)^{1/2} \tag{1.9}$$

where S_y is the monotonic yield stress and a, a_z and $Y(a)$ are as defined previously (plane stress has been assumed).

The residual stress at the current crack tip is assumed to be $S_{red} = S_r - S_{\max}$, where $S_{\max}$ is the current maximum applied stress. The effective maximum and minimum stress levels are defined by $(S_{\max})_{eff} = S_{\max} - S_{red}$ and $(S_{\min})_{eff} = S_{\min} - S_{red}$. If either effective stress is less than zero, it is set equal to zero. The effective stress intensity range and the effective stress ratio, which are defined in terms of the effective maxima and minima, are used in Forman's equation (Eq. 1.4).

This method attempts to account for retardation in fatigue crack growth but cannot model acceleration effects. It has the advantage of only requiring data from crack growth due to constant amplitude loading.

1.4.3 Führing

The Willenborg model has been adapted to account for acceleration and multiple overload interaction effects [Führing, 1981]. Instead of a residual stress estimate, Führing uses phenomenologically based estimates of independent acceleration and retardation parameters, Q_a and Q_r, respectively, such that

$$\Delta K_{eff} = Q_r Q_a \Delta K \tag{1.10}$$

Q_r is calculated from the ratio of current to maximum plastic zone sizes, while Q_a is estimated from a complicated expression based on an empirical parameter. Führing's method produced very good results in the original reference, but was off by an order of magnitude when applied to high R-ratio loadings that showed no sequence effects [Fleck and Smith, 1984].

1.4.4 Barsom's Method (ΔK_{RMS})

Good correlation between crack growth rate and ΔK_{RMS} has been shown [Barsom, 1976; Rolfe and Barsom, 1977] for crack growth in mild steels due to constant amplitude, prescribed increasing and decreasing sequences, and pseudo-random loadings, all at R=~0 (zero minimum stress between each stress peak).

In this case, ΔK_{RMS} is easily defined as the root mean square of the maximum stress intensity.

This method was also used successfully by Hudson [1981] to predict crack growth in aluminum under several specified aircraft flight spectra. These irregular loadings did not have zero minima between each pair of maxima; ΔK_{RMS} was defined to be the difference between $(K_{\max})_{RMS}$ and $(K_{\min})_{RMS}$, where

$$(K_{\max})_{RMS} = \left(\frac{1}{n} \sum_{i=1}^{n} K^2_{\max_i} \right)^{1/2} \tag{1.11a}$$

$$(K_{\min})_{RMS} = \left(\frac{1}{n} \sum_{i=1}^{n} K^2_{\min_i} \right)^{1/2} \tag{1.11b}$$

The stress ratio was defined as $R_{RMS} = (K_{\min})_{RMS} / (K_{\max})_{RMS}$.

The crack growth rate was then assumed to be equal to the growth rate under constant amplitude loading with $\Delta K = \Delta K_{RMS}$ and $R = R_{RMS}$. This approach did as well as other more complicated and computationally difficult methods in estimating time from initial crack size to failure in an ASTM round robin [Chang and Hudson, eds. 1981].

The reason for the success of this method is not known. It may be significant that the crack growth exponent (b in Eq. 1.3) is close to two for the materials used in the studies by Barsom (making the RMS a particularly appropriate measure). The load blocks may also have been short enough that sequence effects would be minimal [Schijve, et.al., 1970]. There is also no reason given as to why Hudson chose the somewhat unusual method for calculating ΔK_{RMS} in Eq. 1.11, except that it provides a means for estimating a stress ratio. The simplicity of the method and its success in the above applications makes it an attractive approach. But the lack of any physical basis for its validity admits the possibility that it may be inaccurate in other applications.

1.4.5 Crack Closure

Elber [1971] observed the change in compliance of a cracked specimen during the application of a tensile loading, which led to the very important discovery that the crack tip remains closed even after some tensile load has been applied. The stress at which the crack tip begins to open is called the *crack opening stress* (reportedly between 35 and 50 per cent of the previous maximum tensile stress). Elber suggested that the effective stress range responsible for

crack growth is the difference between the crack opening stress and the maximum stress. Because the crack opening stress depends on the residual stress and strain around the crack tip, the current effective stress range depends on previous loading. This discovery has opened up a whole new way of looking at the problem of crack growth due to irregular loading. Crack closure is the basis for many of the crack growth models currently in use.

Elber [1976] also made the discovery that during block type loadings (pseudo-random or programmed), the crack opening stress remains relatively constant [Elber, 1976]. He used this fact to calculate an equivalent constant amplitude loading for accelerated testing. Although the equivalent constant amplitude suggestion has not caught on, the idea that the crack opening stress is set by relatively rare, high loads, and remains stable over long periods of loading, has been used effectively, especially in the following approach.

1.4.6 The Nelson Model

Nelson [1978] proposed a crack closure based model that uses only constant amplitude, $R = 0$ crack growth data, The crack opening stress is assumed to be a constant fraction of the largest previously applied stress (overload), and is assumed to remain at that level as long as the crack tip is within the plastic zone created by that overload. When a load large enough to extend the plastic zone is applied, the crack opening stress is reevaluated. The effective stress intensity range is

$$\Delta K_{eff} = K_{\max} - qK_{ol} \tag{1.12}$$

where K_{ol} is the overload stress intensity and q is a constant between 0 and 1 ($0.35 < q < 0.5$ was suggested by Elber [1971]).

The crack growth due to this effective stress intensity range is assumed to be the same as would be produced by constant amplitude loading at the same effective stress intensity range. In constant amplitude loading, where each stress peak is equal to the highest, the effective stress intensity range is $\Delta K_{eff} = K_{\max} - qK_{\max}$. When constant amplitude test data is interpreted in terms of this ΔK_{eff}, the value of q can be anywhere in the suggested range without a major influence on the estimates of crack growth due to blocks of irregular loading. Therefore, without knowing the actual crack opening stress, a good approximation for crack growth life can be made with a minimum of test data.

1.4.7 Kikukawa, Jono, and Others

The most valuable work of the research group composed of Kikukawa, Jono, and several others [Kikukawa et.al., 1981; Jono et.al., 1985] is an experimental validation of some basic concepts that have been used in other models. They conducted crack growth tests in which stress maxima and minima, crack opening stress, and crack growth rate were all monitored. Test loadings included both constant amplitude and blocks of random-amplitude loadings. Their conclusions include the following:

1. With random-amplitude blocks of loading, the crack opening stress is relatively constant throughout the loading and is equal to the crack opening stress in constant amplitude loading with the same largest peak and lowest valley.
2. The threshold effective stress intensity range (below which crack growth ceases in constant amplitude tests) is zero under irregular loading.
3. The crack growth rate due to irregular loadings is accurately estimated by using $\Delta K_{eff} = K_{\max} - K_{op}$, where K_{op} is the measured crack opening stress intensity.

1.4.8 Overview of Crack Growth Models

These models are a few of the many approaches that have been proposed in the effort to predict fatigue crack growth due to irregular loading. They represent a fairly diverse sampling of the available methods. Some comments are listed below:

- Validation of all these methods has been with sample blocks of irregular loading, which are repeated in a closed loop fashion in testing and analysis. The entire loading is not random, but is periodic, and is best described as irregular. These loadings are sometimes called pseudo-random.
- There is a group of modelers, including Elber, Nelson and Kikukawa, who are quite similar in that they seek to represent the crack closure phenomenon by estimating an effective ΔK for each stress range.
- The Wheeler and F*uum*hring models both require empirical estimates of important parameters that depend on the specific load block.
- The Willenborg and Nelson models both require only constant amplitude crack growth data at $R = 0$. Willenborg does not model the crack closure effect while Nelson approximates it.

- Barsom is the only one that attempts to lump the entire loading into a single parameter, ΔK_{RMS}. This avoids the difficulty of calculating crack growth cycle by cycle.
- In all the models, except Barsom's, the maximum stress in a block of loading is a critical parameter. It is identified as the significant event which controls the crack growth retardation.

It is the central importance of the maximum stress peak that seriously limits the ability of all the above methods to model real loadings. As Wei* has observed, the maximum stress in any block of real loading is a random variable. Even the division into blocks is an artificial one that is only done to simplify analysis and testing. Typically, this difficulty has been avoided by selecting a *representative loading,* omitting the highest possible stress peaks, which will usually underestimate the retardation and produce a conservative estimate of time to failure. The amount of conservatism, however, is not known and cannot be obtained from the representative loading.

1.5 Scope and Organization

In the following chapters, fatigue crack growth due to random loading is investigated, showing a variety of approaches that are tailored to the level of complexity required for the application at hand. The emphasis is on creating the simplest models, of both the crack growth process and the random loading, that maintain the desired level of accuracy. Models that include load sequence effects to achieve greater accuracy can be computationally expensive. Because the desired accuracy can vary, approximate models that are simple to implement and require minimal computations are also presented. Examples that illustrate the relative accuracy of the approximations are provided as well.

In Chapter 2, a new crack-growth model, based on a combination of Nelson's and Willenborg's models, is introduced and shown to predict several sets of published test results. The model provides a means of approximating load sequence effects by continuously updating the crack opening stress, accounting for both acceleration and retardation effects in a simplified way. Linear elastic fracture mechanics and a two-dimensional crack geometry are assumed. This model is used in the subsequent chapters as the standard crack growth model

---

* written comment by R.P. Wei, following reference by Barsom, 1976.

that includes sequence effects.

Random load models, which describe the relevant events in the loading necessary to implement the above crack growth model, are outlined in Chapter 3. These models range from simple random variable descriptions that are useful in sequenceless applications to random process simulations that include the relative likelihood of various load sequences. Existing random variable descriptions of narrow-band loadings are shown to be useful approximations for any Gaussian loading. New results that account for the overall peaks and ranges in wide-band loadings are obtained through *racetrack filtering*. An efficient sequential simulation method uses the random variable results to simulate only the most significant events in a random process by breaking the loading into slow (mean variations) and fast (amplitude variations) parts.

Chapter 4 describes practical methods for calculating crack growth life by applying the load models of Chapter 3 to the crack growth model of Chapter 2, and to an alternative model that neglects sequence effects. Inherent difficulties in the traditional, sample-block, load model can be eliminated with a continuously defined loading, which can be obtained by the sequential simulation method. This simulation method is used in studies that illustrate the relative importance of including load sequence effects in crack growth analysis. For stationary Gaussian loadings, sequence effects can often be neglected. Nonstationary random loadings are also simulated and shown to produce greater sequence effects.

As an alternative to simulation, analytical estimates of crack growth life including sequence effects are examined in Chapter 5 using diffusion models. The emphasis is on simplifying the problem (i.e., scalar diffusion models) so that solutions can be obtained with limited computational resources. Solutions for mean and variance of the time to failure due to constant amplitude loading with distinct tensile overloads are presented. The mean time to failure due to stationary Gaussian loading is also estimated. More complete, but computationally expensive, solution methods using vector diffusion models are outlined.

The first four chapters do not assume any background in random process theory by the reader, but attempt to provide the necessary background as the material is presented. Chapter 5 does assume a minimal understanding of random processes and, therefore, moves quickly through the introductory material. The intent is that the reader without probabilistic training would find the early chapters accessible and, perhaps, instructive, while Chapter 5 may be of more interest to the already initiated.

CHAPTER 2

CRACK GROWTH MODEL

2.1 Introduction

There are numerous effects of load sequences on crack growth which have been documented in the past decades. Most of the test data are based on constant amplitude loading with well defined overloads. The applicability of the results of constant amplitude testing to the case of irregular loading is often not well understood. It is therefore not the intent of this crack growth model to quantitatively reproduce all the known responses of crack growth rate to load sequences. It is important, however, to model those known material responses which will cause the most dramatic changes in crack growth rate. Such a model is a useful tool in investigating the relative effects of various combinations of loadings and material properties on time to failure.

The proposed model is capable of accurate fatigue crack growth predictions if sufficient material response data are available, but is also capable of reflecting the relative changes in fatigue life due to differing loadings and material choices when a minimum of data are available. The amount of data required to specify the crack growth response to a random loading is kept to a minimum by including only the most influential parameters in the crack growth model. This is especially important in the early stages of design when it is impractical to obtain test data for all of the alternative materials and geometries.

A simple crack growth model is also valuable when the loading is random and probabilistic analysis or simulation is required. A complex crack growth model could preclude the possibility of an analytical solution. If analytical solutions are still not possible and simulations must be used, a simple crack growth model will reduce the computation time involved in repeated calculations of crack growth.

The intent is to strike a balance between sequenceless analysis and an exhaustive inclusion of all known fatigue crack growth sequence effects. The emphasis, however, is on a model which can reflect relative load sequence effects with a minimum of descriptive parameters. To achieve this, a model is proposed that requires only material properties that describe the yield stress and the

da/dN *vs* ΔK curve for constant amplitude zero-to-maximum loading. All other parameters can be estimated in the absence of test data.

2.2 A Crack Growth Model for Analysis of Load Sequence Effects

2.2.1 Preliminary Definitions

There are a few terms relating to sequence effects which must be defined before the crack growth model can be described. An explicit definition here may help to avoid confusion later.

The application of a large tensile load results in a subsequent slowing of the rate of crack growth known as *retardation.* Any tensile stress large enough to cause retardation is called an *overload* and is referred to by S_{ol}. There is often a time lag between the application of the overload and the maximum retardation, called *delay.* After the retardation has reached its maximum, the crack growth rate gradually returns to the unretarded rate. This is the *decay* of the retardation. A large compressive load has the effect of immediately speeding crack growth, or *acceleration,* followed by a gradual reduction in the acceleration, as was the case for retardation.

The region of material immediately in front of the crack tip, in the path of crack growth, which is plastically deformed is the *crack tip plastic zone.* Although this zone is never perfectly circular, the distance from the crack tip to the maximum extent of the plastic zone is called the *crack tip plastic zone radius,* or usually just the *plastic zone radius,* r_p.

When the loading is irregular, it may not be obvious which load peaks are responsible for retardation. Since the duration of the retardation is associated with the plastic zone size, the overloads are taken to be those loads which increase the plastic zone radius. The stress level which is necessary to reset the maximum extent of the plastic zone is defined as the *reset stress,* S_r. An overload is, therefore, any load peak which exceeds the current reset stress.

The *crack opening stress,* S_{op}, is the stress level necessary to physically open the crack tip. The crack opening stress is modeled as a fraction of the reset stress. The ratio of the crack opening stress to the reset stress is called the *crack opening stress ratio,* q.

The difference between the peak stress, $S_{\max}$, and the crack opening stress is known as the *effective stress range,* $\Delta S_{eff} = S_{\max} - S_{op}$. The stress intensity

associated with it is known as the *effective stress intensity range,* ΔK_{eff}. If the stress peak is less than the crack opening stress, the effective ranges are zero. A negative stress range has no meaning.

2.2.2 Description of the Crack Growth Model

When a tensile overload, S_{ol}, is applied to a cracked body such that the stress intensity factor is $K_{ol} = \sqrt{\pi a}\, Y(a) S_{ol}$ (in which $Y(a)$ is a shape factor), a plastic zone with a radius of approximately r_{ol} is created:

$$r_{ol} = \frac{K_{ol}^2}{\gamma 2\pi S_y^2} \tag{2.1}$$

in which γ is the plane strain constraint factor ($\gamma = 1$ for plane stress and $\gamma = 3$ for plane strain), and S_y is the yield stress.

The extent of the influence of the overload has been suggested to be about twice r_{ol} [Johnson, 1981].

$$d_{ol} = 2r_{ol} = \frac{K_{ol}^2}{\gamma \pi S_y^2} \tag{2.2}$$

The distance between the maximum extent of the influence of the previous overload, $(a_{ol} + d_{ol})$ and the current crack length, a, is d_p, as shown in Fig. 2.1. The reset stress at any time is the stress necessary to produce a plastic zone *diameter* equal to d_p.

$$S_r = \frac{S_y}{Y(a)} \left(\frac{\gamma d_p}{a} \right)^{1/2} \tag{2.3}$$

S_r, therefore, instantaneously increases to S_{ol} when an overload is applied (no delay is modeled) and then gradually decreases as the crack grows through the plastic zone as shown in Fig. 2.2.

The effective stress intensity range due to a stress range from valley $S_{\min}$ to peak, $S_{\max}$, is

$$\Delta K_{eff} = \begin{cases} Y(a)\sqrt{\pi a}\,(S_{\max} - qS_r) & S_{\max} > qS_r\,,\ S_{\min} < qS_r \\ Y(a)\sqrt{\pi a}\,(S_{\max} - S_{\min}) & S_{\max} > qS_r\,,\ S_{\min} \geq qS_r \\ 0 & S_{\max} \leq qS_r \end{cases} \tag{2.4}$$

The crack growth rate is assumed to depend on ΔK_{eff} in a way that is analogous to Paris' Law:

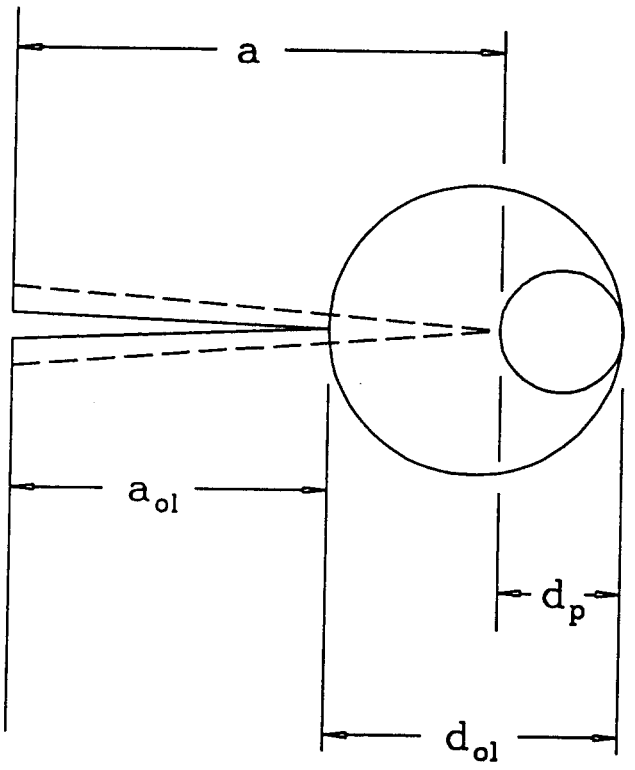

Fig. 2.1 Schematic of crack growth through the overload affected zone from a_{ol} to $a_{ol}+d_{ol}$.

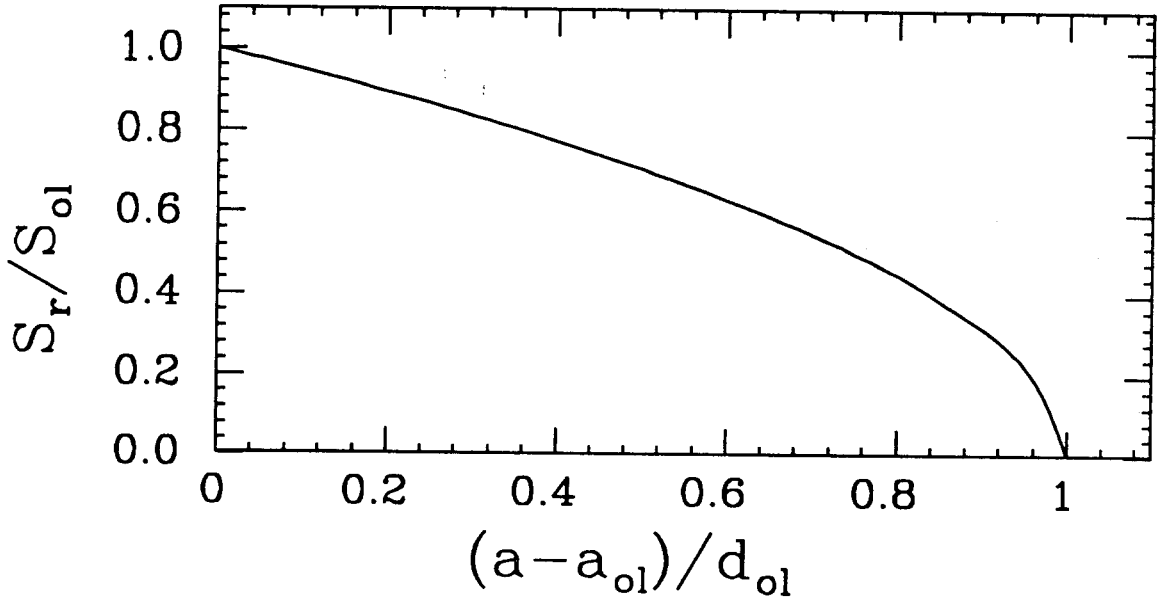

Fig. 2.2 Variation in reset stress, S_r, as the crack grows through the overload affected zone from a_{ol} to $a_{ol}+d_{ol}$.

$$\frac{da}{dN} = C\Delta K_{eff}^{b} \tag{2.5}$$

Several studies of constant amplitude loading have shown q to be a function of stress ratio, R, as well as $S_{\max}$. The empirical relationship between effective stress range and applied stress range is often expressed in terms of the parameter U, which is the ratio of effective stress range to total stress range given by

$$U = \frac{\Delta S_{eff}}{\Delta S} = \frac{S_{\max} - S_{op}}{S_{\max} - S_{\min}} = \frac{1 - q}{1 - R} \tag{2.6}$$

Estimates of U as a function of R include forms ranging from linear [Elber, 1971] to fourth order polynomials [Schijve, 1981; Chand and Garg, 1983]. U and q are related by

$$q = 1 - U(1-R) \tag{2.7}$$

When the relationship is plotted in terms of q instead of U, as was done by Schijve, the deviations from a straight line are not great over a fairly wide range of R. Figure 2.3 illustrates the assumed dependence of q on R given by three authors. The solid lines are linear approximations to the dependence of q on R given by

$$q = q_o \left(1 + \frac{R}{|R_o|}\right) \tag{2.8}$$

where q_o is the crack opening stress ratio at $R = 0$ and R_o is the (negative) stress ratio at which q becomes zero. Plots for $R_o = -2$ and $R_o = -5$ are shown. This range of R_o values allows the linear relationship to adequately represent the variation in q for stress ratios near or less than zero. When $S_{\min}$ is greater than S_{op}, it is as if $q = R$. Effectively, the crack opening stress ratio is bilinear as shown by the solid lines in Fig. 2.3.

The above stress ratio, R, is traditionally the ratio of the minimum to the maximum stress in constant amplitude loading. For a loading defined by a sample block, R is defined by the highest and lowest stresses in the block. In a random loading, for which there is no block structure, it is not obvious what the local stress ratio should be. Since the crack growth rate is dependent on the changes in q with stress ratio in a secondary way, any number of methods of determining a local R can produce equivalent results. In the absence of block structure, an arbitrary block length of one thousand cycles is used to update a

local R.

There is a documented tendency for q to decrease as $S_{\max}$ increases [Newman, 1981; 1982; Chand and Garg, 1983], but this dependence on $S_{\max}$ is not always evident [Jono et. al., 1984; 1985]. Dependence of q on the maximum stress is not included in this model.

The threshold stress intensity range is reportedly zero when the effective stress intensity range is used to calculate crack growth rate for irregular loadings [Kikukawa, et. al., 1981]. Even if there is a threshold for crack propagation, it would not be a bad approximation to assume zero threshold because for irregular loadings, the small amplitude effective stress ranges account for a very small fraction of the total crack growth. A zero threshold is assumed in this work.

2.2.3 Sequence Effects Included in the Model

The most prominent sequence effect, retardation of the crack growth rate due to a tensile overload, is modeled by making the crack opening stress a function of the reset stress. This reset stress is set equal to the magnitude of a tensile overload at the time of application. The magnitude of the retardation effect is tied to the size of the overload by making the crack opening stress a fraction, q, of the reset stress. The crack opening stress governs crack growth rates because the effective stress range is the difference between the maximum stress and the crack openings stress.

Decay of the retardation is modeled by reducing the reset stress gradually as the crack grows through the overload induced plastic zone. This approach to decay is similar to that used in conjunction with other crack growth sequence effect models [Willenborg, et. al., 1971; Johnson, 1981].

Acceleration is modeled in an indirect way by relating q to the stress ratio, R. When a large compressive load is applied, R decreases and q also decreases (Eq. 2.8), resulting in an increased ΔS_{eff}, which yields an accelerated crack growth rate.

2.2.4 Sequence Effects Neglected by the Model

The neglected effect that could have the greatest impact on predictions of fatigue crack growth life is the possible dependence of q on maximum stress. There is conflicting evidence on this effect. The association between q and $S_{\max}$ is neglected here for the sake of simplicity.

The delay of retardation after an overload arrival is also neglected. This delay accounts for a decrease in life for one very special load history [Larsen and Annis, 1980] but is likely to be inconsequential in a random loading.

The magnitude of the retardation can be increased if a number of overloads are applied in one clump [Trebules, et. al., 1973; Gardner and Stephens, 1974]. Although this effect is well documented for constant amplitude loading with distinct clumps of overloads, it is not clear how this would be manifest in a random loading environment where each load peak is different. Since the additional effect of repeated overloads is smaller than the effect of the first one, and it is unlikely that a large number of overloads will occur in succession during a random loading, no differentiation is made in this model between single and multiple overloads.

2.2.5 Crack Growth Rate Constants

The constants in Eq. 2.5, C and b, are defined in terms of the effective stress intensity range, ΔK_{eff}. These constants are derived from the relationship between crack growth rate fit of the $R = 0$ test data to the usual Paris law equation is first obtained:

$$\frac{da}{dN} = C_o \Delta K^b \tag{2.9}$$

The effective stress intensity range when $R = 0$ is

$$\Delta K_{eff} = \Delta K(1-q_o) \tag{2.10}$$

To predict the same crack growth rate from both Eq. 2.5 and 2.9 for $R = 0$ tests, C must be related to C_o by

$$C = C_o(1-q_o)^{-b} \tag{2.11}$$

The crack growth exponent, b, is unchanged.

Without changing the basic assumptions of the model, it is possible to formulate other crack growth equations. The prime assumption is that the crack growth rate is determined by the effective stress range which is in turn determined by the crack opening stress. The assumption that has worked well in predicting crack growth rates for irregular loadings is that the crack opening stress will be the same as for a constant amplitude loading with the same maximum and minimum stress [Socie, 1977; Jono, et. al., 1984]. The crack growth rate should be the same as for constant amplitude loading with the same

effective stress range. Therefore, alternate crack growth rate equations which maintain the equivalence of growth rates for similar effective stress ranges are consistent with this modeling approach. One such alternative is to apply a Forman-like equation [Forman, et. al., 1967].

$$\frac{da}{dN} = \frac{C_F \Delta K_{eff}^b}{(1-R_{eff})} \tag{2.12}$$

in which R_{eff} is the effective stress ratio of each cycle, which depends on the crack opening stress:

$$R_{eff} = \begin{cases} \dfrac{S_{op}}{S_{\max}} & S_{op} > S_{\min} \\ \dfrac{S_{\min}}{S_{\max}} & S_{\min} > S_{op} \end{cases} \tag{2.13}$$

The crack growth constants are determined as before by fitting to constant amplitude $R = 0$ data using the equation

$$\frac{da}{dN} = \frac{C_o \Delta K^b}{(1-R)} \tag{2.14}$$

When $R = 0$, $R_{eff} = q_o$. As before, b is the same for both equations and C_F is related to C_o by

$$C_F = C_o(1-q_o)^{1-b} \tag{2.15}$$

Both of these formulations account for constant amplitude stress ratio effects in roughly the same way. Figure 2.4 shows the crack growth rates for nonzero stress ratios divided by $R = 0$ crack growth rates for the two formulations. The ratio of crack growth rates is almost identical for the two approaches as long as the minimum stress is less than the crack opening stress ($R < q_o$).

The purpose of including the Forman-like variation to the crack growth equation is to exemplify the flexibility of this modeling approach and to show the effect of such model variations on life predictions. The approach does not depend on the exact form of the crack growth equation, but rests on the definition of the reset stress, which governs the variations in the crack opening stress.

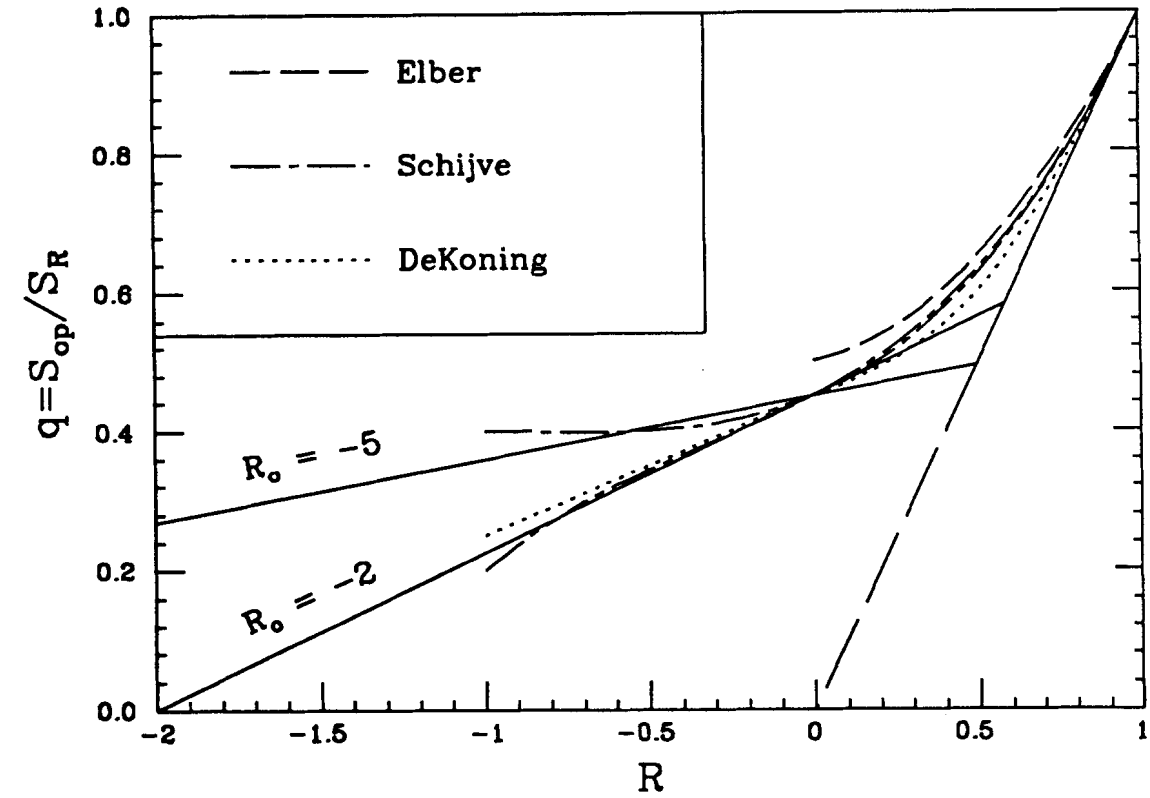

Fig. 2.3 Comparison of the relationship between q and R assumed in the model (solid line) with those suggested by Elber [1971], Schijve [1981], and De Koning [1980].

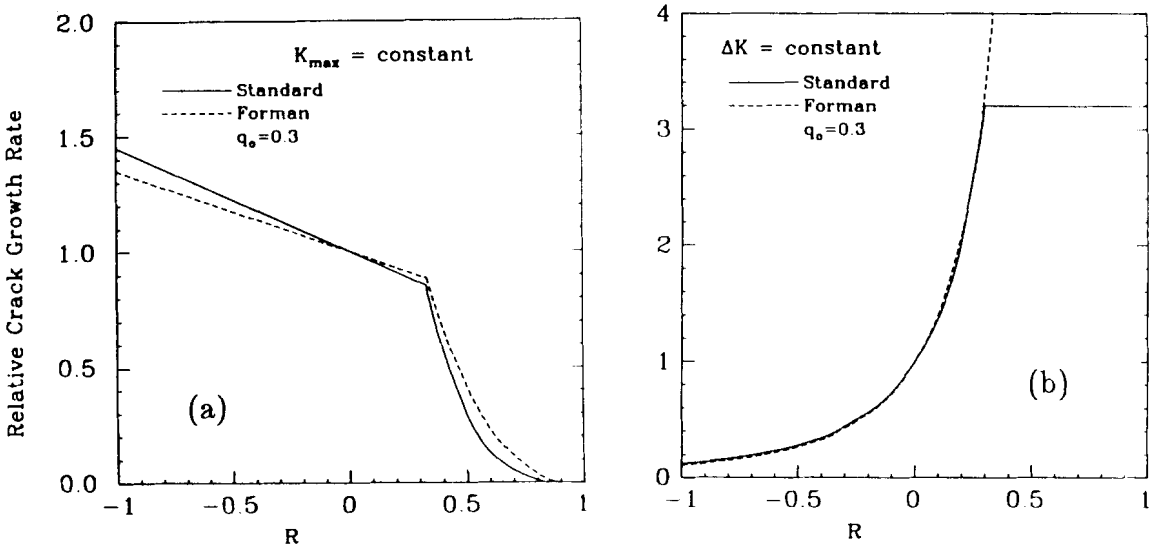

Fig. 2.4 Crack growth rate as a function of R divided by the crack growth rate when $R = 0$. a) Maximum K fixed. b)ΔK fixed. ($q_o = 0.3$, $b = 3.64$)

2.2.6 Model Assumptions

It has been assumed that linear elastic fracture mechanics applies to the loaded crack. This requires that the loading be nominally elastic with plasticity limited to the vicinity of the crack tip. Mode I crack growth, which is based on uniaxial loading perpendicular to the crack surfaces, is also assumed throughout. The expressions for the size of the plastic zone are for a two dimensional geometry and depend on a homogeneous, isotropic material which is linear elastic up to the yield stress. No time dependent material behavior is modeled so high temperature effects are also excluded.

2.3 Comparison of Model Predictions with Test Results

2.3.1 Overview

The proposed model is applied to several published irregular load histories. These loadings consist of blocks of sequential stress peaks and valleys tabulated in two special publications, one by the American Society for Testing and Materials (ASTM) [Chang and Hudson, eds., 1981] and the other by the Society of Automotive Engineers (SAE) [Wetzel, ed., 1977].

The four ASTM histories were computer generated while the SAE loadings were selected load measurements from three different automotive components. The specimens were aluminum 2219-T851 center cracked tension specimens for the ASTM tests and steel keyhole notched plates for the SAE tests. The SAE testing was conducted at a number laboratories while the ASTM tests were done at a single facility. The SAE and ASTM test and analysis series were published in 1977 and 1981 respectively .

Both test series share the methodology of defining the load history with a single block of sequential load peaks and valleys. A fatigue test is conducted by repeating the load block in a continuous loop fashion until either the specimen fails or the test is suspended. Although the term *random* is often applied to these loadings, a better description might be *irregular*. The block structure gives well defined minimum and maximum stress levels which repeat at time intervals equal to the block length. In a random loading, the maximum and minimum stress levels in any fixed block of time will be random variables, as will the time between local extrema.

2.3.2 The ASTM Test Series

The purpose of the ASTM test series was to "*assess whether data from constant amplitude fatigue crack growth tests on center cracked tension (CCT) specimens can be used to predict fatigue crack growth lives of CCT specimens subjected to random load sequences*" [Chang and Hudson, eds., 1981].

The ASTM load histories are examples of the types of loadings experienced by fighter aircraft wings. The loads were not taken directly from measurements, but were derived from power spectral densities (PSDs) which were calculated from hours of actual flight data [Dill and Saff, 1977]. The load histories were divided into three types: Air-to-Air (AA), Air-to-Ground (AG), and Instrumentation-and-Navigation (IN). From a combination of these three, a fourth type of loading, called Composite Fighter (CF), was generated.

Simplified versions of the PSDs used to generate the time series for the AA, AG, and IN load histories are shown in Fig. 2.5. Unique random time series were generated by discretizing the PSDs, assigning random phase angles to each frequency component and computing the inverse discrete Fourier transform. (The topic of simulating random loadings is given more detailed treatment in Chapter 3.)

One sample block of loading was selected for the AA, AG, and IN load histories. Peaks and valleys were determined by quadratic interpolation and all ranges smaller than 10% of design limit stress (DLS) were removed. Valleys were replaced with a fixed magnitude compressive load at regular intervals to simulate the *ground load*. A ground load of -5% of design limit stress (DLS) was used in the AA and IN histories while -10% of DLS was used in the AG history.

Sample blocks of sequences of peaks and valleys are tabulated for each load type [Chang, 1981]. Figure 2.6 contains plots of a sample of the sequential peaks and valleys of the AA, AG, and IN histories. The load magnitudes are defined as fractions of DLS. The DLS levels used in the test series were 20, 30, and 40 ksi for the AA, AG, and CF histories, and of 30 and 40 ksi for the IN history.

The stress intensity factor for the ASTM specimen includes a finite width correction factor in the geometric term $Y(a)$.

$$K = \sqrt{\pi a}\ Y(a)S \tag{2.16}$$

where

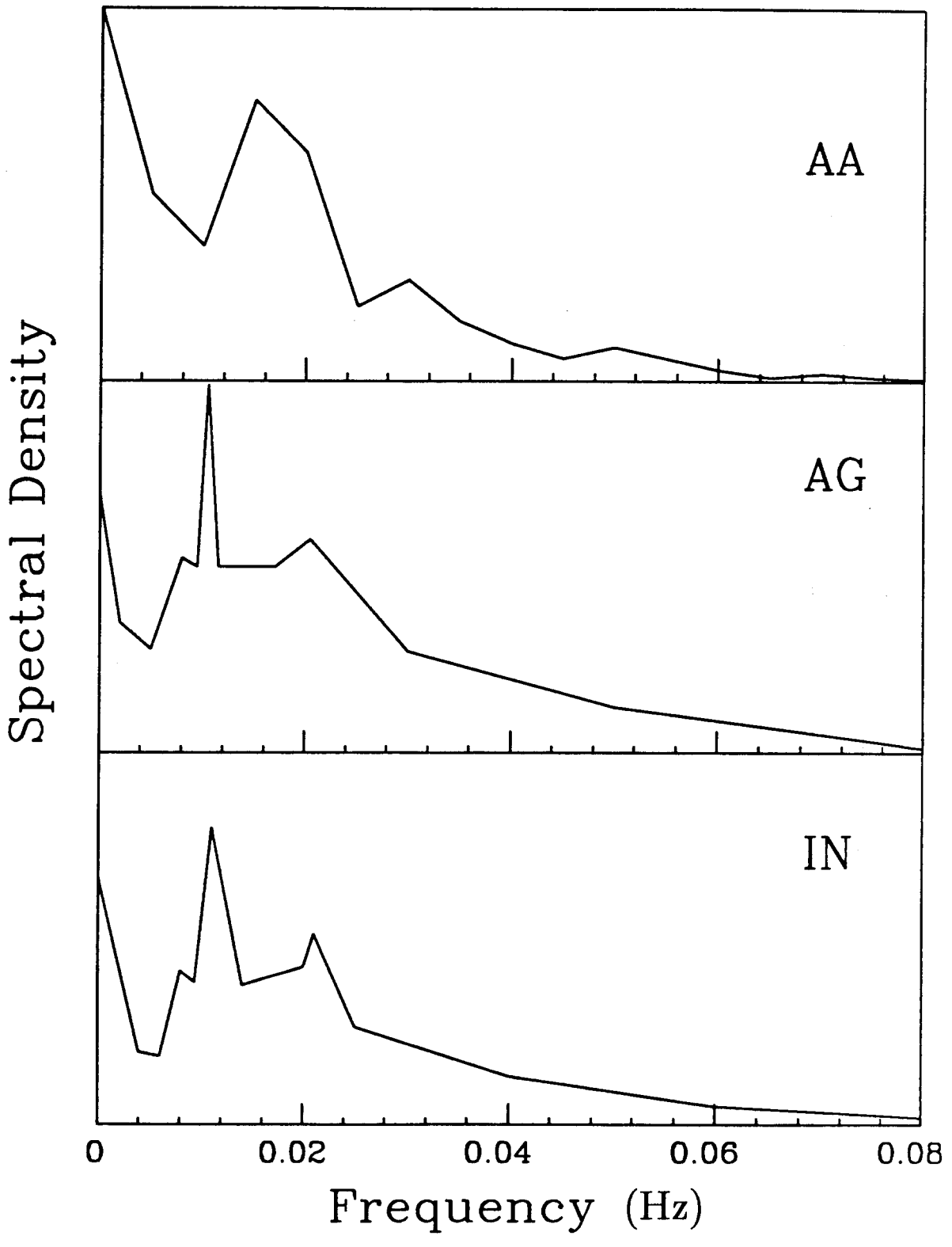

Fig. 2.5 Simplified power spectral densities (PSDs) of the ASTM loadings.

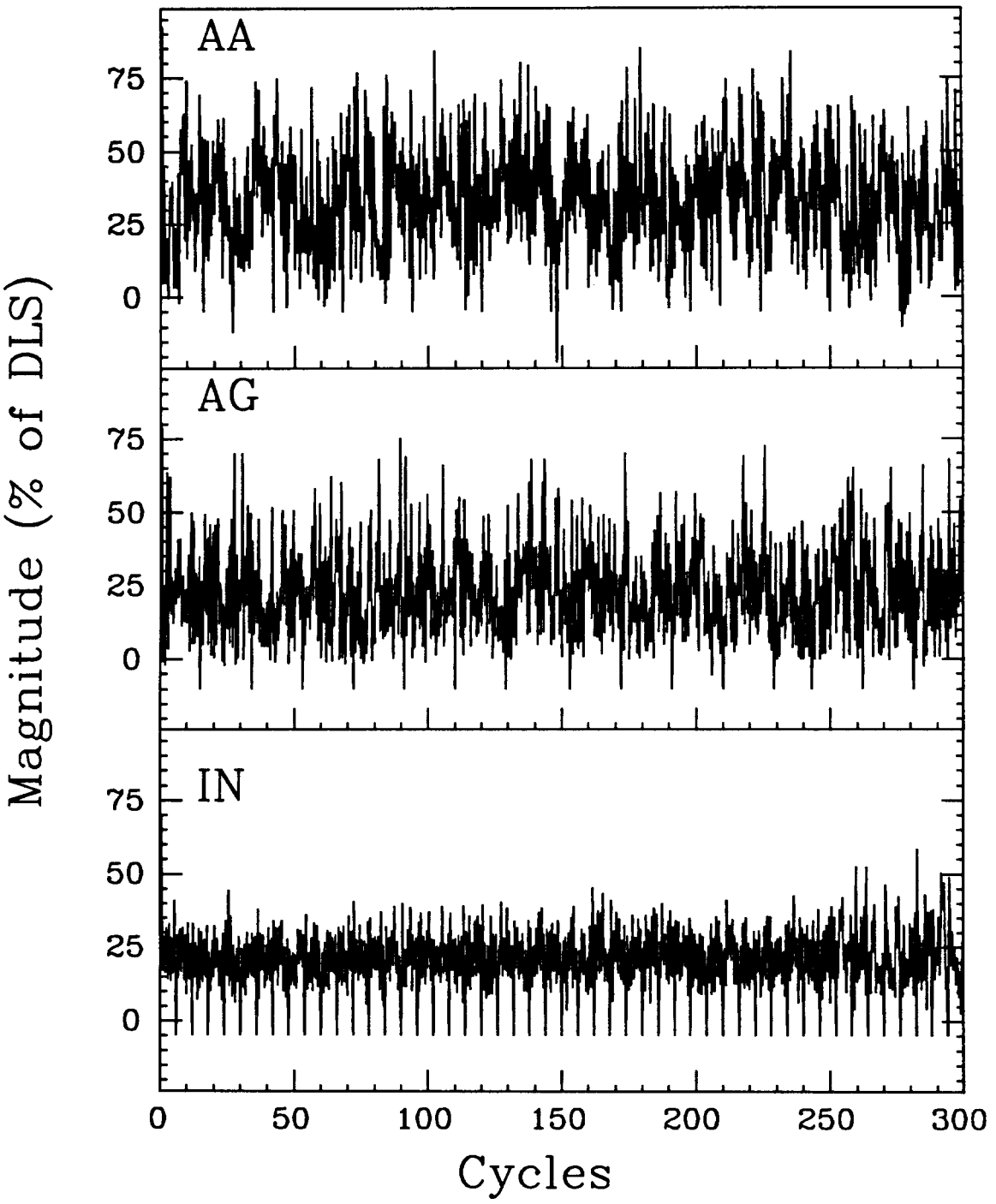

Fig. 2.6 Plots of a sample of the sequences of peaks and valleys for the ASTM test series.

$$Y(a) = \left[secant \left(\frac{\pi a}{W} \right) \right]^{1/2}$$

and W is the specimen width.

The relevant material properties (S_y, C_o, and b), which are taken from Chang, Szamossi and Liu [Chang, et. al., 1981], are listed in Table 2.1. Only $R = 0$ crack growth rate data was used to calculate C_o and b.

Crack growth testing was conducted by repeating the load blocks until the crack had grown from the initial precracked half crack length of about 0.15 inches to failure. The precise initial and final crack lengths and the number of cycles to failure are listed in Table 2.2 for all eleven tests. Only one test was conducted for each combination of load history and load magnitude.

Table 2.1 - Material constants for the ASTM and SAE test series.

Material	Specification	Yield Stress, ksi	b^*	C_o^*
Aluminum	2219-T851	50	3.64	8.4×10^{-10}
Steel	Manten	48	2.81	4.6×10^{-10}
Steel	RQC-100	95	3.03	2.7×10^{-10}

($^*b, C_o$ for crack growth rate in inches/cycle and stress intensity range in ksi$\sqrt{in.}$)

Table 2.2 - ASTM crack lengths and number of cycles of loading.

Load Type	Scale Factor	Initial crack length (in.)	Final crack length (in.)	Number of Cycles
AA	0.2	0.16	0.5125	115700
AA	0.3	0.15	1.395	58585
AA	0.4	0.15	0.9175	18612
AG	0.2	0.175	2.2	268908
AG	0.3	0.144	1.735	95642
AG	0.4	0.1525	1.29	36397
IN	0.3	0.15	1.805	380443
IN	0.4	0.15	1.5125	164738
CF	0.2	0.1525	2.03	218151
CF	0.3	0.15	1.4225	65627
CF	0.4	0.15	1.1625	22187

2.3.3 The SAE Test Series

The Society of Automotive Engineers (SAE) initiated this test series to provide guidance in "*how to handle complex load histories*" [Wetzel, ed., 1977]. The selection of the specimen geometry and material as well as the choice of load histories were intended to make the test series simulate a real life situation. The tests, which started with an initially smooth notch, monitored *crack initiation* and subsequent growth to failure. The portion of the test from crack initiation to failure is used here to test the ability of the proposed crack growth model to predict test results.

Many of the tests in the series included substantial plasticity extending well beyond the notch root. Since the proposed model is limited to linear elastic fracture mechanics, those tests are not considered here. In addition, some of the tests were either suspended prior to crack initiation or contained insufficient documentation of initial and final crack lengths. Twenty one of the tests, eleven using Manten and ten using RQC-100, are applicable for comparison with model predictions.

The material properties for these two steels, taken from published estimates [Socie, 1977], are included in Table 2.1. The only material properties which are required to implement the crack growth model are the ones listed in the table.

The load histories are sample measurements made on three different ground vehicle components. The *suspension* history (SP) is a record of the load in a vehicle suspension component when driven over an accelerated durability course. This loading has a large compressive mean. The *bracket* history (BR), measured on a mounting bracket while the vehicle was operated on a rough road, is an almost classic narrow band random vibration with near zero mean stress. The *transmission* history (TR) is a torque measurement on the transmission of a front-end loader equipped tractor during heavy duty operation. A portion of each loading is shown in Fig. 2.7. Tables of peaks and valleys are published in the special SAE publication [Tucker and Bussa, 1977]. Condensed tables of extrema are given by Nelson [Nelson and Fuchs, 1977]. The number of cycles in each block was reduced to 10 percent of the original using the *racetrack filtering* technique [Fuchs, et. al., 1977]. (An examination of the racetrack filtering algorithm is included in Chapter 3.) The condensed load history is used for the bracket history. All tensile peaks are included in the suspension loading. The entire set of peaks and valleys are used to evaluate the transmission load history.

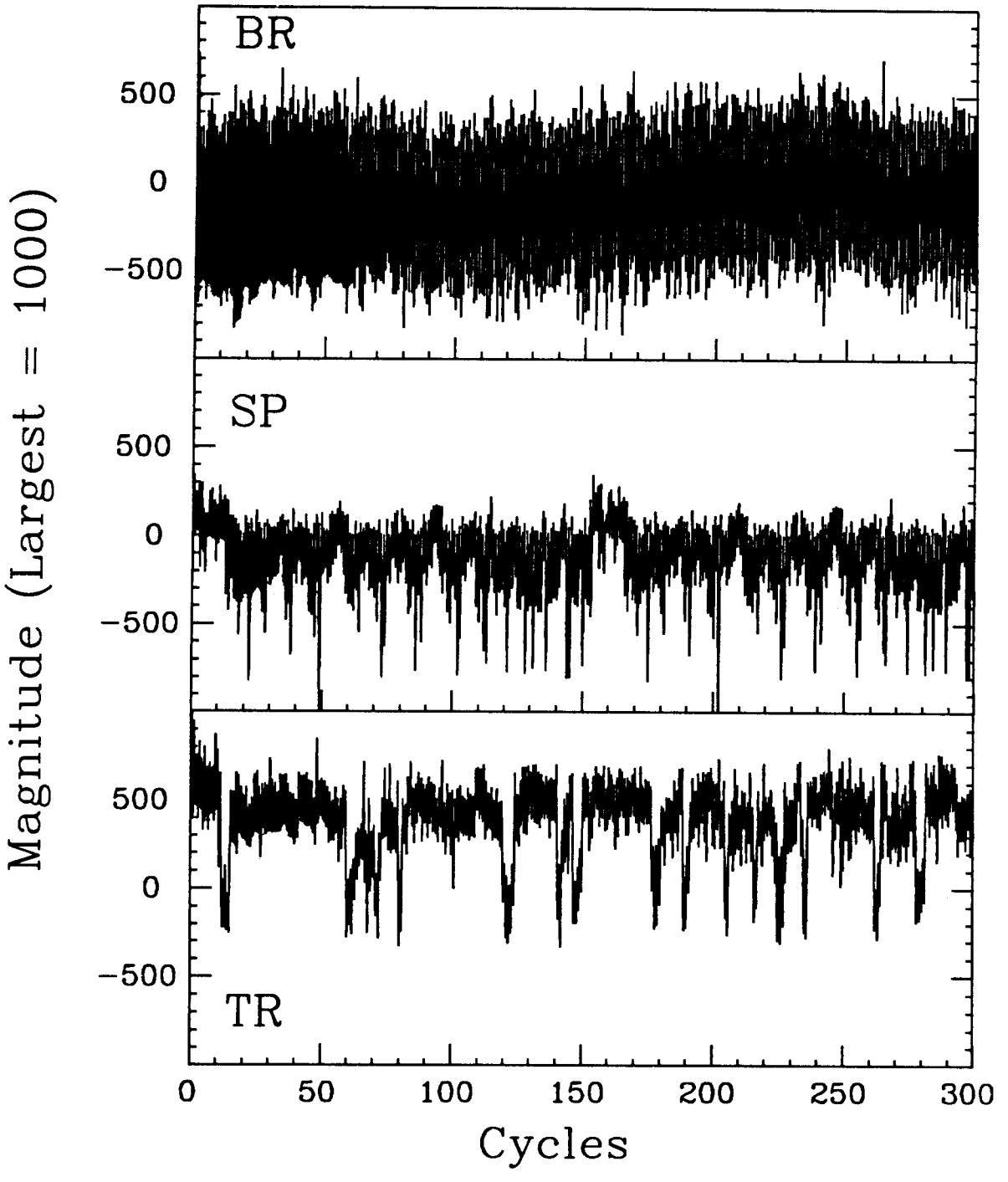

Fig. 2.7 Plots of a sample of the sequences of peaks and valleys for the SAE test series. Only the peaks used in the crack growth analysis are plotted.

Table 2.3
SAE crack lengths and number of blocks of loading in crack growth.

Test ID	Max. load (kips)	Initial crack length (a_i/W)	Final crack length (a_f/W)	Number of Blocks
SM3-1-FS	-6.0	.3777	.7669	22402
SM3-2-FS	-6.0	.3723	.7669	28448
SM3-3-W	-6.0	.3524	.6831	23932
SM4-2-MTS	-4.5	.3501	.7026	19100
BM3-1-MTS	-3.5	.3507	.8263	3262
BM3-2-MTS	-3.5	.5993	.7169	32
BM3-3-FS	-3.5	.3507	.7669	2062
BM4-2-FS	-3.0	.3669	.4209	6543
BM4-3-MTS	-3.0	.3561	.7777	1306
TM3-2-FS	+3.5	.3858	.6764	979
TM3-3-MTS	+3.5	.3507	.6418	2137
SR2-2-GM	-9.0	.3520	.3696	3490
SR3-2-FS	-7.0	.3608	.7804	38053
BR2-1-FS	-8.0	.3561	.5264	80
BR2-2-FM	-8.0	.3547	.6545	59
BR2-3-JD	-8.0	.3520	.7318	94
BR3-1-MTS	-3.5	.3507	.5966	4901
BR3-3-FS	-3.5	.4520	.7709	774
TR2-1-FM	+8.0	.3677	.5494	27
TR2-2-JD	+8.0	.4628	.6561	11
TR2-3-GM	+8.0	.3547	.5588	43

The test specimen is the keyhole notched plate shown in Fig. 2.8. The stress in the test section is a combination of axial and bending with a stress concentration at the notch. The loadings selected for analysis have notch root yield zones that do not extend to the crack tip. The initial crack length is 0.35 times the width, W (crack lengths are measured from the load line). For purposes of comparison with predictions, the exact initial crack length at the time of a measurement was used; this usually does not correspond to exactly $0.35W$. The initial and final crack lengths as well as the material and number of blocks to grow from initial to final crack length are listed in Table 2.3.

The stress intensity factor for the keyhole notch specimen is defined separately over segments of the crack length domain while maintaining continuity of the function and its first derivative [Nelson, 1978]. The stress intensity factor is defined in terms of the applied load, P (in lbs.), by

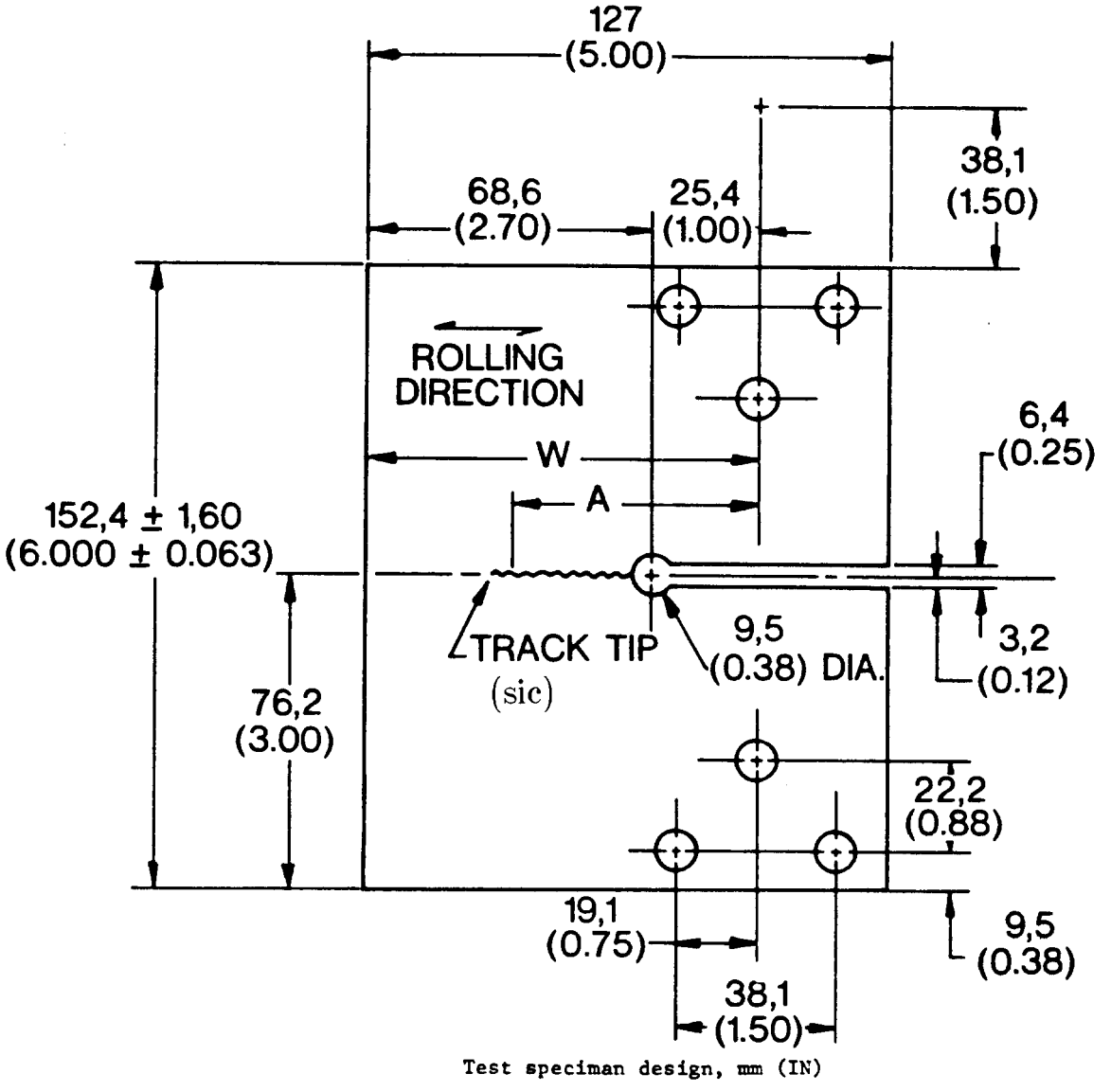

Fig. 2.8 Keyhole notched specimen used in the SAE test series [from Tucker and Bussa, 1977].

$$K = PY(a) \tag{2.17}$$

where

$$Y(a) = \begin{cases} 6.35[7.13 - 38.44(\frac{a}{W}) + 63.31(\frac{a}{W})^2]^{1/2} & .350 < \frac{a}{W} < .525 \\ 6.35[97.10 - 381.17(\frac{a}{W}) + 389.72(\frac{a}{W})^2]^{1/2} & .525 < \frac{a}{W} < .730 \\ 1.80(2 + \frac{a}{W})(1 - \frac{a}{W})^{-3/2} & .73 < \frac{a}{W} < 1.0 \end{cases}$$

2.3.4 Comparison of Model Predictions with Test Results

The only required material properties are the crack growth rate constants, C_0 and b, and the yield stress, S_y, which are given in Table 2.1 for the ASTM and SAE test materials. The other quantities that must be specified are: γ, the plane strain constraint factor; q_0, the $R = 0$ crack opening stress ratio; and R_0, the $q = 0$ intercept of q *vs* R. Each of these quantities can be determined by testing or by elastic-plastic analysis of the crack tip stress field. In the absence of such information, some simple approximations can be made.

For plane strain conditions γ is equal to 3, while for plane stress γ is 1. Plane stress prevails when r_p is greater than the specimen thickness. The ASTM guidelines for determining the plane strain fracture toughness require a specimen thickness of about four times the plane stress r_p before plane strain is fully developed. For thicknesses between one and four r_p, γ can take on values between 1 and 3, with $\gamma = 2$ being a good intermediate approximation.

Values of q_0 have been reported ranging from 0.2 [Jono, et. al., 1985] to 0.5 [Elber, 1970]. As mentioned previously, q_0 may also depend on the maximum stress. The value of q_0 can have substantial influence on the crack growth estimates when the loading is nearly constant amplitude with occasional overloads. But when variations in load amplitude are less distinct, q_0 can be fixed in the middle of the range at about 0.35 as a simplification that recognizes realistic uncertainties in knowledge of q_0 while preserving reasonable accuracy [Nelson, 1978].

The change in crack opening stress ratio, q, with stress ratio, R, has been given many representations including dependence on maximum stress as well as stress ratio. Test data would be valuable in defining the relationship, but in the

absence of test data a linear decrease in q with decreasing R, independent of maximum stress (Eq 2.8), can be used. de Koning suggests $R_0 = 2.25$ when $q_0 = .45$ [de Koning, 1980]. Values of R_0 between -2 and -5 cover most of the published range of q *vs* R [Schijve, 1981; Newman, 1982]. q would be practically constant if $R_0 < -5$ which would minimize the effect on the model of crack growth acceleration due to compressive loading. Different choices of R_0 have a minor effect on crack growth predictions except at relatively large negative stress ratios (R near R_0).

The values of γ, q_0, and R_0 for the ASTM test series are taken from the crack tip plastic zone analysis done by Newman [1981]: $\gamma = 2.3$, $q_0 = 0.3$, and $R_0 = -3.5$. For the SAE test series, there were no estimates of these parameters available so the midrange values were selected for each: $\gamma = 2.0$, $q_0 = 0.35$, and $R_0 = -3.5$.

Predicted cycles to failure are plotted against test cycles to failure for the ASTM test series in Fig. 2.9. Predictions using both the Standard model and the Forman crack growth equation are included. All predictions are within a factor of two of the test results and most are much closer. There is a tendency for the model to overestimate life at lower stress levels (long lives). This is consistent with other predictions for these data [Chang and Hudson, eds., 1981] and has generally been attributed to an insufficient fit to the $R = 0$ crack growth data at low stress intensity levels [Chang, 1981].

Predictions of the number of blocks of loading to failure for the SAE test series are shown in Fig. 2.10. This figure shows a great deal more scatter than the ASTM test series. The major source of variability can be found by comparing the scatter in prediction ratios (ratios of predicted life to test life) within each load/material grouping to the prediction ratios of all the tests. The groupings with the most replicates are: four tests with the SP loading of Manten, five tests with the BR loading of Manten, and five tests with the BR loading of RQC-100. The coefficients of variation (standard deviation divided by the mean) of the prediction ratios for these three groups are 0.90, 0.76, and 0.53, respectively. The coefficient of variation of prediction ratios for the entire SAE test series is 0.76. This indicates that the variability from specimen to specimen within a grouping is the source of most of the scatter in Fig. 2.10.

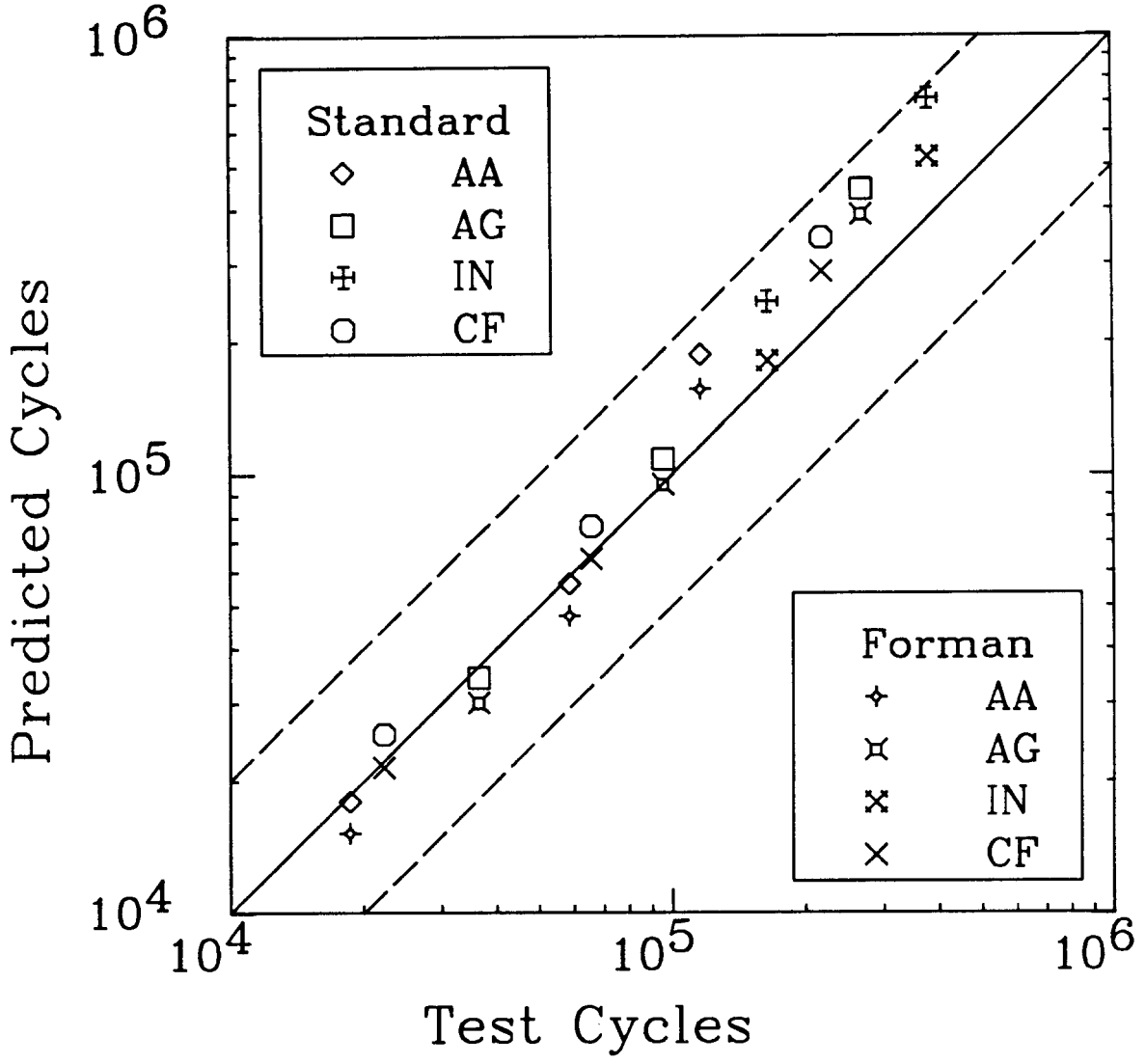

Fig. 2.9 ASTM test results and model predictions.

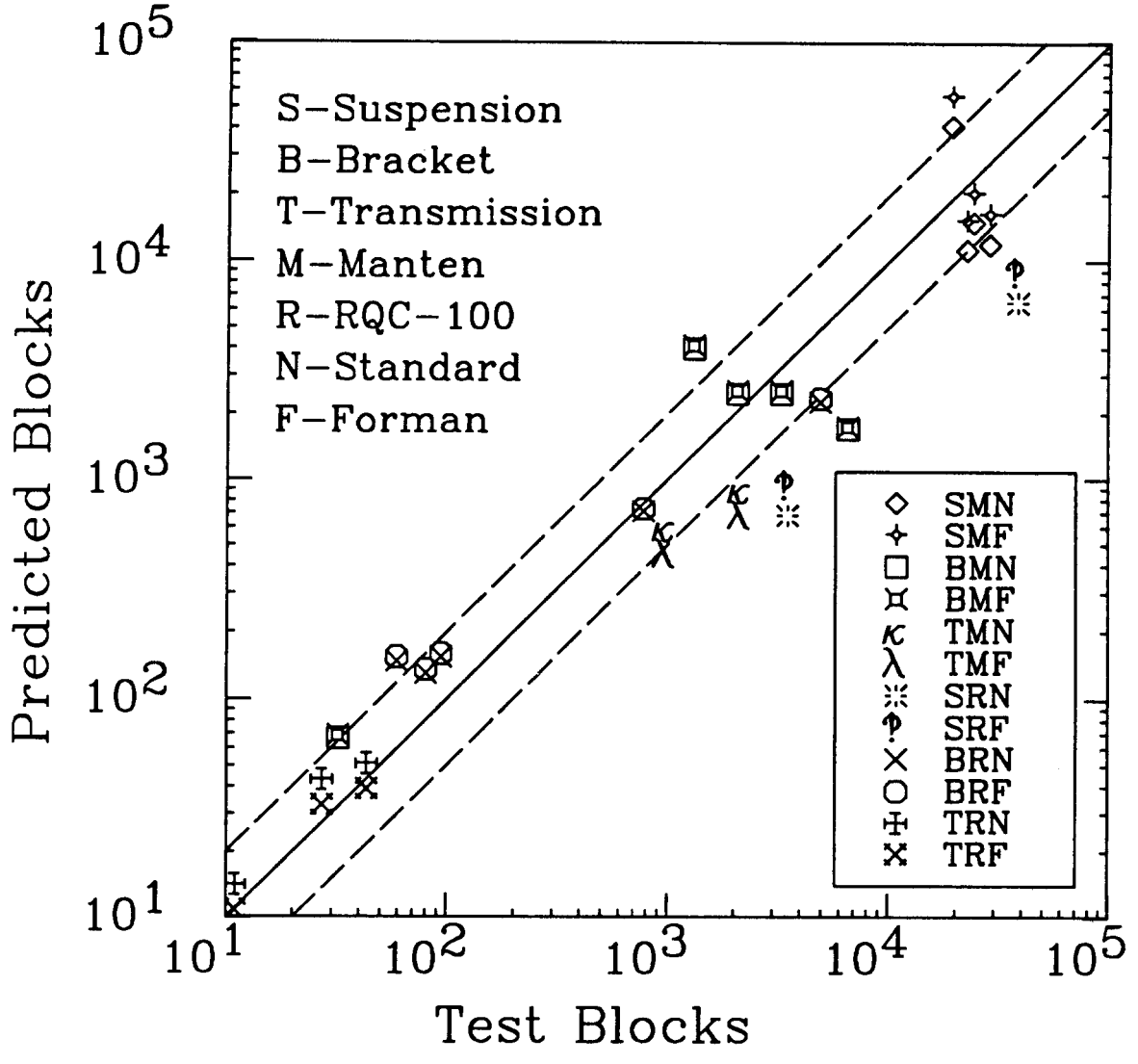

Fig. 2.10 SAE test results and model predictions.

2.4 Discussion

When one load peak in a block type loading is much higher than all the others, it will be the only load to set the reset stress, which governs the crack opening stress. This is true of the ASTM IN loading where one load peak is 70% of DLS and all other peaks are much lower. All the other test cases have many peaks near the maximum. The IN history is the most sensitive to variations in the crack growth parameters, especially q_0. Reducing q_0 decreases life and increasing q_0 increases life. If q_0 is varied between the practical limits of 0.2 and 0.5, the predicted IN life changes by a factor of 4.1. The change for the AA loading, for example, is only a factor of 1.8. The IN loading sensitivity is caused by the one large overload which creates a crack opening stress very near the mean of the rest of the ranges. Small changes in q_0 produce large changes in the crack opening stress relative to the size of the smaller stress ranges. The IN loading most closely resembles the constant amplitude with occasional overload testing which has been used so often to demonstrate retardation effects.

Even when there are several load peaks near the highest one, it is the highest peak that will determine the reset stress for some time during the block. When γ and S_y are both small, the plastic zone will be large and the one highest stress will determine the reset stress for the entire block. This will lead to some sensitivity in the choice of q_0. When the plastic zones are small, the reset stress will decay rapidly and will be reset often leading to less sensitivity to the choice of parameters.

The acceleration effect is negligible in all but the SAE suspension and bracket histories. R is about -3 for the suspension loading and about -1 for the bracket loading. All the other test cases have near-zero minimum stresses that make R close to zero. When R is close to R_0 (-3.5 in this case) the model predicts a near-zero crack opening stress regardless of the maximum or minimum stresses. This acceleration may be too great as can be seen by the underestimated life for the RQC-100 specimens under the suspension loading.

Another possible explanation for underestimating life for the suspension history is the maximum stress influence on q. The maximum stress in the suspension history is lower than any other SAE loading. If low maximum stresses tend to increase q, then the crack opening stress would have been higher and the predicted life would also be longer. The mild tendency in the SAE test cases for over-predicting at high stresses and under-predicting at low stresses is also consistent with this explanation. For the ASTM test series, q was shown to be

insensitive to variations in maximum stress [Newman, 1981]. This would not have been true if there had been plane stress conditions for the ASTM tests. It is also interesting that the SAE tests were close to plane stress conditions during most of the crack growth.

The two crack growth equations, the *Standard* and the *Forman*, are quite close in their predictions. The main difference is in the way that they treat crack growth when the minimum stress is greater than the crack opening stress. The Standard model has a limit on the crack growth rate while the Forman equation continues to predict higher growth rates as the maximum stress increases (for a fixed ΔK). When the minimum stress is almost always negative (as in the bracket history) the two predictions are almost identical.

When sufficient analysis has been done to determine all the input parameters, as was provided by Newman for the ASTM test series, the predictions can be quite accurate. Even when these parameters, q_0, R_o, and γ, are not known, reasonable choices from the middle of the practical range of values can also yield reasonable life predictions as shown by the SAE test series results. This simplified crack growth model may not be quantitatively correct in all instances, but it contains the appropriate effects to model the qualitative behavior of the crack growth and produce estimates of life which are within the band of uncertainty inherent in fatigue testing.

CHAPTER 3

MODELS OF RANDOM LOADING

3.1 Introduction

Although crack growth rates are generally defined in terms of constant amplitude loadings, service loads on fatigue-susceptible structures are rarely constant amplitude. Variable amplitude loads can be described by an actual sequence of peaks and troughs or by a limited number of statistics that reflect, on average, various load characteristics. The statistical description may be both more efficient and more consistent with the extent of knowledge of the loading. The purpose here is to find a minimally sufficient set of load statistics for fatigue crack growth applications. Random load models are provided here (1) for analytical life estimates that ignore sequence effects, and (2) for numerical life estimates based on load simulation methods that reflect the likelihood of various load sequences.

One common way to represent variable amplitude loads is to list the precise sequence of peaks and valleys in a sample block. This sample may be derived either from actual load measurements, as was done for the SAE test series described in Chapter 2, or from a load simulation technique, as was done for the ASTM loadings. The sample block is used in both analysis and testing by repeating the block until failure. This method has the advantage of providing an accurate sample of load sequences, but the disadvantage that only a single sample of all possible load sequences is represented. It has the additional drawback that an artificial sequence effect may be introduced by the periodic repetition of the largest loads in the sample block.

Another way of specifying a random loading is through a *frequency of exceedance* diagram, which defines the number of times within a block that the load will exceed any given level. This is equivalent to describing the peaks of a loading as a random variable. Simple random variable models of various useful load parameters (peaks, ranges, mean stresses, etc.) are shown here. This type of model provides a more complete description of the relative frequency of peak amplitudes than does the sample block, but at the expense of all information on load sequences. For crack growth analysis without sequence effects, these

random variable models provide an efficient method of calculating crack growth by summing contributions from all cycles at each specified stress level, avoiding the need for cycle-by-cycle integration.

To retain a complete description of both (1) the load peaks and ranges and (2) the possible load sequences, the loading dynamics must be described. Modeling load dynamics requires the description of the load as a random process [Madsen, et.al., 1986]. Random loadings are often specified by their frequency content through the power spectral density (PSD) and simulated by fast Fourier transform (FFT) methods. This method was suggested for generating test loadings soon after the discovery of sequence effects in crack growth [Swanson, 1968]. This FFT based approach was used to generate the sample loading blocks used in the ASTM test series. Because published data for the ASTM test series includes both illustrations of the PSDs, and tables of the peaks and valleys, these loadings will be used as examples of load generation techniques in this chapter.

The full specification of a random process load model is often unnecessary for fatigue analysis, which is most sensitive to the overall behavior of load peaks and troughs. Minimal load statistics are suggested here to reflect this dynamic behavior. An efficient *sequential* load simulation method is also presented to preserve these important dynamic aspects, while avoiding the computational expense of PSD based random process simulation.

3.2 Definitions of Random Loading

In common, nontechnical usage, the term *random* implies completely unpredictable, haphazard and patternless. Technically, if a process is random it means simply that it is not possible to predict the value of the process with certainty at any time in the future. Many loadings that are technically random are treated deterministically because, even though foreknowledge of the loading is not certain, it is sufficiently complete for the desired purpose. Loadings that are typically called random are those in which the amount of uncertainty is sufficient to cause difficulty in predicting the effect of the loading on a structure. Estimating the effect of a random loading requires knowledge of both the appropriate loading statistics and analysis techniques that make use of these statistics. Random loading statistics are presented here that describe the loading at the level of complexity necessary for crack growth analysis either with or without sequence effects. A brief discussion of random variables and random

processes is included first.

For the purpose of the following discussion, it is assumed that the random process is both *stationary* and *ergodic*. A stationary process is said to be in a *steady-state* condition, i.e. the mean, variance and other statistics are constant in time. Also, the correlation between the process at any two points in time depends only on the time between the points and not on the absolute time. It is rare that any real process is stationary in a strict sense, but loading processes can often be divided into time segments with stationary behavior in each segment. The ergodic property is that ensemble averages are equivalent to time averages, which means that averaging the value of different realizations of the process at a single time is the same as averaging a single realization over time.

3.2.1 Random Variables

Two basic descriptors of a stationary, ergodic, random loading, $X(t)$, are its average or mean value, m_X, and standard deviation or RMS, σ_X. The mean is the central tendency and the RMS is the spread about that central value. (Strictly speaking, the RMS, as the *root mean square,* includes the squared mean while the *standard deviation* measures the variation about the mean. The term RMS will be used here as the root mean square of the process with the mean removed, making it equivalent to the *standard deviation.*)

The magnitude of a stationary random loading at any point in time is a random variable. The probability that $X(t)$ is between X and $X+dX$ at any time is $p(X)dX$ where $p(X)$ is the probability density function (PDF) of X. (Here, the notation is employed that uses X as both the random variable and the value of the random variable.) The PDF shows the distribution of probability as a function of load magnitude. Actual probabilities of any event depend on the integral of the PDF over the range of magnitudes in the event. The cumulative distribution function (CDF) of X, $P(X)$, is the integral of the PDF from minus infinity up to the argument of the CDF:

$$P(X) = \int_{-\infty}^{X} p(u)du \tag{3.1}$$

Thus, the CDF is the probability that the random variable is less than the argument at any time, as well as the average fraction of time for which the load is less than the argument (by the ergodic property).

While it would be very helpful to know the exact distribution of the loading, it requires more information than is usually available. In practice, the best that can be done is to estimate some statistics of the distribution. Moments of the distribution are useful descriptors; for example, the first moment of the distribution is the mean, m_X:

$$m_X = \int_{-\infty}^{\infty} X\, p(X) dX \tag{3.2}$$

which can also be written as $m_X = E[X]$ where $E[\cdot]$ is known as the expectation operator. Expectation is a linear operator defined as the integral of the operand times the PDF. The n^{th} moment of the distribution of X is therefore $E[X^n]$.

The variance, σ_X^2, is the expectation of $(X-m_X)^2$ or, equivalently, the second moment of the distribution minus the squared mean:

$$\sigma_X^2 = \int_{-\infty}^{\infty} X^2 p(X) dX - m_X^2 = E[X^2] - (E[X])^2 \tag{3.3}$$

The RMS, σ_X, is the square root of the variance.

Two random variables, X and Y, have a joint PDF, $p(X,Y)$. The probability that $X(t)$ is between X and $X+dX$, and that $Y(t)$ is between Y and $Y+dY$ is $p(X,Y)dXdY$. If X and Y are independent, then the joint PDF is equal to the product of the individual PDFs, $p(X,Y) = p(X)p(Y)$. Expectation of an operand which contains both X and Y is done by integrating the product of the operand and the joint PDF over both variables. For independent random variables, the expected product is the product of the expectations; $E[XY] = E[X]E[Y]$.

If a *usual* functional form for the PDF is assumed, only a few moments of the distribution are needed to complete the specification. For example, if the process is the linear structural response to Gaussian forcing, the process will be Gaussian as well. The Gaussian distribution is completely defined by the first two statistical moments or, equivalently, by the mean and RMS. The Gaussian model is both simple to implement and often accurate so it is usually assumed until there is evidence that shows otherwise. *It is assumed that* $X(t)$ is Gaussian for the remainder of this chapter.

3.2.2 Dynamic Behavior

The dynamic, or time varying, nature of the loading is described by the correlation between the load at any two (or more) times through the autocorrelation function, $R(\tau)$. The autocorrelation of a stationary process depends only on the time lag, τ, and is defined by

$$R(\tau) = E[X(t)X(t+\tau)] \tag{3.4}$$

Notice that when $\tau = 0$, the autocorrelation is equal to the mean square, $E[X^2]$. When τ is very large, $X(t)$ and $X(t+\tau)$ are usually uncorrelated so the autocorrelation equals the squared mean; $R(\tau) = E[X(t)]E[X(t+\tau)] = E[X]^2$. A normalized correlation function, $\rho(\tau)$, which takes on a maximum value of unity at $\tau = 0$ and decays to zero for large time lags, can be defined as

$$\rho(\tau) = \frac{R(\tau) - m_X^2}{\sigma_X^2} \tag{3.5}$$

The integral of this normalized correlation function provides a measure of the duration of significant fluctuations in the random process called the *fluctuation scale,* θ_X [Winterstein and Cornell, 1985].

The PSD, $S(f)$, is defined as the Fourier transform of $R(\tau) - m_X^2$. Since the autocorrelation is a real valued function which is symmetric about $\tau = 0$, the PSD is also real and symmetric. To avoid negative frequencies, a *one-sided* PSD, $G(f)$, is often defined for positive frequencies only, with twice the magnitude of the *two-sided* PSD ($G(f) = 2S(f)$; $f \geq 0$). The integral of the PSD is equal to the variance of the process. In this way, the PSD shows the distribution of variance as a function of frequency in the same way that the PDF shows the distribution of probability (i.e., the variance between frequencies f and $f + df$ is equal to $G(f)df$).

Although it is mathematically expedient to define the PSD as the Fourier transform of the autocorrelation, it is more insightful to think of the PSD as the normalized, squared magnitude of the Fourier transform of the time history. PSDs are usually estimated from time series by just such a procedure. The PSD can thus be visualized as the variances of sine waves at different frequencies that when added together yield the original process.

Wide-band processes are composed of frequency components from a wide band of frequencies. Figure 3.1 shows a sample PSD and time series of a wide-band loading. Narrow-band processes have most of their variance concentrated

in a narrow band of frequencies, as shown in Figure 3.2.

Some useful measures of load bandwidth can be calculated as weighted averages of $G(f)$ [Winterstein and Cornell, 1985]. For example, the spectral moments,

$$\lambda_n = \int_0^\infty f^n G(f) df \tag{3.6}$$

can be combined to form the quantity

$$\alpha_n = \frac{\lambda_n}{\sqrt{\lambda_o \lambda_{2n}}} \tag{3.7}$$

Various measures follow from different choices of n. In general, α_n is a unitless quantity varying between zero (wide-band limit) and unity (narrow-band limit). For relatively narrow bandwidths, the α_n values become proportional: $\alpha_n \approx n\,\alpha_1 \approx n\,\alpha_2/2 \cdots$.

The closer a process is to being sinusoidal, the more *regular* the process is said to be. As Figures 3.1 and 3.2 show, the narrow-band process is more regular in that it is nearly sinusoidal with slowly changing amplitude while the wide band process is far from sinusoidal. The more peaks (local maxima) in a process between up-crossings of the mean, the more wide band the process. For a Gaussian process, the rate of peaks, f_p, and the rate of mean up-crossings, f_o, are related to the spectral moments [Rice, 1944; 1945]:

$$f_o = \left(\frac{\lambda_2}{\lambda_0}\right)^{1/2} \tag{3.8}$$

$$f_p = \left(\frac{\lambda_4}{\lambda_2}\right)^{1/2} \tag{3.9}$$

In fact, a regularity measure equal to the ratio of mean up-crossings to peaks is exactly α_2, which can also be expressed as

$$\alpha_2 = \frac{f_o}{f_p} = \frac{\lambda_2}{\sqrt{\lambda_o \lambda_4}} \tag{3.10}$$

For this reason, α_2 is sometimes called the *regularity* of the process.

Another way to visualize the regularity of the time history is to pass an envelope over the process through all the peaks, as shown in Figure 3.3. A wide band process has an envelope almost as irregular as the process itself while a narrow-band process has an envelope, $A(t)$, which varies slowly in time.

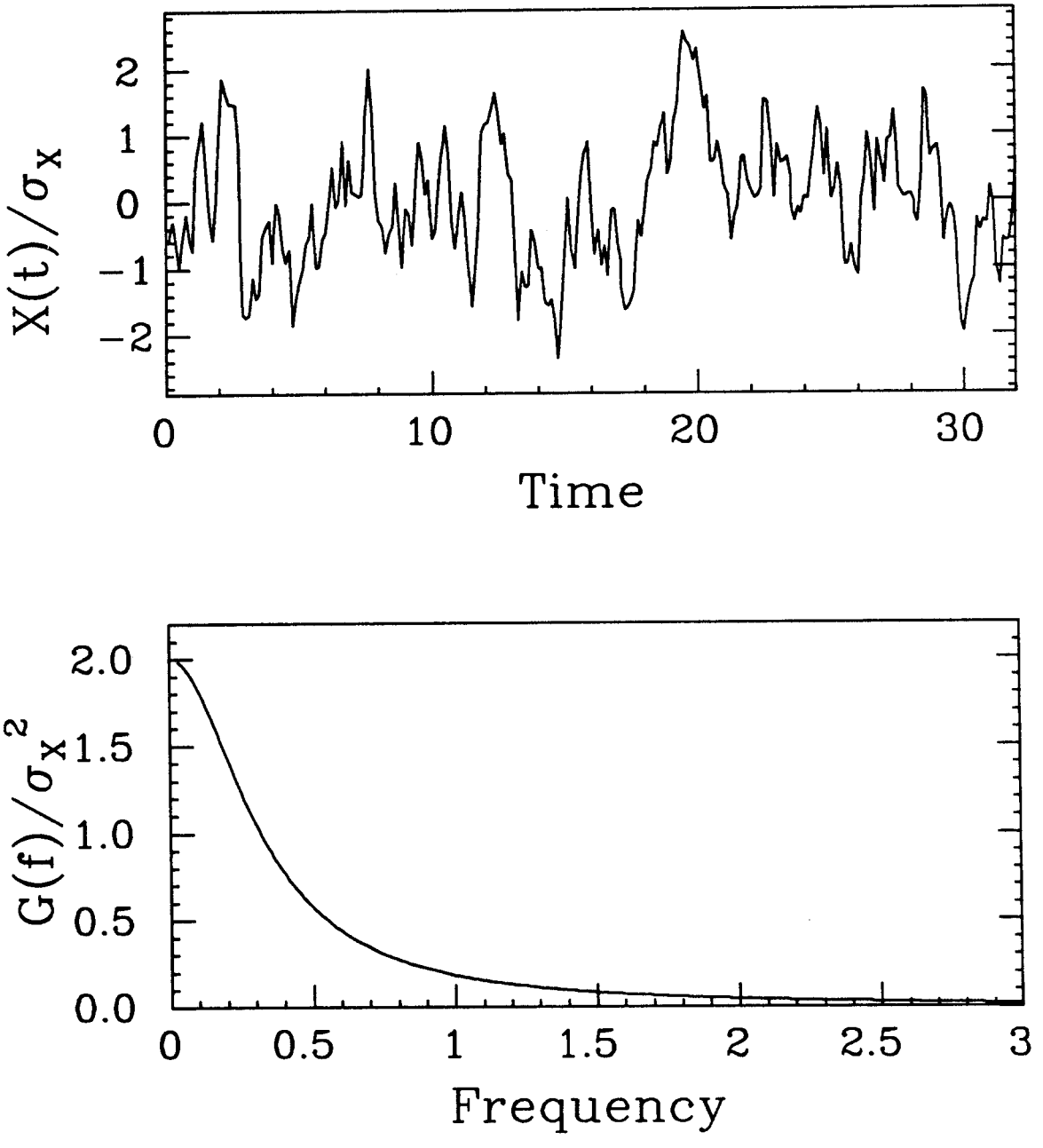

Fig. 3.1 Example of a time series (top) and a PSD (bottom) of a wide-band loading.

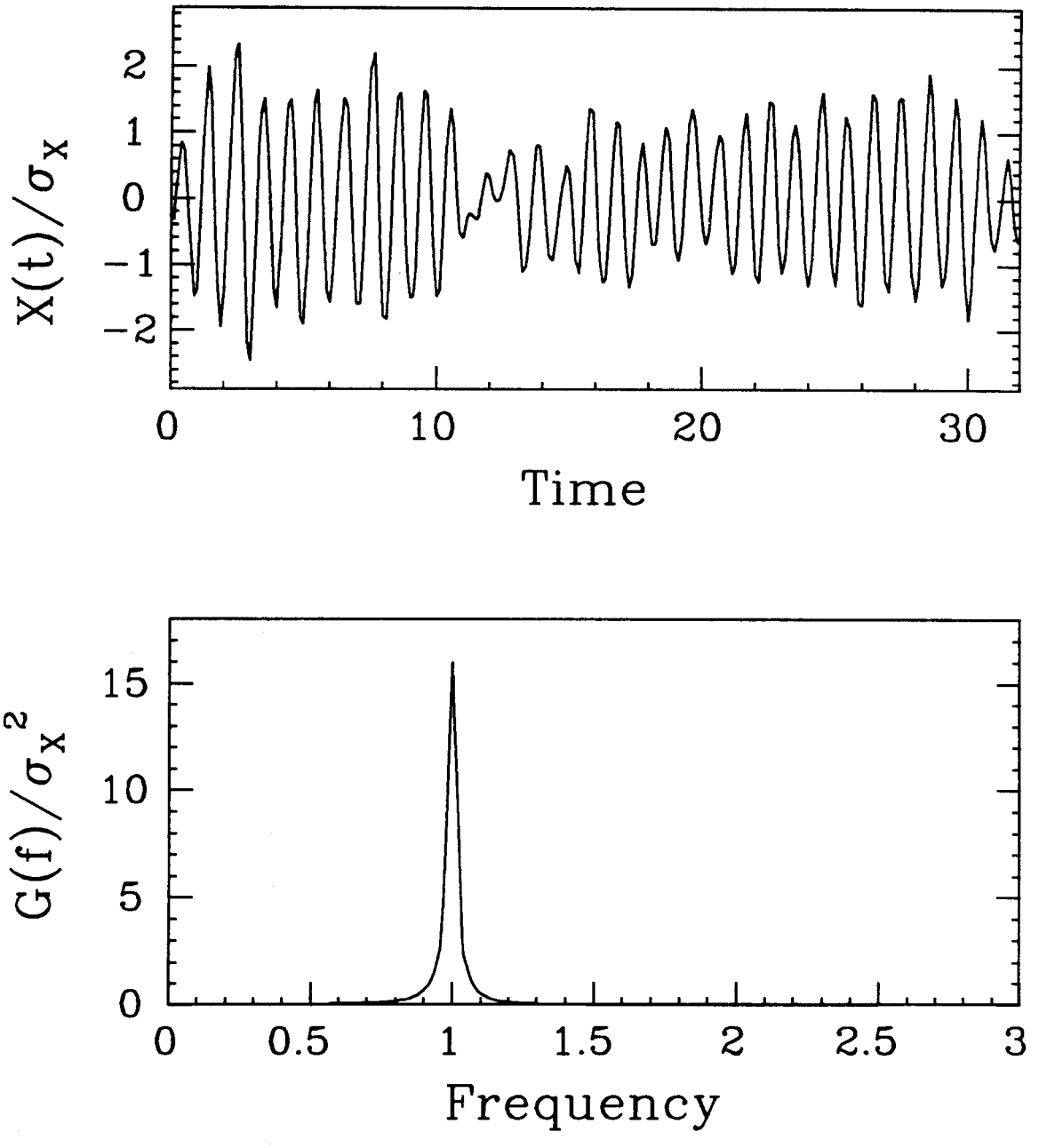

Fig. 3.2 Example of a time series (top) and a PSD (bottom) of a narrow-band loading.

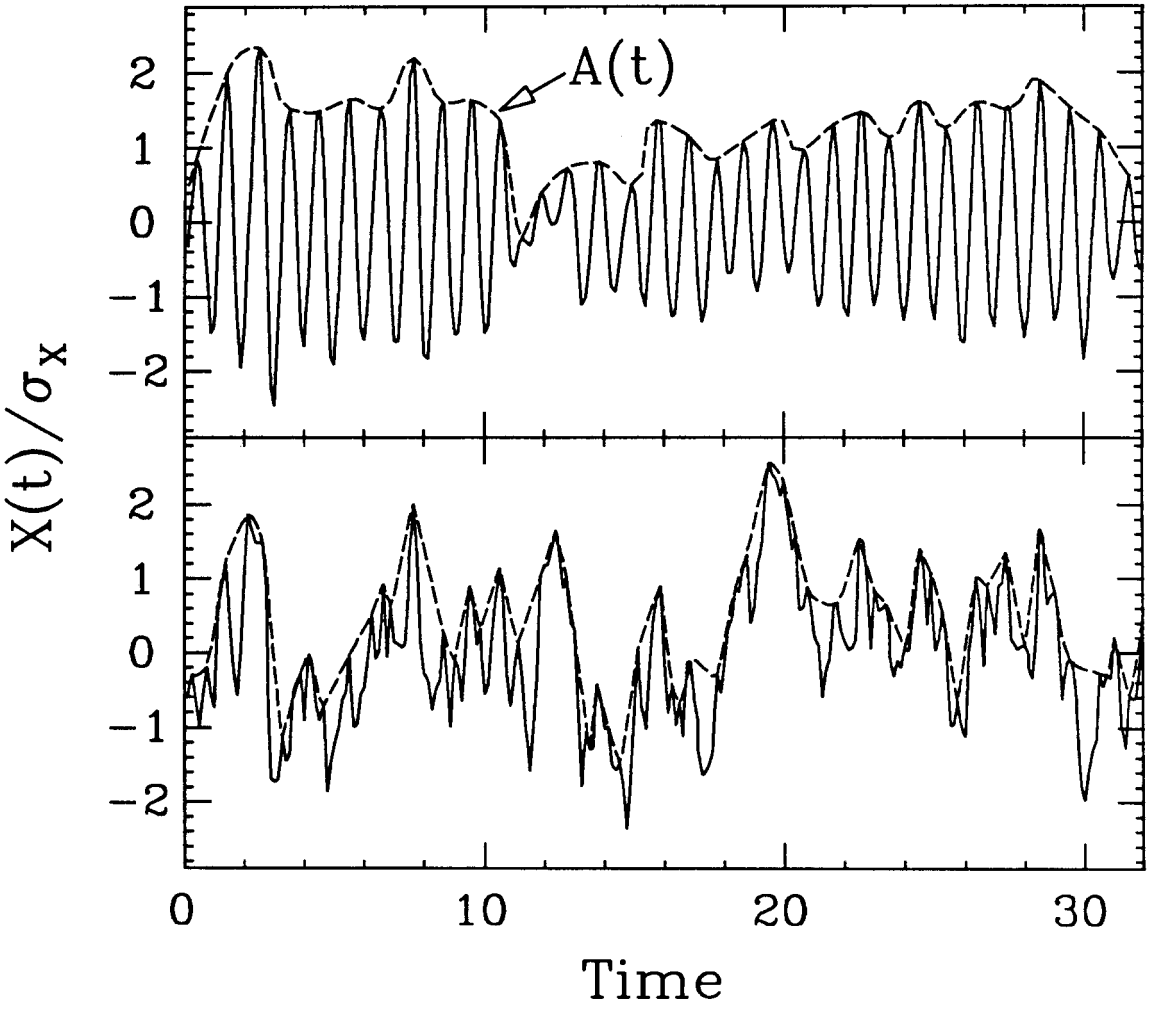

Fig. 3.3 Envelopes of narrow- and wide-band loadings.

Therefore, the wide band envelope is uncorrelated even for short time lags while the narrow-band envelope is highly correlated for several cycles. The bandwidth measure θ_E is the *fluctuation scale* of the squared envelope, $E(t)=A^2(t)$. Because the correlation function of this envelope, $\rho_E(\tau)$ is likewise the squared envelope of the original correlation function, $\rho(\tau)$, θ_E can be defined by any of the following relationships [Winterstein and Cornell, 1985]:

$$\theta_E = \int_{-\infty}^{\infty} \rho_E(\tau)d\tau = 2\int_{-\infty}^{\infty} \rho^2(\tau)d\tau = \frac{1}{\sigma_X^4}\int_0^{\infty} G^2(f)df \tag{3.11}$$

Physically, θ_E is the time duration over which the envelope (and therefore the peaks) has significant correlation. As bandwidth decreases, θ_E increases because the duration of envelope correlation is increasing (i.e., the envelope becomes smoother).

3.2.3 Distributions of Peaks and Ranges

The PDF of peaks, $p(P)$, of a Gaussian process can be written in terms of the bandwidth of the process through the regularity, α_2 [Rice, 1944; 1945]:

$$p(P) = \frac{\sqrt{1-\alpha_2^2}}{\sigma_X\sqrt{2\pi}} \exp\left[-\frac{1}{2}\left(\frac{P-m_X}{\sigma_X\sqrt{1-\alpha_2^2}}\right)^2\right] + \alpha_2\frac{P-m_X}{\sigma_X^2}\exp\left[-\frac{1}{2}\left(\frac{P-m_X}{\sigma_X}\right)^2\right]\Phi\left(\frac{\alpha_2(P-m_X)}{\sigma_X\sqrt{1-\alpha_2^2}}\right) \tag{3.13a}$$

and the CDF of peaks, $P(P)$ is

$$P(P) = \Phi\left(\frac{P-m_X}{\sigma_X\sqrt{(1-\alpha_2^2)}}\right) - \alpha_2\exp\left[-\frac{1}{2}\left(\frac{P-m_X}{\sigma_X}\right)^2\right]\Phi\left(\frac{\alpha_2(P-m_X)}{\sigma_X\sqrt{(1-\alpha_2^2)}}\right) \tag{3.13b}$$

where $\Phi(\cdot)$ is the standard Gaussian CDF.

It is more illuminating to view the peak of each cycle by an equivalent representation, as the sum of two independent random variables; a Gaussian mean value, X_0, and a Rayleigh distributed amplitude, A [Madsen, 1982]. The PDFs are

$$p(X_o) = \frac{1}{\sigma_X \sqrt{2\pi(1-\alpha_2^2)}} \exp\left[-\frac{1}{2}\left(\frac{X_o - m_X}{\sigma_X\sqrt{1-\alpha_2^2}}\right)^2\right] \tag{3.14}$$

$$p(A) = \frac{A}{(\alpha_2\sigma_X)^2} \exp\left[-\frac{1}{2}\left(\frac{A}{\alpha_2\sigma_X}\right)^2\right] \qquad A \geq 0 \tag{3.15}$$

In the narrow-band limit, α_2 approaches unity, the mean of each cycle, X_o, becomes fixed at the mean level, m_X, and the PDF of peaks becomes Rayleigh. The ranges of a narrow-band process are approximately equal to twice the peak value and are therefore Rayleigh distributed as well. Even when the loading is wide band, the ranges, R, between adjacent peaks and valleys (local ranges) are approximately Rayleigh distributed [Winterstein, 1984], as is suggested by Eq. 3.15, with σ_X replaced by $2\sigma_X$:

$$p(R) = \frac{R}{(2\alpha_2\sigma_X)^2} \exp\left[-\frac{1}{2}\left(\frac{R}{2\alpha_2\sigma_X}\right)^2\right] \qquad R \geq 0 \tag{3.16}$$

There are other more complicated models of range distributions, which depend on more than one bandwidth measure and are therefore less tractable [Yang, 1974]. The Rayleigh distribution of ranges gives an exact first moment and is conservative with respect to rainflow-counted ranges for higher moments (using Eq. 3.16 with $\alpha_2 = 1$ and the rate of cycles equal to f_o) [Wirsching and Light, 1980; Madsen, 1982].

The distributions in Eqs. 3.13-3.16 are not always directly applicable to fatigue analysis. Because they reflect all of the peaks, valleys, and ranges between adjacent peaks and valleys, the numerous small amplitude excursions in a random loading can obscure the more important, slower cycles, especially in wide-band loadings. If these overall cycles are neglected, fatigue damage can be significantly underestimated [Socie and Kurath, 1983]. Rainflow counting is a method of accounting for both the small excursions and overall cycles. Unfortunately, there is no known method for predicting the distribution of rainflow-counted ranges in a random loading. In addition, rainflow counting does not preserve the sequence of the load peaks. Racetrack filtering provides a solution by removing small amplitude ranges from the time series without disturbing the sequence, mean, or range of the significant load excursions. In this way, the distribution of racetrack-filtered ranges, which can be estimated, becomes an approximation for that of rainflow-counted ranges.

3.3 Racetrack Filtering

3.3.1 Definition of Racetrack Filtering

Racetrack filtering [Fuchs, et.al., 1977; Nelson and Fuchs, 1977] was created to condense load histories, for analysis or testing, without unduly sacrificing fatigue-damaging characteristics. The method works as follows. Suppose that a segment of loading, as shown by the lower set of peaks and valleys in Fig. 3.4, is converted into a *racetrack* by offsetting its profile by a selected *track width* or threshold level, R_{th}. A race car driver, taking the shortest line through this course would follow the dashed line in Figure 3.4. Peaks and valleys on the original segment of loading, corresponding to locations where turns are made involving a change in direction from northerly to southerly, or vice versa, are identified by letters. For the value of R_{th} used in Fig. 3.4, a condensed segment of loading is created by a line from valley A to peak B to valley C to peak D to valley E. Smaller load fluctuations are *filtered* out. Peaks and valleys that were separated by smaller ranges in the original loading become adjacent, creating larger local ranges such as the one from D to E. Because it preserves the sequence of important loads, racetrack filtering can be followed by an analysis that either includes sequence effects or not.

The most extreme points in the random loading are always retained after racetrack filtering. If a very small threshold had been selected, all the peaks shown in the figure could have been retained. If a larger threshold had been selected, points C and D would also have been filtered leaving only A, B, and E. If only adjacent peaks and valleys (local ranges) are used, the larger filtering level would have identified a larger range from B to E while eliminating the three smaller ranges from B to C, from C to D, and from D to E. The tradeoff is between small thresholds that save all the ranges and miss the overall ranges, or large thresholds that capture the large ranges at the expense of the small to medium size ranges. Some guidelines are provided in Section 3.3.3 for selecting the appropriate threshold.

3.3.2 The Effects of Racetrack Filtering

Racetrack filtering reduces the number of load peaks and makes the load more *regular* (i.e., more nearly narrow-band). This reduction in f_p and increase in α_2 is estimated below for Gaussian loadings, as functions of load bandwidth and R_{th}, from simulation results. Significantly, Eqs. 3.13-3.16, with these

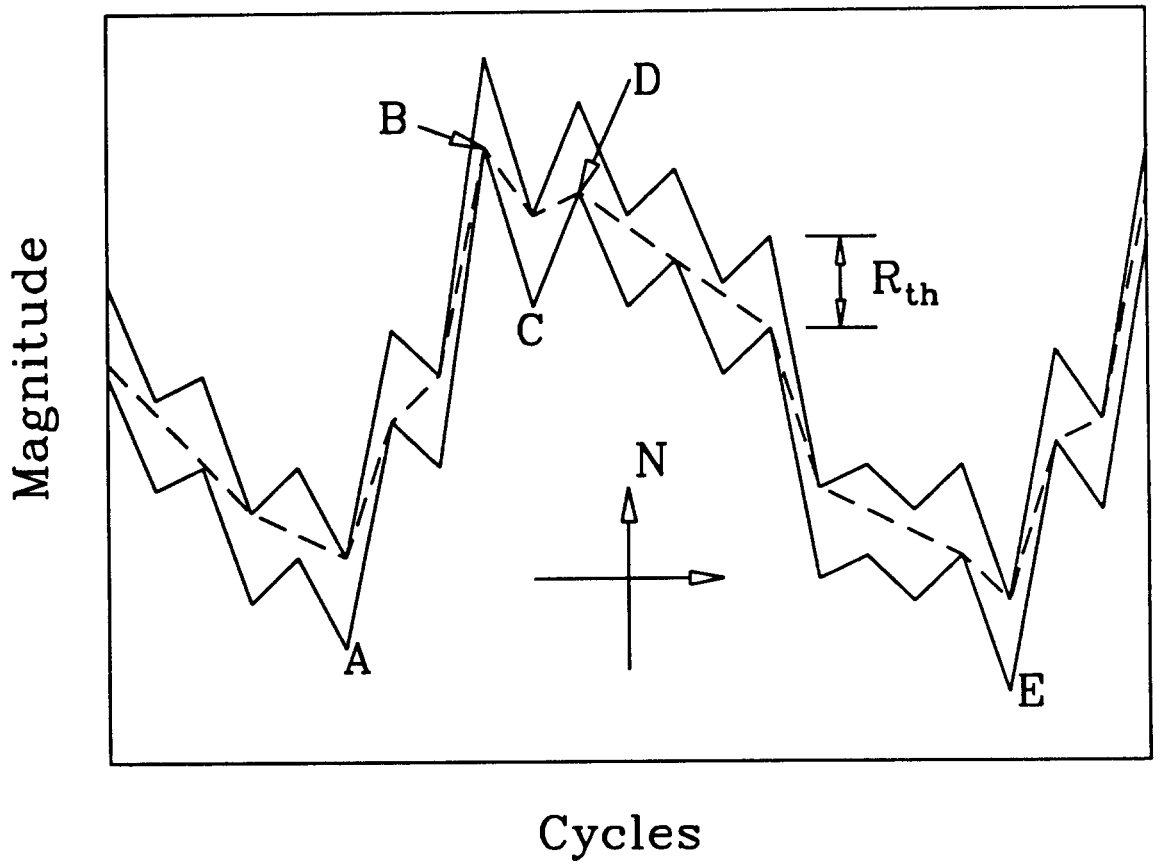

Fig. 3.4 Schematic of racetrack filtering a segment of wide-band loading.

adjusted parameters, are found to still give useful models of the post-filtered stress cycles. (It may be argued that because racetrack filtering is similar to the linear operation of time-averaging, the post-filtered process may be nearly Gaussian and Eqs. 3.13-3.16 still appropriate.)

As an example of the effect of racetrack filtering on the statistics of peaks and ranges, the ASTM data sets are examined. Each of those data sets was filtered at a threshold level of 0.1 times the design limit stress (DLS). The exact filtering algorithm is unknown, but the result is very similar to racetrack filtering [Chang, 1981]. In terms of the RMS level, this results in thresholds of $0.61\sigma_X$ for the AA loading, $0.67\sigma_X$ for the AG loading, and $1.33\sigma_X$ for the IN loading.

The statistics of the pre-filtered loadings are calculated using the published PSDs [Dill and Saff, 1977] in Eq. 3.7. The regularities, α_2's, are 0.54, 0.60, and 0.59 for the AA, AG, and IN loadings, respectively. The tabulated data sets (which are filtered at the above levels) have $\hat{\alpha}_2$'s of 0.80, 0.86, and 0.95, respectively. (All post-filtered statistics are designated by the "$\hat{}$" symbol.) Clearly, racetrack filtering makes the loading more regular (i.e., more narrow band). The higher the threshold with respect to the RMS of the loading, the more regular the filtered loading will be. This is especially important because the more regular the loading, the less important the effect of the cycle counting method on the fatigue analysis. A perfectly narrow-band process will produce the same result whether rainflow-counted ranges or local ranges are used. Therefore, the more narrow band the loading, the more useful statistics of local ranges become.

The CDFs of peaks are plotted in Figure 3.5a for the tabulated data together with theoretical results from Eq. 3.13b using regularities that are both pre-filtered (α_2) and post-filtered ($\hat{\alpha}_2$). Notice that the observed distributions are well represented by the theoretical results when $\hat{\alpha}_2$ is used.

Figure 3.5b shows the filtered range distributions with the Rayleigh approximations, again using both α_2 and $\hat{\alpha}_2$. The theoretical distribution is a truncated Rayleigh; all ranges below the threshold level, R_{th}, are eliminated. The truncated Rayleigh CDF is given by

$$P(R) = \begin{cases} 0 & R < R_{th} \\ 1 - \exp\left[-\dfrac{R^2 - R_{th}^2}{2(2\hat{\alpha}_2\sigma_X)^2} \right] & R \geq R_{th} \end{cases} \tag{3.18}$$

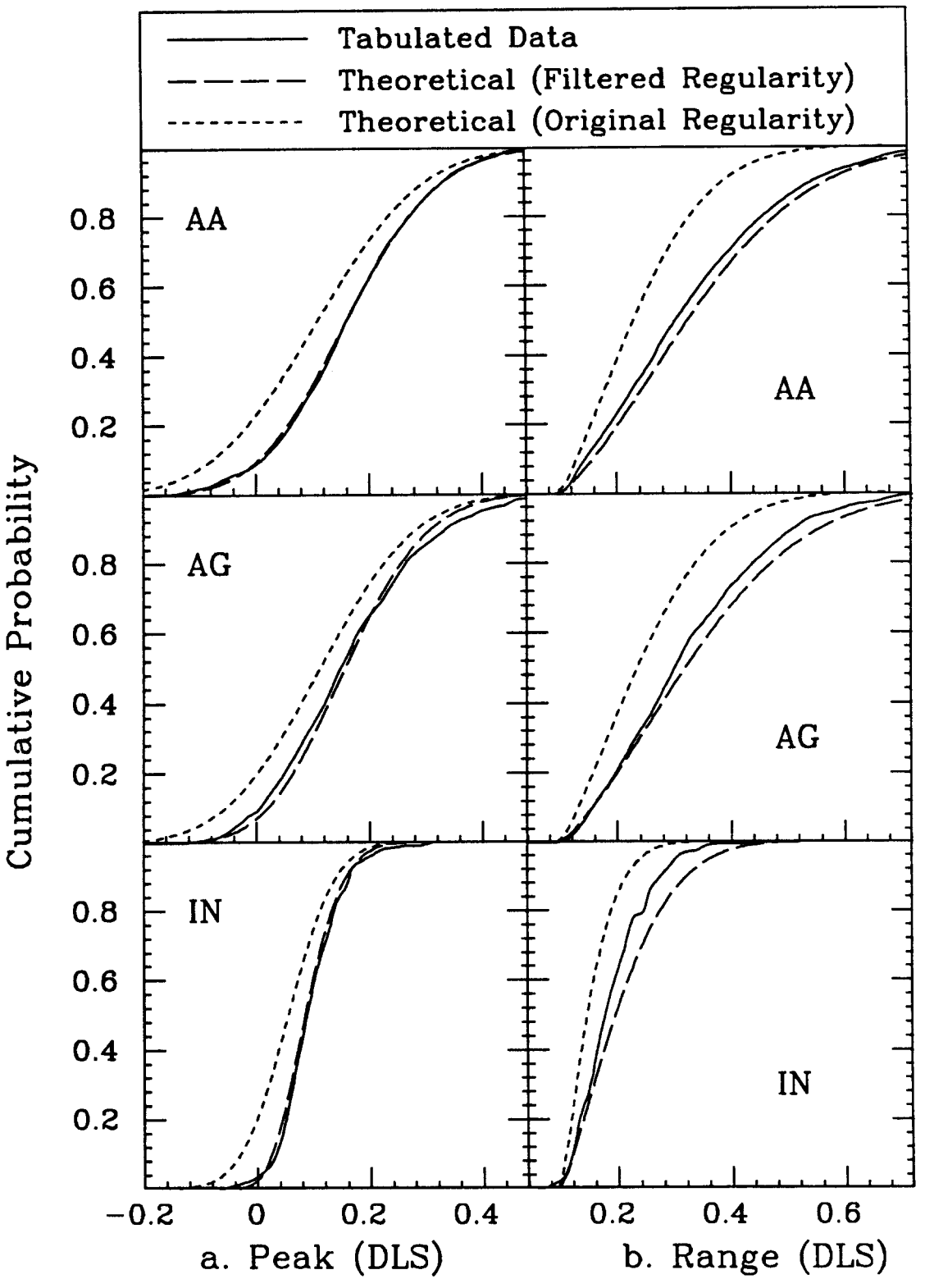

Fig. 3.5 Comparison of CDFs of the tabulated ASTM loadings to the theoretical results for (a) peaks and (b) ranges using the pre-filtered regularity (α_2) and post-filtered regularity ($\hat{\alpha}_2$).

A good approximation to the post-filtered range distribution is also obtained using $\hat{\alpha}_2$. The approximation becomes conservative as the filtering level increases. This is more readily demonstrated by filtering the AA history at successively higher thresholds, as shown in Figure 3.6 for filtering levels of 1.0, 1.5, and 2.0 times the RMS.

Obtaining a satisfactory fit to the distributions of both peaks and ranges depends on $\hat{\alpha}_2$, and not the original α_2. The regularity, in turn, depends on the threshold level, R_{th}. Finally, R_{th} must be selected to balance the loss of small ranges with concatenation of larger ranges so that the damaging potential of the process is best preserved. The effects of racetrack filtering on loadings with various spectral bandwidths are examined in the next section with the aid of simulations.

3.3.3 Simulations of Racetrack Filtering

To investigate the effects of racetrack filtering, simulations of loadings with a wide variety of spectral shapes are racetrack filtered at several threshold levels. The necessary statistics of the loading before and after filtering are calculated so that empirical estimates of these statistics, based on threshold level and bandwidth, can be generated.

The spectral shapes are obtained by varying the sizes and shapes of the two boxes that form the PSD illustrated in Figure 3.7. The PSD is defined by six parameters: low frequency variance V_l, high frequency variance V_h (these variances are the areas of the boxes), f_l and f_h (the center frequencies of the boxes), $2L$ and $2H$ (the width of each box). After fixing both total variance and mean frequency, there are four dimensionless quantities that can be selected to achieve a variety of spectral shapes: V_h/V_l, f_h/f_l, L/f_l, and H/f_h. Table 3.1 gives the values of these parameters used in the simulations. The spectral densities are summed wherever the boxes overlap. These variations result in almost 400 different spectral shapes (there are a few redundant shapes when $f_h/f_l = 1$). Each simulation was filtered at eight different thresholds in increments of $0.25\sigma_X$. Each spectral shape was simulated ten times to obtain an estimate of the spread in the calculated statistics, which indicated that the variability from one simulation to another is negligible compared to the variability from one spectral shape to another.

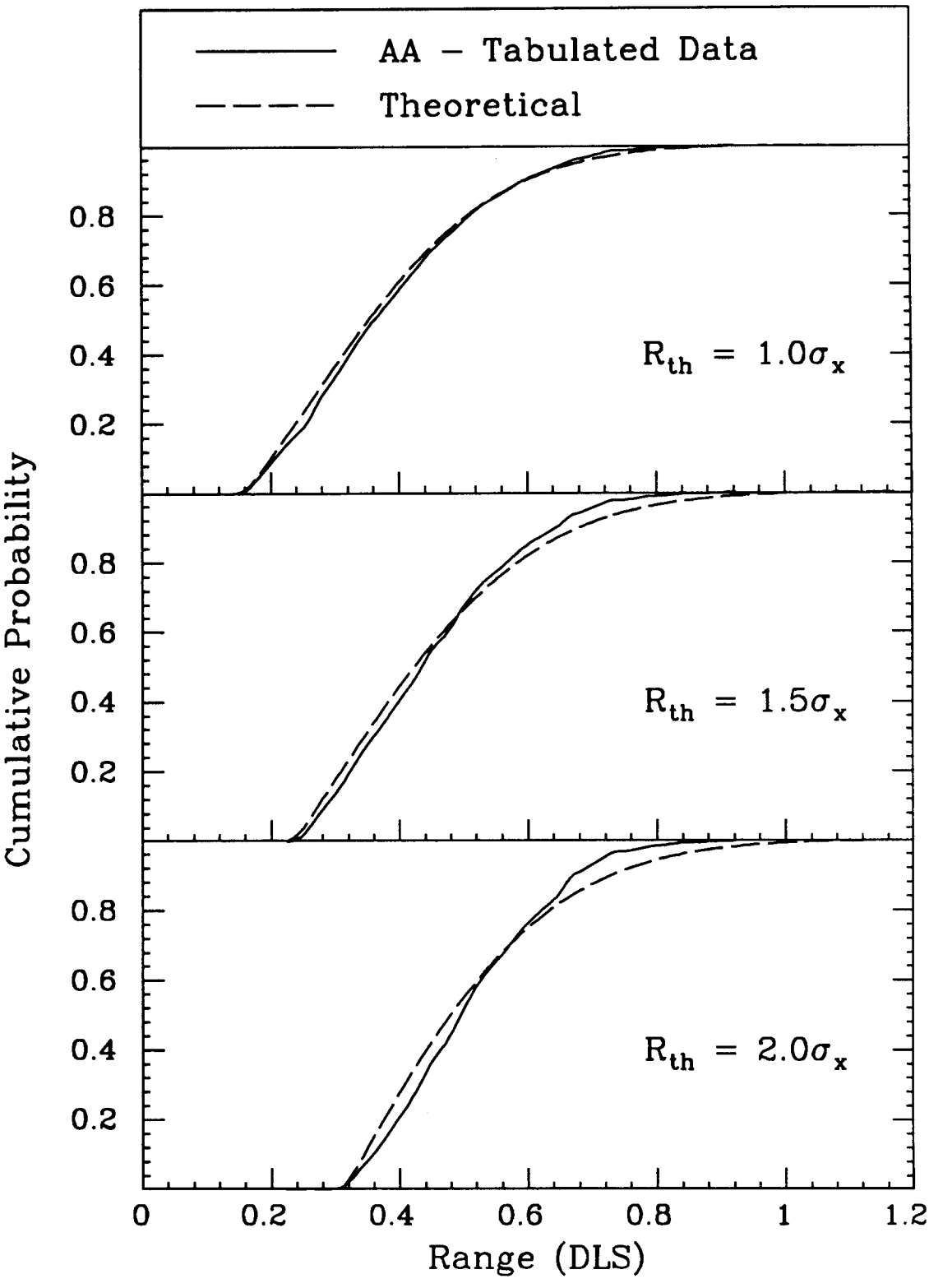

Fig. 3.6 Comparison of CDFs of the AA load history ranges to the theoretical predictions at three racetrack filtering thresholds.

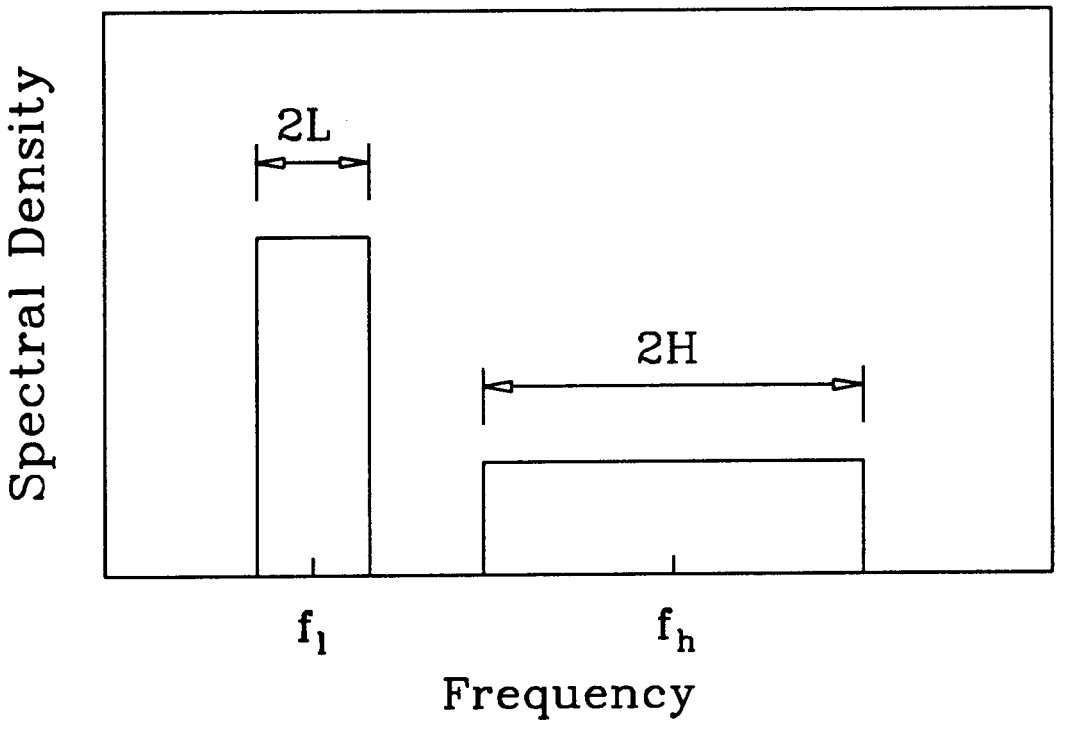

Fig. 3.7 Spectral shape parameters used in the simulations with racetrack filtering.

Table 3.1
Values of the dimensionless parameters used to define the spectral shapes for the simulations with racetrack filtering.

V_h/V_l	f_h/f_l	L/f_l	H/f_h
0.25	1.0	0.25	0.25
0.5	2.0	0.5	0.5
1.0	3.0	0.75	0.75
2.0	4.0	1.0	1.0
4.0	5.0	. . .	. . .

The central purpose of the simulation study is to estimate $\hat{\alpha}_2$ and $\hat{f}_p$ based on the statistics of the pre-filtered process. The original α_2 can be calculated from the PSD by Eq. 3.10. Figure 3.8 is a plot of $\hat{\alpha}_2$ vs the original α_2 when $R_{th} = \sigma_X$. The scatter in this plot is a reflection of the way that racetrack filtering removes all high frequency content that does not produce oscillations larger that R_{th}. When α_2 is estimated from the PSD, it is based on the second and fourth moments of the PSD (Eq. 3.10). The fourth moment is very sensitive to high frequencies that produce many peaks with small local ranges, which are subsequently filtered. The net result is a poor correlation between initial and filtered α_2's.

The regularity measure, α_1, is based on the first and second spectral moments and is therefore less sensitive to high frequencies than α_2. The fit between pre- and post-filtered parameters is also enhanced by defining *irregularity* factors, z_1 and z_2, which are zero for perfectly narrow band loadings and increase as bandwidth increases. In general terms, z_n is related to α_n, and therefore the spectral moments, by

$$z_n = \frac{\sqrt{1-\alpha_n^2}}{\alpha_n} = \left(\frac{\lambda_{2n}\lambda_0}{\lambda_n^2} - 1\right)^{1/2} \tag{3.19}$$

For narrow-band processes, z_2 is approximately the conventional spectral bandwidth measure $\epsilon = \sqrt{1-\alpha_2^2}$, and z_1 is roughly equal to $\delta = \sqrt{1-\lambda_1^2/\lambda_0\lambda_2}$, the lower-order bandwidth parameter of Vanmarke [1970]. Unlike these conventional parameters, z_1 and z_2 can increase beyond unity as the bandwidth grows.

The filtered regularity, $\hat{\alpha}_2$, is obtained from $\hat{z}_2$ by inverting Eq. 3.19.

$$\hat{\alpha}_2 = \frac{1}{\sqrt{\hat{z}_2^2 + 1}} \tag{3.20}$$

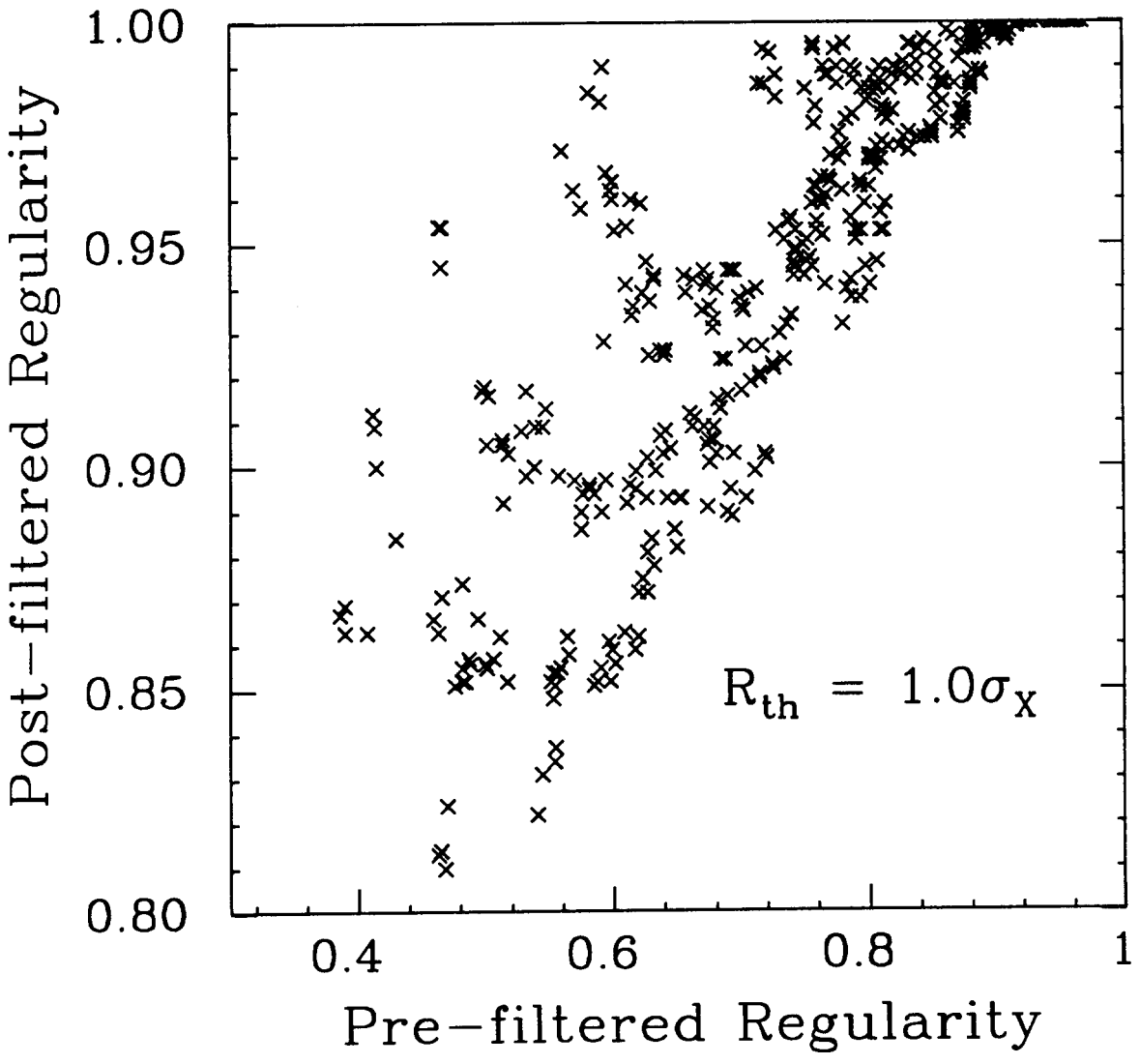

Fig. 3.8 Pre-filtered regulatity (α_2) vs. post-filtered regularity ($\hat{\alpha}_2$) for a racetrack-filtering level of σ_X.

The irregularity of the filtered time series, $\hat{z}_2$, is plotted against the original z_1 (calculated from the PSD) in Figure 3.9 for three filtering threshold levels. By eliminating the sensitivity to high frequencies in the PSD, a much better fit to the filtered irregularity is obtained. Also shown is a linear fit between z_1 and $\hat{z}_2$ given by

$$\hat{z}_2 = M(R_{th})z_1 + B(R_{th}) \tag{3.21}$$

The slope, $M(R_{th})$, and intercept, $B(R_{th})$, depend on R_{th} in a way that is approximated by the following functions;

$$M(R_{th}) = 1.7 - 0.8\frac{R_{th}}{\sigma_X} \tag{3.22a}$$

$$B(R_{th}) = 0.18\left(\frac{R_{th}}{\sigma_X}\right)^2 - 0.36\frac{R_{th}}{\sigma_X} \tag{3.22b}$$

There is low correlation when $R_{th} \geq 1.5\sigma_X$, but when the threshold is that high, all of the filtered processes are essentially narrow band ($\hat{z}_2<0.4$, $\hat{\alpha}_2>0.93$) regardless of the original regularity.

Another factor that determines the fatigue damaging potential of a loading is the rate at which ranges occur, which is equal to the rate of peaks, f_p. The post-filtered rate is significantly reduced, to $\hat{f}_p$, by filtering. Fig. 3.10 shows the average reduction in the rate of peaks, $\hat{f}_p/f_p$, as a function of R_{th} for initially narrow-band ($z_1<0.2$), moderately wide-band ($z_1\approx 0.5$), and very wide-band ($z_1>0.9$). Plus and minus one standard deviation error bars are shown on the simulation results. Also included are the approximations for $\hat{f}_p/f_p$ as functions of z_1 and R_{th}, which are given by

$$\frac{\hat{f}_p}{f_p} = \exp\left[-\frac{1}{2}\left(\frac{R_{th}}{2\sigma_X}\right)^2\right] - \frac{3z_1^2}{5z_1+1}\left(1 - \exp\left[-\frac{3R_{th}}{\sigma_X}\right]\right) \tag{3.23}$$

In summary, starting with a PSD of a random loading, the distributions of local ranges and range means after racetrack filtering can be estimated using the above relationships. The regularity, $\hat{\alpha}_2$, which is a necessary statistic of the distributions, depends on R_{th}, as does the rate of ranges, $\hat{f}_p$. Therefore, it is important to select the appropriate threshold for the filtering in order to produce the distribution and frequency of local peaks and ranges that best approximates the damaging potential of the loading. If R_{th} is too small, small ranges can split up larger overall ranges and too little damage might be predicted. If R_{th} is too

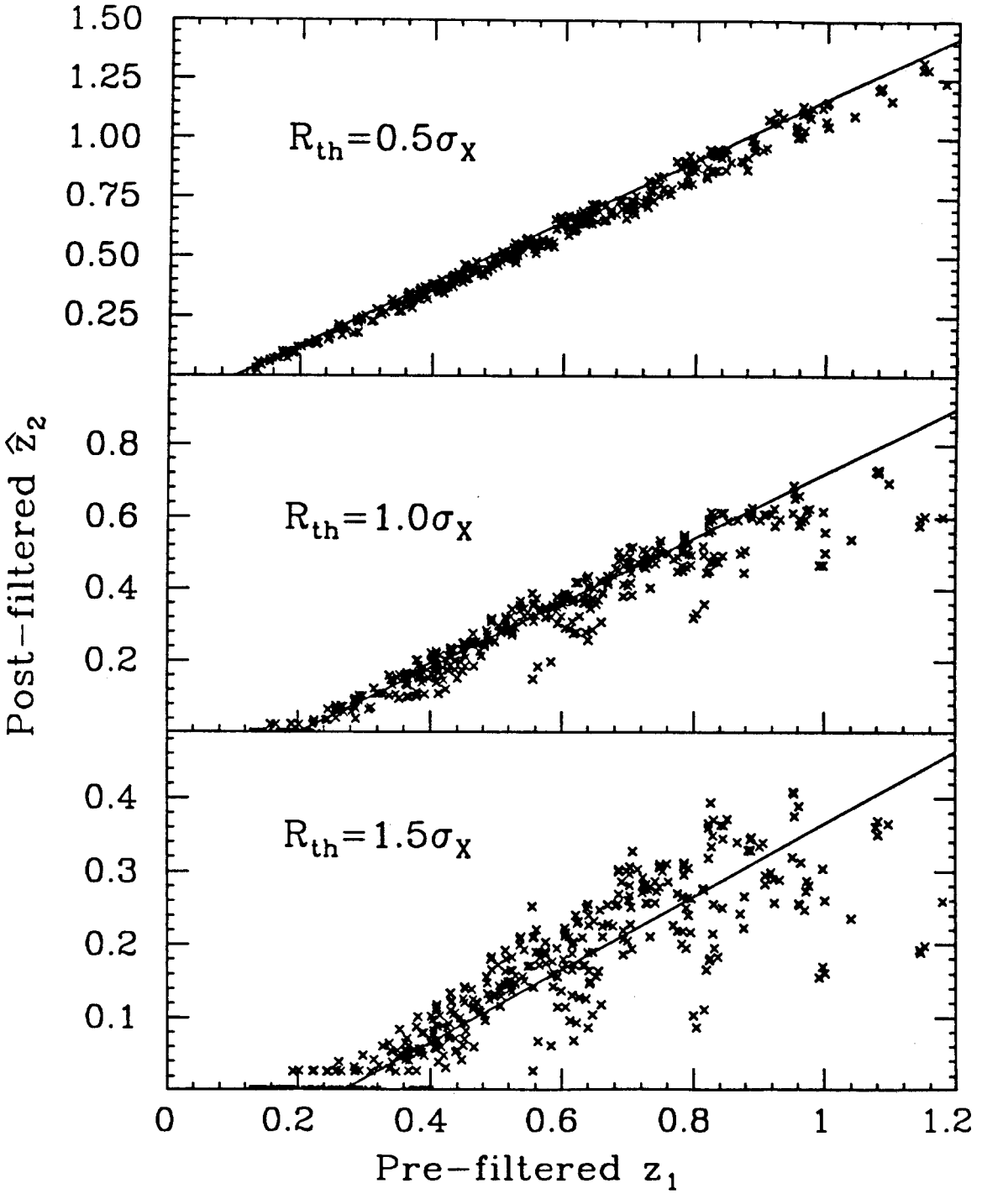

Fig. 3.9 Irregularity measures before (z_1) and after ($\hat{z}_2$) racetrack filtering at three threshold levels.

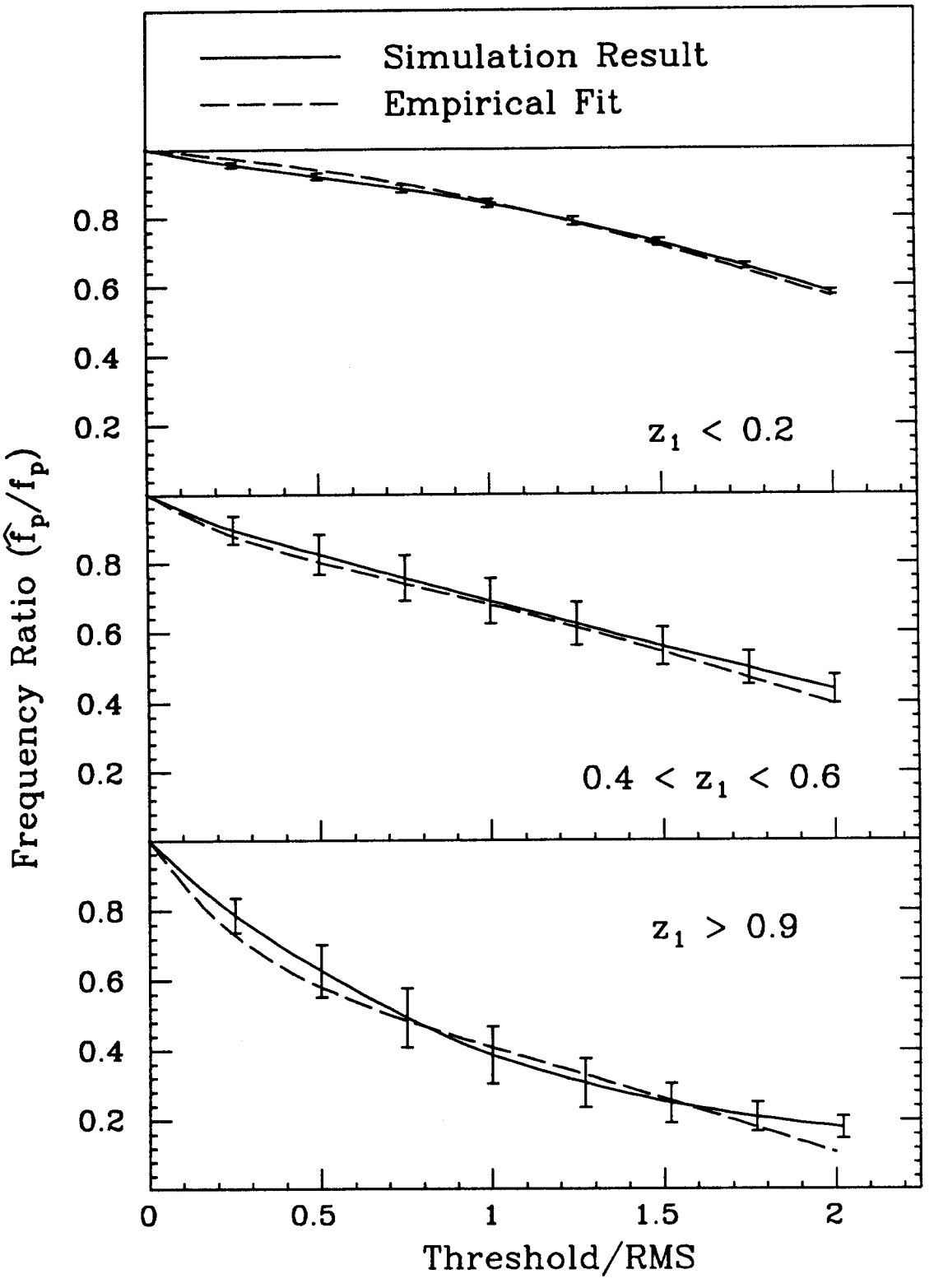

Fig. 3.10 Reduction in frequency of peaks as a function of racetrack filtering threshold.

large, many significant ranges will be removed and damage can again be under-predicted.

To illustrate the effects of racetrack filtering on *damage*, a damage measure, D, is defined as

$$D = \sum_{i=1}^{N} R_i^b \tag{3.24}$$

This is equivalent to a Palmgren-Miner damage summation neglecting mean stress effects. A normalization factor, D_{norm}, is the average damage that would be calculated from a narrow-band process ($\alpha_2 = 1$) with the same RMS and mean up-crossing frequency. D_{norm} is the sum of the Rayleigh distributed ranges raised to the b^{th} power. In this case, in N cycles one expects $N \cdot p(R)dR$ ranges between R and $R+dR$ so that, for large values of N, the damage is well approximated by

$$D_{norm} = \sum_{i=1}^{N} R_i^b \approx \int_0^{\infty} R^b [N \cdot p(R)dR] = T f_o (2\sqrt{2}\sigma_X)^b (b/2)! \tag{3.25}$$

for a load duration of T and number of cycles, $N = T f_o$. If $b/2$ is not an integer, $(b/2)!$ can be evaluated through the widely tabulated Gamma function [Abramowitz and Stegun, 1964]. D_{norm} is the theoretical maximum damage from a Gaussian random vibration loading [Powell, 1958].

Plots of damage, D/D_{norm}, from the simulations are shown in Fig. 3.11 for b equal to 2, 4, and 8. Plus and minus one standard deviation error bars are included on the simulation results. Damage estimates derived from the theoretical distribution of filtered ranges in Eq. 3.18 with the adjustments to α_2 and f_p given by Eqs. 3.20-3.23 are shown in Fig. 3.12. Both damage estimates depend on load bandwidth and racetrack threshold level as shown in the figures. The difference between the simulation results and the empirically adjusted analytical estimates is mostly due to the conservatism in assuming that the range distribution is the truncated Rayleigh. Also, the empirical estimates of the post-filtered statistics begin to deteriorate as R_{th} approaches twice the RMS.

In the narrow-band case, there is virtually no change in damage with R_{th} because filtering the already regular loading only removes small amplitude ranges; it does not concatenate small ranges into larger ones. In fact, damage decreases when $b = 2$, because the low exponent makes small ranges relatively more important. In the wide band case, as R_{th} is increased from zero, there is

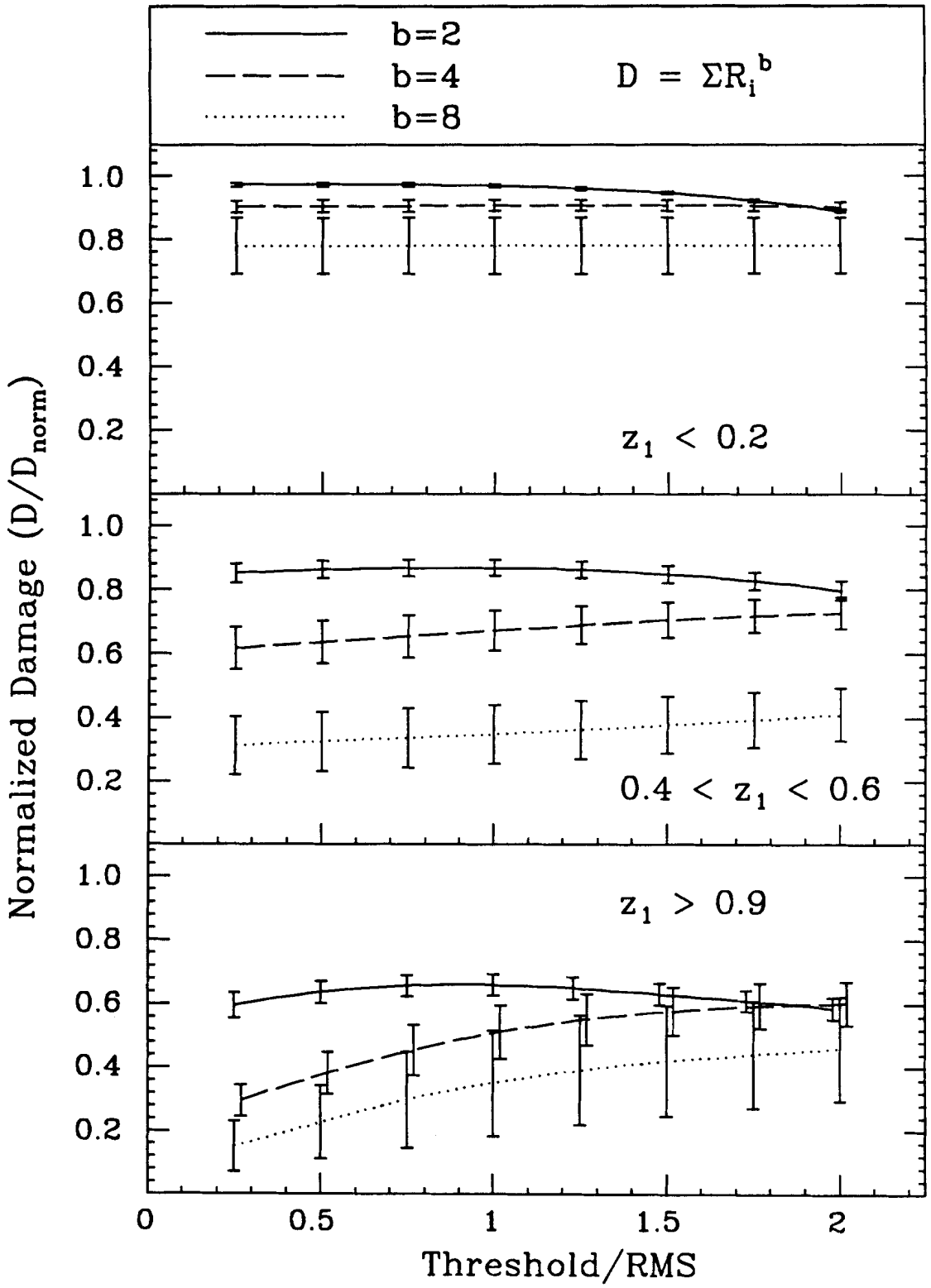

Fig. 3.11 Normalized damage due to local ranges from simulations.

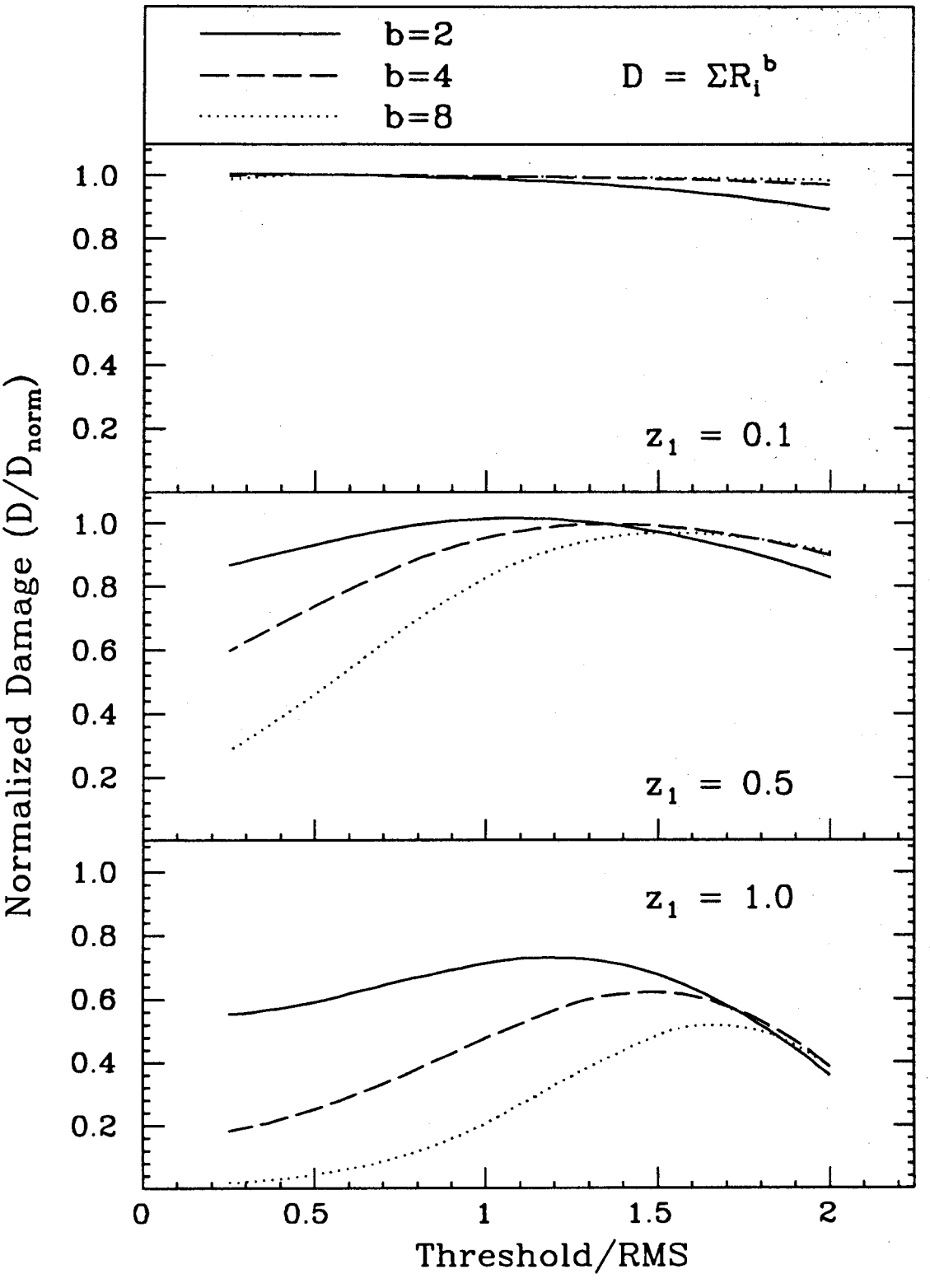

Fig. 3.12 Normalized damage due to local ranges from adjusted theoretical distributions.

more concatenation of local ranges resulting in increased damage, in spite of the fact that the total number of ranges is greatly decreased.

The theoretical estimates of this damage measure are conservative with respect to local ranges over most combinations of bandwidth and threshold. It should be observed that the damage measure plotted in Figs. 3.11-3.12 is a measure of the accuracy of the range distribution. The curves in Figs. 3.11-3.12 are based on full ranges while fatigue crack growth is often based on tensile ranges or peaks, which generally fit the theoretical distributions better than full ranges (see Fig. 3.5).

It is also important to know how damage calculated using local ranges compares to damage calculated from rainflow-counted ranges. The simulated loadings were used to estimate damage in two ways: first, by rainflow counting the ranges and, second, by using the local ranges after racetrack filtering at several threshold levels between 0 and $2\sigma_X$. Fig. 3.13 shows the ratio of estimated damage based on local ranges to damage based on rainflow-counted ranges. For narrow-band loadings ($z_1 < 0.2$) there is little difference, even for large b. Again, for wider-band loadings, the joining of smaller amplitude ranges, accomplished by filtering the intervening sub-threshold size ranges, results in a better match between local and rainflow-counted ranges. When b is small (≤ 4) as in fatigue crack growth applications, local ranges can account for over 80% of the damage that rainflow counting identifies if the appropriate racetrack-filtering threshold is used. When $b \geq 8$, as in high cycle crack initiation, the thresholds investigated here will only produce local ranges about half as damaging as rainflow-counted ranges when the loading is wide-band.

To get the most conservative analytical estimate of damage or crack growth from a wide-band loading, the adjustments to the loading statistics should be calculated using $R_{th} \approx 1.0\sigma_X$ when $b = 2$ and $R_{th} \approx 1.5\sigma_X$ when $b = 4$. These analytical estimates should be used with caution for wide-band loadings when $b > 4$ both because errors in the distributions are magnified and because local ranges can underestimate damage by a factor of about two (which may still be acceptable in view of other uncertainties in estimating life).

3.4 FFT Simulations of Random Loading

In the previous section, limited information on the random process (λ_1 and λ_2) was used to produce random variable models of load peaks and ranges for use in crack growth analysis where sequence effects may be neglected. In this

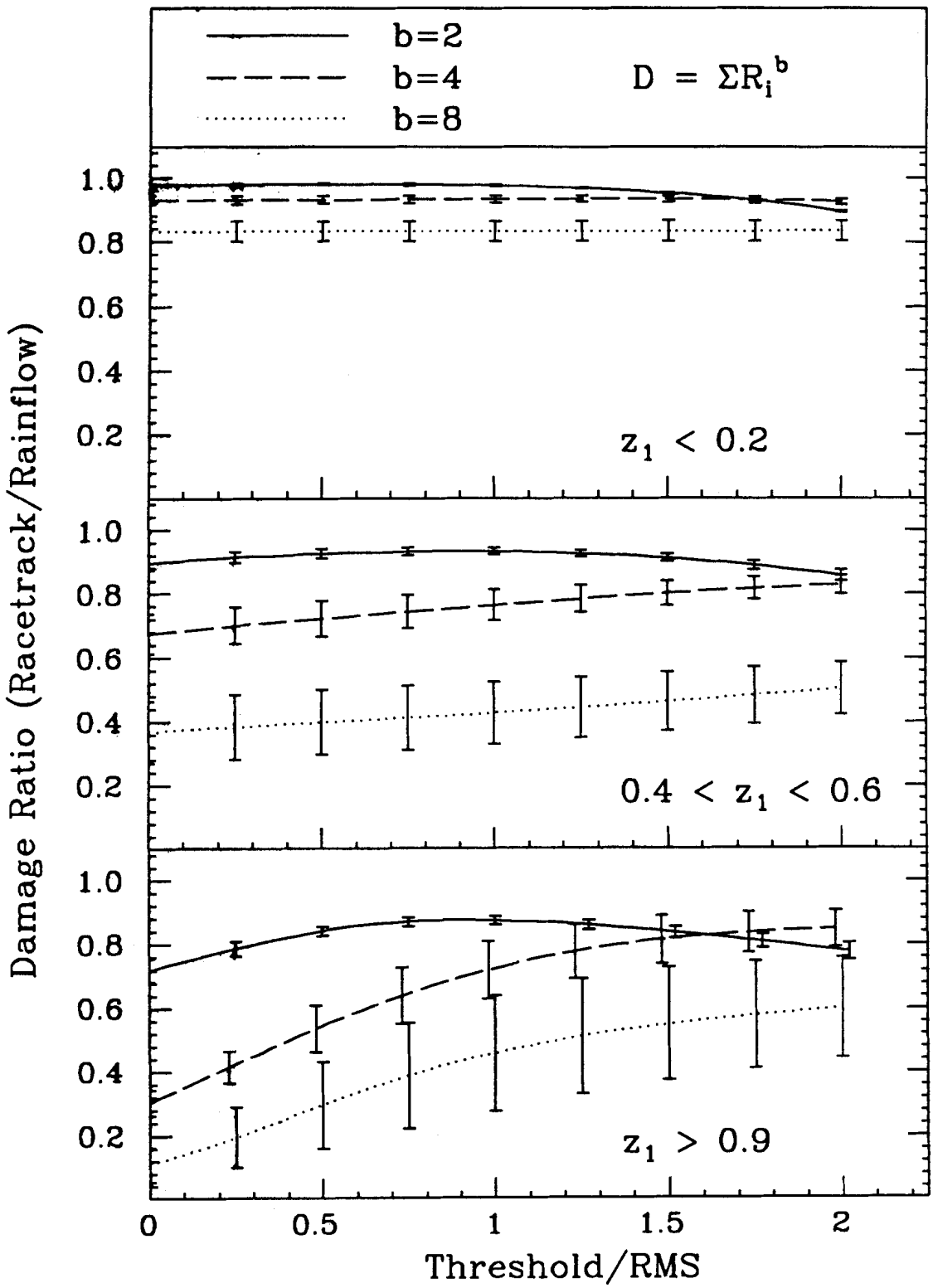

Fig. 3.13 Simulation results for the ratio of damage due to local ranges to damage due to rainflow counted ranges.

and the next section, methods of simulating random loadings are described for the situation in which sequence effects are important and crack growth must be calculated cycle-by-cycle.

3.4.1 Generating a Time Series from a PSD

The PSD defines the distribution of variance in a random process as a function of frequency. A time domain realization of the random process can be generated by discretizing the PSD into frequency bands and summing sine waves at frequencies corresponding the center frequency of each band. The random nature of the process is preserved by making the relative phase of each sine wave an independent, uniformly distributed, random variable on the interval from zero to 2π. The resulting time domain realization will approach a Gaussian process as the number of frequency components becomes large [Shinozuka and Jan, 1972].

In practice, actual sine waves are rarely added together to simulate a time series. The fast Fourier transform (FFT) does the same calculations much more efficiently provided the frequency spacing is constant from zero to the maximum frequency. (The fastest algorithms also require the number of frequency components to be an integer power of 2.) The Fourier series representation, $\tilde{X}(f_j)$, is found by equating the variance in each frequency band with the variance of a single complex component of the Fourier series and splitting it into real and imaginary parts with a random phase angle.

$$\tilde{X}(f_j) = \sqrt{(G(f_j)\,\Delta f)/2}\,\left(\cos(\phi_j) + i\,\sin(\phi_j)\right) \tag{3.26}$$

where Δf is the frequency spacing, ϕ_j is the j^{th} random phase, and i is the square root of -1. To produce a real time series, negative frequency components in the Fourier series must be defined to be the complex conjugates of the positive frequency components.

The time series is generated by inverse Fourier transforming the above Fourier series. This time series will have exactly the same variance and frequency content as the original PSD. Each new set of random phase angles will produce a unique realization of the process. The maximum and minimum values of each sample will themselves be random variables just as they would be if the samples were taken from measured data.

One of the difficulties with using FFT's to generate time series for use in fatigue analysis is the stringent resolution requirement caused by the need to raise ranges to a power that is usually greater than 2 (Eq. 3.24). Since the FFT

creates a time series that is composed of samples of the process at discrete times, it always underestimates the magnitudes of peaks and ranges. For example, if damage is defined as $\sum R_i^b$, where R is a rainflow-counted range, many points per cycle must be simulated to accurately simulate the damage. Figure 3.14 shows how the estimated damage from a narrow band random time series increases with the number of points per cycle for three values of b. This error is reduced by fitting a parabola to the three points nearest each peak and extrapolating to the true peak value. Figure 3.14 also shows that about sixteen points per cycle are required to accurately estimate the damage from FFT generated time series, even with a parabolic extrapolation. This need for high resolution requires that the PSD be prescribed out to frequencies eight times the natural frequency of a narrow-band loading to simulate sixteen points per cycle.

An accurate representation of the PSD shape requires that the Fourier series be defined with a small Δf. The net result is that a very large data array is required to accurately capture both the shape of the PSD and the peaks of the time series. It can be much more efficient to simulate the peaks and ranges of the process directly, as outlined in section 3.5.

Another difficulty with FFT simulations is that each FFT generates a separate block of data. If a very long continuous realization of the process is desired, several blocks of data may need to be joined. The mismatch between adjacent blocks can be eliminated by tapering and overlaying a small portion of each block [McNerney and Veers, 1984].

3.4.2 ASTM Simulated Time Series

The ASTM test series [Chang and Hudson, eds., 1981] was based on loading blocks which were generated with the FFT technique. The estimated shapes of the PSDs for the three types of loading (AA, AG, and IN) are shown in Figure 2.5. The PSDs were estimated from figures in the reference; exact definitions are not available. Samples of the tabulated sequences of peaks and valleys are shown in Figure 2.6. Since these loadings will be used as example cases for future simulations, these loadings have been resimulated with the FFT method as a check on the accuracy of the estimated PSDs. For purposes of comparison, it is useful to work with the Gaussian process which is obtained directly from the inverse FFT of the PSDs.

The ASTM load histories contain modifications to the FFT-generated time series, which either provide better simulations of several observed phenomena or

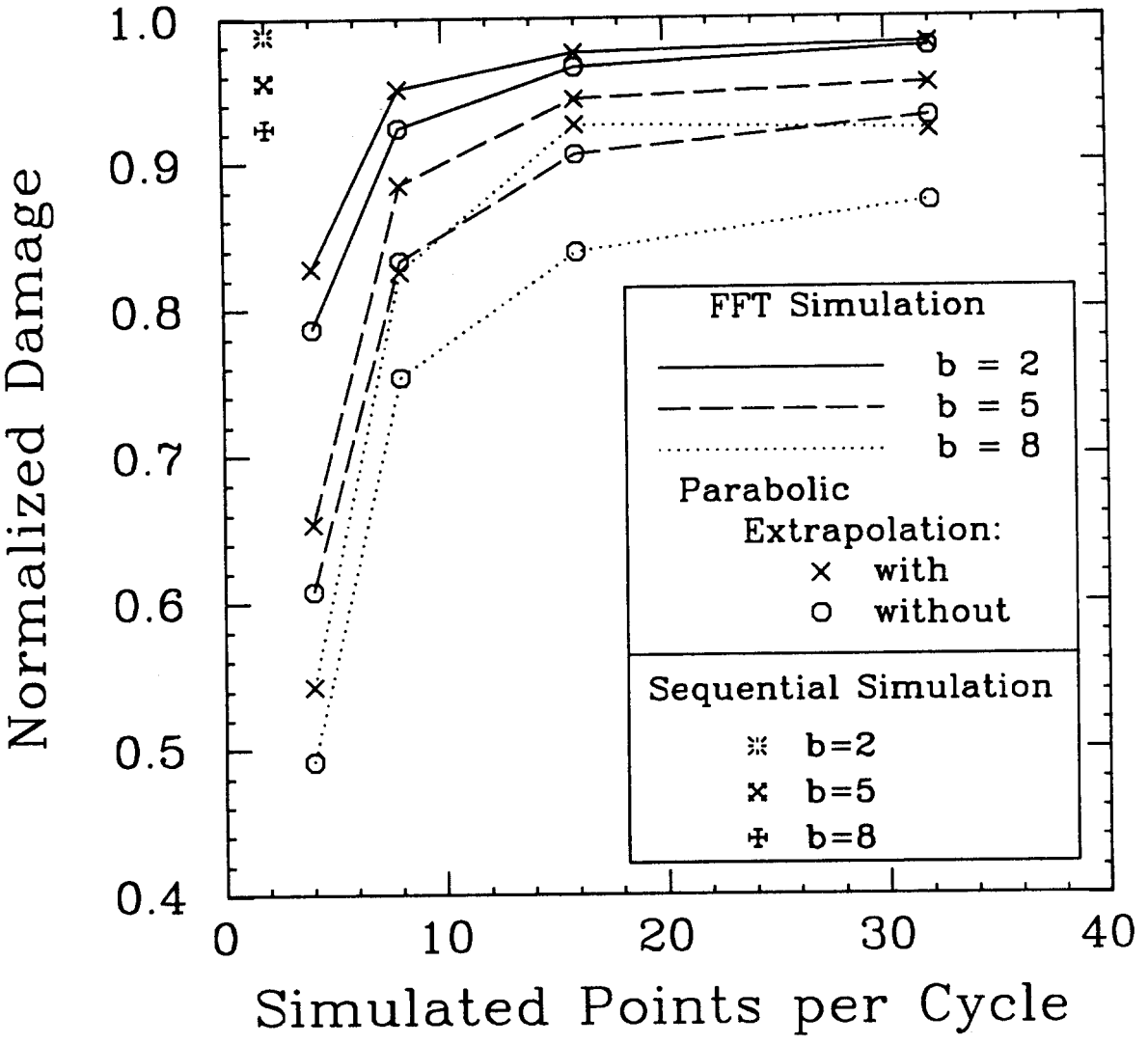

Fig. 3.14 Normalized damage calculated from FFT (with and without parabolic extrapolation for the peaks) and Sequential simulation methods as a function of the number of simulated points per cycle of narrow-band loading. (The sequential method simulates only two points per cycle, peak and valley.)

make testing easier. The small amplitude ranges (below 10% of design limit stress, DLS) were filtered from the time series to reduce the number of peaks and valleys necessary to define each load block. The peaks and valleys were also skewed to match a non-Gaussian frequency of exceedance diagram. The skewing was accomplished by raising the absolute value of each peak and valley (in units of DLS) to the power of 1.128 [Dill and Saff, 1977]. The other modification was the introduction of *ground loads* at regular intervals after all other alterations were completed.*

Another addition to the ASTM tabulated loads was a single peak of 0.7DLS included as the first peak in each load history. This peak is not the highest in the AA or AG loadings, but it is by far the highest peak in the IN loading. The major significance of this peak lies in its effect on crack growth life as observed in Chapter 2.

The first step backward to the FFT generated time series is to remove the ground cycles. The remaining peaks and valleys were then un-skewed to return the tabulated peaks and valleys to the original Gaussian state. The mean and standard deviation were then estimated. These estimates apply to the Gaussian process that results from using the FFT simulation technique. Table 3.2 lists the mean, RMS, and a few other parameters (discussed in the next section) for the three load types.

The distributions of peaks and ranges in the unskewed tabulated data (with ground loads extracted) are compared with FFT simulation results in Figure 3.15. Differences between the tabulated data and the FFT simulations are due to inaccuracies in the estimates of PSD shape and magnitude (RMS) and must be tempered by the knowledge that the tabulated results are a single sample of the loading.

* Saff, C.R., private correspondence, 1986.

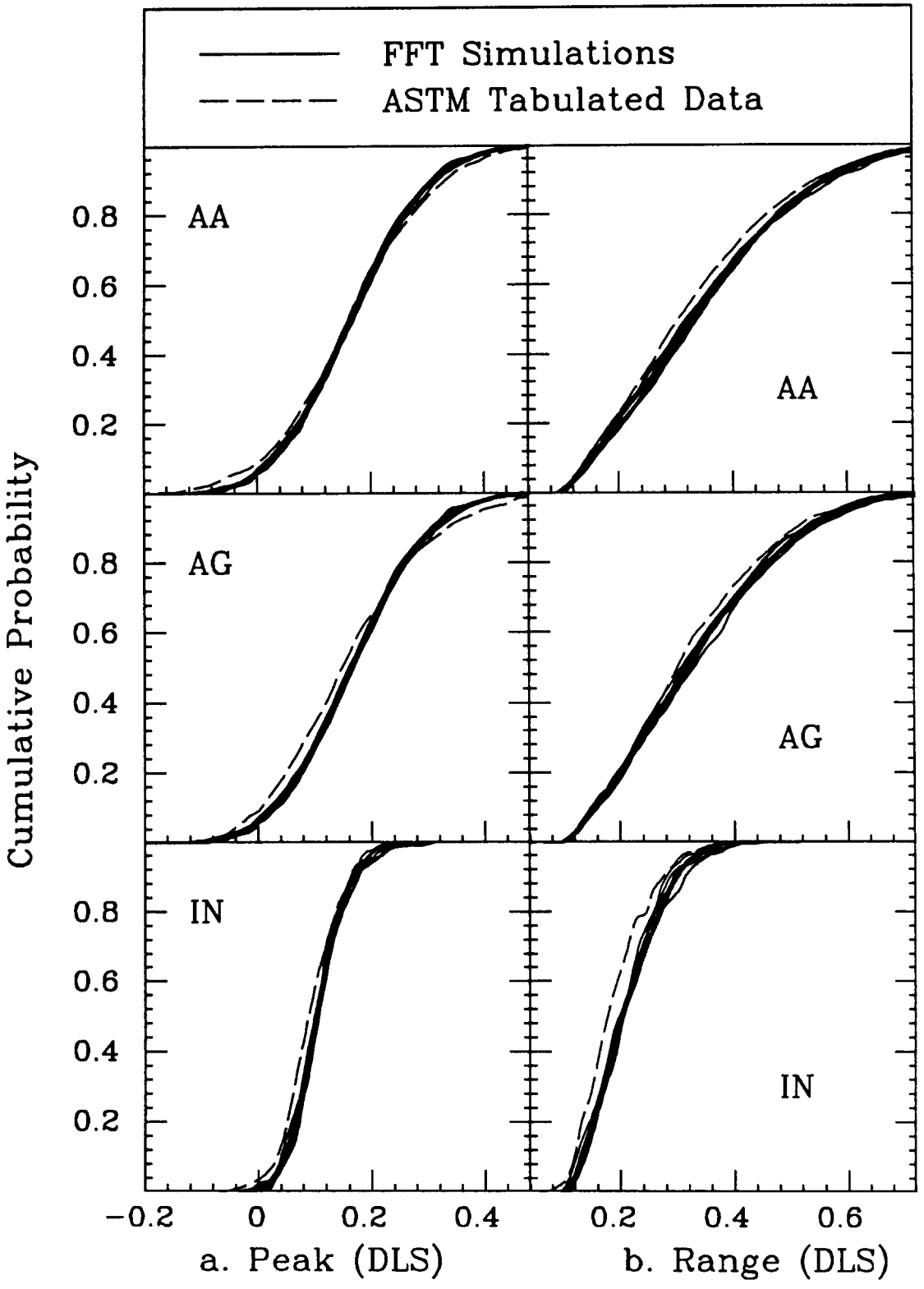

Fig. 3.15 Comparison of CDFs of the tabulated ASTM loadings with CDFs of the FFT simulations for (a) peaks and (b) ranges.

Table 3.2
Parameters of the ASTM loadings and statistics for sequential simulations.

Load Type	m_X (DLS)	σ_X (DLS)	σ_S (DLS)	σ_F (DLS)	f_n (hz)	θ_X (sec)	θ_E (sec)
AA	.3733	.163	.0904	.1356	.0196	76.5	29.3
AG	.2712	.150	.0774	.1285	.0246	51.5	20.6
IN	.2615	.075	.0391	.0640	.0230	63.3	22.2

3.5 Sequential Simulation of Random Loading

To predict fatigue crack initiation or growth, only the correlated set of load peaks and troughs needs to be accurately simulated. To adopt conventional FFT simulation techniques for these purposes, the load must first be simulated with high resolution and then searched to find the significant peaks and ranges. A more efficient *sequential* simulation method, which simulates the sequence of load peaks and troughs directly (two points per cycle) is outlined here [Winterstein, 1984]. This method simulates the sequential random variables which make up successive load peaks and valleys, which means that the significant peaks and ranges (identified by racetrack filtering) can be generated directly.

A correlated sequence of Gaussian random variables with one step memory (each element in the sequence depends only on the one previous element), called a Gauss-Markov process, is the basic building block of this method. The wide-band process in Figure 3.1 is very similar to a Gauss-Markov process.

A Gauss-Markov process can be generated from uncorrelated unit-variance Gaussian random variables, ξ_n, by

$$U_{n+1} = U_n\, e^{-2\Delta t/\theta_X} + \xi_n\, \sigma_X \left(1 - e^{-4\Delta t/\theta_X}\right)^{1/2} \tag{3.27}$$

in which Δt is the time step between simulated values and θ_X is the length of time over which the process is significantly correlated (the fluctuation scale). θ_X can be calculated from either the spectral density, $G(f)$, or the correlation function, $\rho(\tau)$, of the Gauss-Markov process [Vanmarke, 1979]:

$$\theta_X = \frac{G(0)}{2\sigma_X^2} = \int_{-\infty}^{\infty} \rho(\tau)\, d\tau \tag{3.28}$$

Several Gauss-Markov processes, each simulated as in Eq. 3.27, can be combined to directly simulate peaks and troughs of both narrow- and wide-band loads.

3.5.1 Narrow-Band Sequential Simulation

The peaks of a narrow-band random loading can be defined in terms of the envelope of the process, $A(t)$, as shown in Figure 3.16a. The envelope can be thought of as the square root of the *energy,* $E(t)= A^2(t)$, in the loading. The form of the energy changes from potential (large displacement) to kinetic (large velocity) in each cycle while the total energy varies slowly in time (see Fig. 3.3).

Values of the envelope can be generated from two Gauss-Markov sequences, U_n and V_n, through the relation

$$A_n = (U_n^2 + V_n^2)^{1/2} \tag{3.29}$$

The underlying values of U_n^2 and V_n^2 are somewhat analogous to the potential and kinetic components of the energy, and A_n^2 to the total energy. If the load standard deviation is σ_X, consistent levels of amplitude correlation are ensured by generating U_n and V_n from Eq. 3.27 with $\theta_X= 2\theta_E$, in which θ_E, the *energy fluctuation scale,* is the correlation time of the energy envelope, $E(t)$, as defined in Eq. 3.11. For a lightly damped single degree of freedom oscillator with natural frequency f_n, and damping coefficient, ς, θ_E can be approximated by

$$\theta_E \approx \frac{1}{2\pi f_n \varsigma} \tag{3.30}$$

Taking Δt as half the period of load cycles, successive amplitude values from Eq. 3.29 can be alternately added and subtracted from the mean, m_X, to simulate peaks and valleys of a narrow band loading. Significantly, this sequential simulation technique leads to accurate damage estimates, which the FFT method approaches only asymptotically as the number of points increases (Fig. 3.14). The sequential approach, which needs to simulate only two points per cycle, has been found to require less than one fifth of the computation time of the FFT method when sixteen points per cycle are generated.

3.5.2 Wide-Band Sequential Simulation

Wide-band loadings can be simulated in a similar sequential fashion. The key is to split the wide-band process into a slowly varying Gaussian part, $X_0(t)$, which gives the mean of each cycle, and a quickly varying narrow-band part, with envelope $A(t)$, to produce the wide-band envelope shown in Fig 3.16b.

Three Gauss-Markov sequences are now required to simulate the peaks and troughs: one to simulate $X_0(t)$ and two, as in Eq. 3.29, to simulate $A(t)$. The

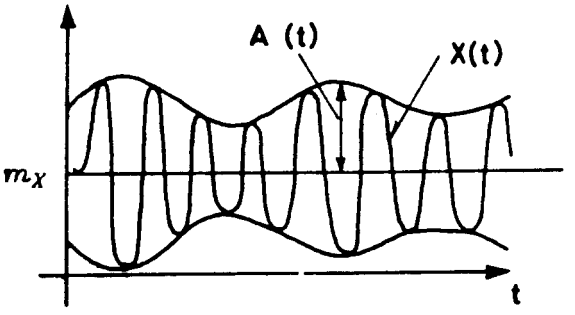

(a)

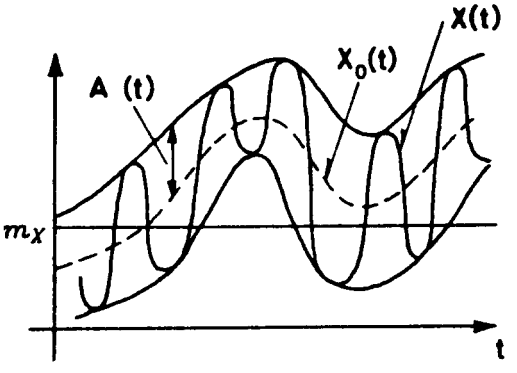

(b)

Fig. 3.16 Schematic of (a) narrow-band and (b) wide-band loadings showing the range amplitude, A, and mean, X_0 (from Madsen, 1982).

A's are again added and subtracted from the cycle mean, X_0, at intervals of half the cycle period to obtain peaks and troughs. Because the mean process varies slowly, it is sufficient to simulate X_0 values only once per cycle, taking Δt as the total cycle period in Eq. 3.27.

There are two additional considerations in wide-band sequential simulation: (1) The total variance, σ_X^2, must be split between slow variance, σ_S^2, and fast variance, σ_F^2 (where $\sigma_X^2 = \sigma_S^2 + \sigma_F^2$). σ_X should be replaced, in Eq. 3.27, with σ_S when simulating X_0, and with σ_F when simulating both U_n and V_n values that comprise the amplitude, A. In view of Eqs. 3.14-3.15, the simulated peaks and valleys will have the correct probability distributions if we take $\sigma_F = \alpha_2 \sigma_X$ and $\sigma_S = \sqrt{1-\alpha_2^2}\,\sigma_X$. (2) Although θ_X is inherently related to the low frequency (slow) part of the PSD through $G(0)$ in Eq. 3.28, θ_E should reflect the correlation in only the high frequency (fast) part of the PSD, rather than the entire PSD as suggested by Eq. 3.11.

To simulate a racetrack-filtered loading, the filtered regularity, $\hat{\alpha}_2$, and filtered frequency of peaks, $\hat{f}_p$, should be used. Also, simulated amplitudes smaller than half the racetrack threshold should be censored to approximate racetrack filtering of small ranges. θ_E of the fast process can be approximated from Eq. 3.11 if the PSD of the fast process, $G_F(f)$, with variance $\sigma_F^2 = (\hat{\alpha}_2 \sigma_X)^2$ is used. The exact shape of $G_F(f)$ is somewhat arbitrary; the original PSD can simply be truncated from below, or an averaging filter can be applied (see Eq. 3.31 below).

The σ's and θ's for a simulation of a wide band process that has not been racetrack filtered can be derived from the shape of the PSD. Since the sequential simulation is composed of samples of a process that is the sum of a Gauss-Markov slow part and a modulated-Markov fast part, the simulated PSD can be viewed as the sum of Gauss-Markov and modulated-Markov PSDs. The necessary parameters for the simulation, σ_S and σ_F, can be chosen to preserve the total variance, zero frequency intercept ($G(0)$), and some central frequency measure (e.g., median frequency). Although there is no unique way to satisfy these constraints, a practical way of deriving the necessary parameters is illustrated below.

The total variance, σ_X^2 and median frequency must first be calculated from the PSD. The low frequency (slow) part is obtained by low pass filtering the process with an averaging filter, defined in the time domain by

$$X_S(t) = \frac{1}{T_n} \int_t^{t+T_n} X(\tau) d\tau \tag{3.31a}$$

and in the frequency domain by

$$G_S(f) = H^2(f)\, G(f) = \left(\frac{\sin(\pi f / f_n)}{\pi f / f_n} \right)^2 G(f) \tag{3.31b}$$

where $f_n = 1/T_n$ is the fast process natural (or modulating) frequency. The PSD of the fast process is the difference between that of the total process and the slow part; $G_F(f) = G(f) - G_S(f)$. θ_X can be estimated from $G_S(0)$ by Eq. 3.28. Once the PSD has been split into slow and fast parts, all the simulation model parameters (σ_S, σ_F, θ_X, and θ_E) can be calculated. The difficulty is that f_n, which controls the filter in Eq. 3.31, is not uniquely defined. The following iterative method can be used to find appropriate values for the above parameters and f_n such that the correct median frequency is obtained.

To start, approximate f_n by the median frequency of $G(f)$. Then:

(1) Low pass filter the original process, splitting it into slow and fast parts using $H^2(f)$ from Eq. 3.31 to calculate the resulting PSDs.

(2) Calculate σ_S and σ_F for the slow and fast parts, respectively, by integrating $G_S(f)$ and $G_F(f)$.

(3) Calculate θ_E from $G_F(f)$ using Eq. 3.11 and θ_X from $G_S(0)$ using Eq. 3.28.

(4) Estimate the simulation PSD, $G^*(f) = G_S^*(f) + G_F^*(f)$, where

$$G_S^*(f) = \frac{2\sigma_S^2 \theta_X}{1 + (\pi f\, \theta_X)^2} \tag{3.32a}$$

is the PSD of the Gauss-Markov slow part, and

$$G_F^*(f) = \frac{\sigma_F^2}{\theta_E} \left(\frac{1}{(1/\theta_E)^2 + (\pi(f - f_n))^2} + \frac{1}{(1/\theta_E)^2 + (\pi(f + f_n))^2} \right) \tag{3.32b}$$

is the PSD of the modulated-Markov fast part. (The * superscript distinguishes the simulation model PSDs from the original process PSDs.)

(5) Calculate the median frequency of the simulation from $G^*(f)$.

(6) If the median frequencies of the simulation and original PSDs are significantly different, select a new modulating frequency, f_n, and go back to step (1). As a first step, $f_n/2$ can be added or subtracted from the initial guess to bracket the desired modulating frequency. A Newton-Raphson

iteration afterward usually converges in about four to six iterations.

The simulation parameters derived from the above iterative method are listed in Table 3.2 (see Section 3.4.2). The original and simulation PSDs for the AA, AG, and IN ASTM loadings are shown in Figure 3.17. Most of the details of the PSDs are lost in the sequential simulation; only the overall distribution of frequency content is preserved.

The AA, AG, and IN load peaks and valleys were sequentially simulated repeatedly using the parameters in Table 3.2. These simulations were then racetrack filtered at the same levels as the tabulated ASTM loadings so that CDFs of load peaks and ranges could be compared as shown in Figure 3.18. It is apparent that the sequential simulation sometimes does not produce as many small amplitude peaks and ranges. Fortunately, fatigue damage is heavily dependent on the larger peaks and ranges, which are accurately simulated by this sequential technique.

3.6 Summary

The type of fatigue crack growth analysis that is required for each application determines the level of complexity of the load model needed to supply the necessary information. There are two fundamentally different types of crack growth analyses, depending on whether load sequence effects must be included or not. Investigations of when sequence effects are likely to be important are included in Chapter 4.

For fatigue analyses in which load sequence effects can be neglected, random variable models for both narrow- and wide-band loadings provide all the necessary loading information. Analytical results from the narrow-band model are conservative for most cases of practical interest, regardless of the actual bandwidth of the Gaussian loading.

Adjustments to the theoretical distributions of load peaks and ranges are provided, through racetrack filtering, to make the theoretical distributions more accurate models for fatigue analysis. Basic analytical results from the Gaussian model can still be used; it is necessary only to modify the regularity ($\hat{\alpha}_2$) and the frequency of peaks ($\hat{f}_p$) to reflect the racetrack-filtering threshold and initial bandwidth (Eqs. 3.20-3.23). These adjusted theoretical distributions account for over 80% of the *damage* that is identified by rainflow counting, for small fatigue exponents ($2 \leq b \leq 4$), which is the usual case in crack growth applications.

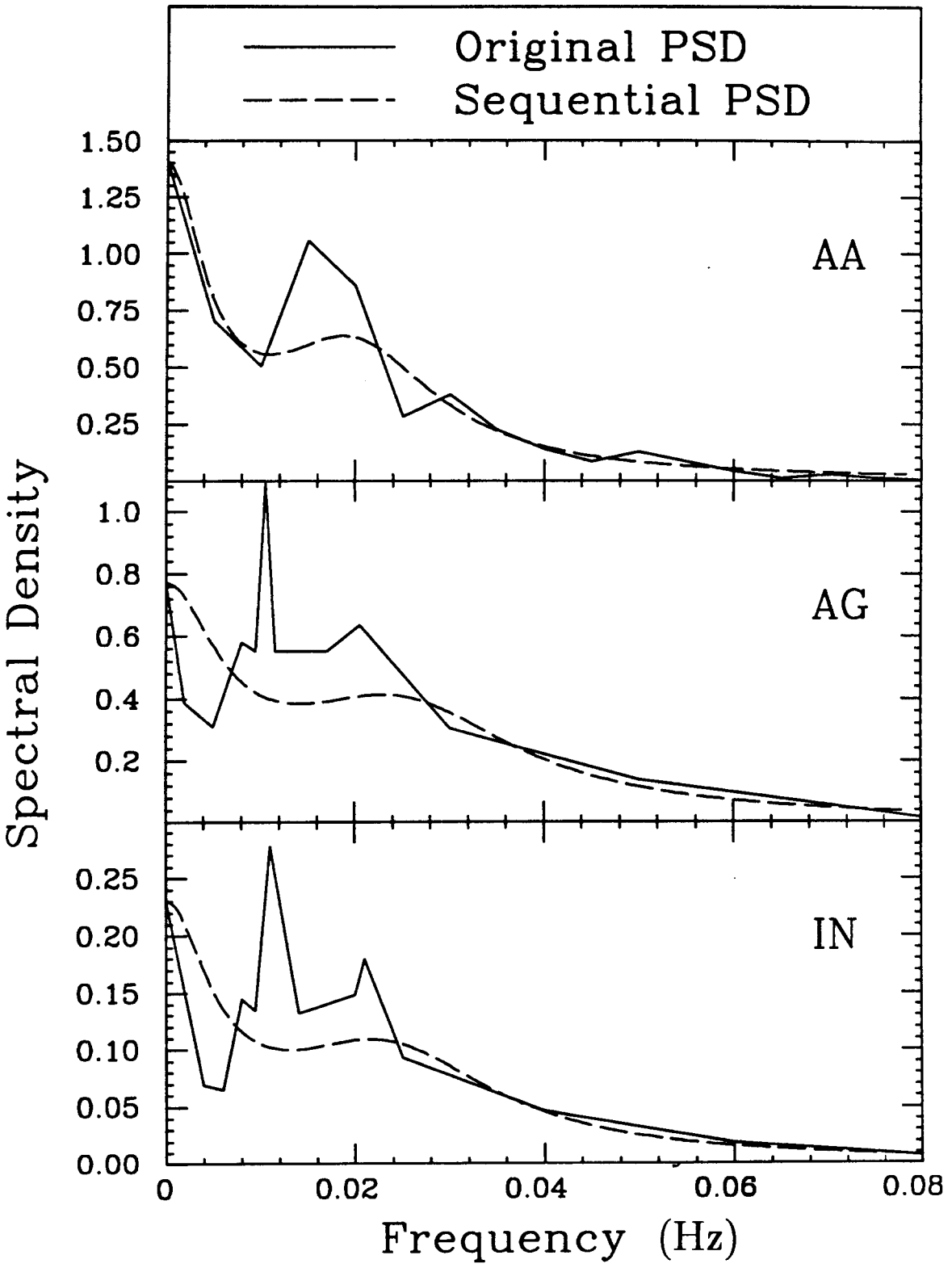

Fig. 3.17 PSDs of the ASTM loadings with the approximate PSDs from the sequential simulations.

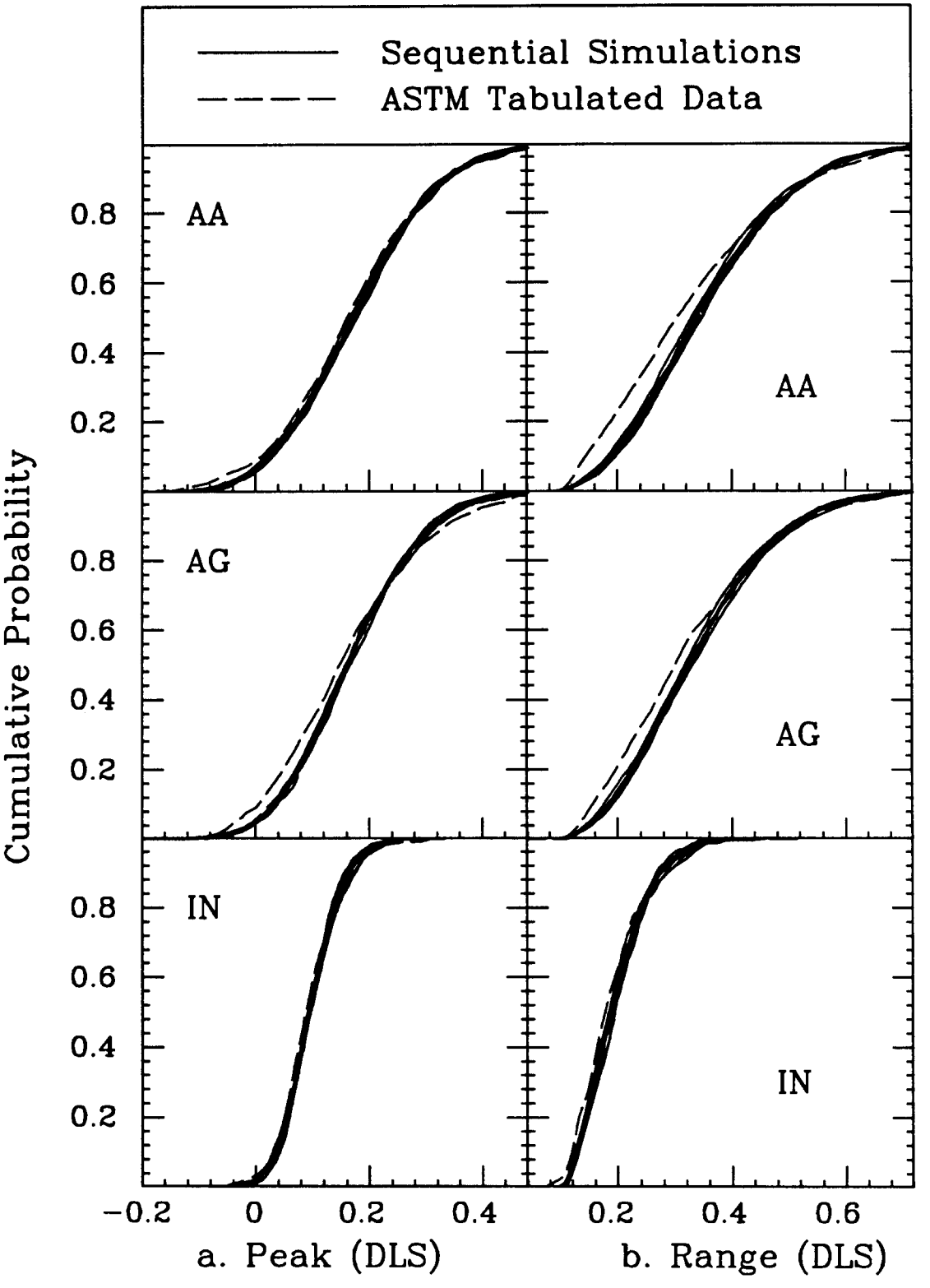

Fig. 3.18 Comparison of CDFs of the tabulated ASTM loadings with CDFs of the sequential simulations for (a) peaks and (b) ranges.

When sequence effects must be included in the analysis, the loading dynamics must also be modeled, and simulation is usually required to track the history dependence of the crack opening stress. Traditional FFT simulation methods can be used, but a more efficient method directly simulates a sequence of load peaks and troughs for either narrow- or wide-band loadings. Narrow-band peaks are generated by simulating the process envelope at intervals of half the natural period. Wide-band simulations require splitting the process into high frequency (fast) and low frequency (slow) parts; the slow process and the envelope of the fast process represent the mean and amplitude, respectively, of each load cycle. An iterative technique is provided to estimate the parameters of the sequential simulation from the PSD. If the parameters of the simulation reflect the results of racetrack filtering ($\hat{\alpha}_2$ and $\hat{f}_p$), this sequential simulation technique reproduces those peaks and ranges in the loading that are most important in fatigue crack growth.

CHAPTER 4

CALCULATING CRACK GROWTH WITH RANDOM LOAD MODELS

4.1 Introduction

The purpose of this chapter is to use the crack growth model of Chapter 2 to show the appropriate applications and relative accuracies of the random load models of Chapter 3. The level of complexity of the random load models varies from the simple use of a sample block of the loading, to random variable models that neglect sequence effects, to the use of simulations that reproduce both distributions of load peaks and ranges as well as the most probable sequences. The specific application will determine which model is appropriate (How much accuracy is needed? Are load sequences important? etc...). Efficient methods of calculating crack growth life are shown here, matching crack growth models with and without sequence effects to the appropriate load model. Simulation results are then used to illustrate the relative importance of including sequence effects in the crack growth calculation. The fatigue analyst may find these comparisons useful in deciding which analysis/load model is appropriate for the individual application.

The order of the presentation of topics is as follows:

(1) Block loading retains sequence effects by specifying a sample of the loading peaks and valleys. While this accurately describes load sequences within the sample, it provides an incomplete description of all load statistics because it is only a single sample out of all possible loadings. The crack growth model of Chapter 2, which includes sequence effects, is used to evaluate the implications of block loading on crack growth calculations and testing.

(2) The simplest statistical model describes the load peaks and valleys (or, equivalently, cycle means and amplitudes) as random variables which neglect sequence effects. A sequenceless crack growth model is introduced to show how crack growth can be calculated from random variable load models when sequence effects are negligible. Both narrow- and wide-band random loadings can be modeled in this way, as described in Chapter 3.

(3) The question of when sequence effects can be neglected is treated by simulating random loadings and calculating crack growth, cycle-by-cycle, with and without sequence effects. Gaussian random loadings are simulated with the sequential algorithm, introduced in Chapter 3, which creates a series of peaks and valleys directly, without the need for extrapolation to find extrema. Regions of applicability of sequenceless crack growth models are suggested by the simulation results.

(4) If the intensity (RMS) of the loading is also varying in time, the highest peaks can be even more rare than for a stationary random loading. Simulations that include variations in RMS level show how these intensity fluctuations influence crack growth predictions.

(5) Sequence effects in crack growth have long been demonstrated when there are large tensile overloads present in the loading [von Euw, et.al., 1972; Trebules, et.al., 1973]. This can be the case, for example, when the overloads are caused by a different source than the loading responsible for most of the crack growth. If these loadings are defined as sample blocks, the overloads occur at regular intervals of the block size throughout the crack growth life. Simulation studies showing the influence of the regularity of overload spacing on cycles to failure are included here. Analytical results for cycles to failure due to simple loadings with randomly occurring overloads are also possible, and will be presented in the following chapter.

4.2 Block Loading Effects

4.2.1 Definition and Purpose of Block Loading

One common way to represent a random loading is to list the precise sequence of peaks and valleys in a sample block, as was done for both the ASTM and SAE test series introduced in Chapter 2. This load block is used in both testing and analysis. Testing is easily programmed by repeating the load block until failure. Calculation of the crack growth life is possible cycle-by-cycle, again repeating the block until calculated crack growth exceeds the final crack length. The loading that results from the block approach is no longer random, but has peaks that repeat periodically at intervals of the block length.

Analysis is also simplified by calculating the increment in crack growth, δa_i, due to one block of loading at a crack lengths of a_i (which can be chosen to be an *integration point*). Thus, an estimate of the crack growth rate per block at

each integration point is $(da/dB)\big|_{a=a_i} = \delta a_i$. The number of blocks to failure, N_B, is then estimated by summing over the integration points:

$$N_B = \int_0^{N_B} dB = \int_{a_o}^{a_f} \frac{da}{(da/dB)} \approx \sum_{i=1}^{n} \frac{\Delta a_i}{\delta a_i} \tag{4.1}$$

where Δa_i is the size of the interval associated with the i^{th} integration point and n is the number of integration points between initial and final crack lengths (a_o and a_f). By selecting ten to twenty uniformly spaced integration points and calculating crack growth at those selected crack lengths, the number of blocks to failure can be estimated without cycle-by-cycle integration over the entire life. If failure is predicted after thousands of blocks, this represents a tremendous savings in computation time. The number of integration points can be further reduced (to from three to six) if the intervals are logarithmically, rather than uniformly, spaced between a_o and a_f (for a_f about 10 times a_o).

4.2.2 Implications of Block Loading

The ASTM AA load history is an example of block loading, which is composed of 1300 tabulated peak-valley pairs produced by the FFT simulation method (see Section 3.4) [Dill and Saff, 1977]. One hundred more statistically equivalent blocks have been simulated here using the same procedure and input data as was used to create the tabulated AA block. The highest peak in the tabulated AA block is 92.5% of design limit stress (DLS) while the highest peak in the 100 simulations varies between 87% and 115% of DLS with a mean of 101% of DLS. Assuming that each of these blocks is repeated in a closed loop fashion, the resulting crack growth life is predicted using the crack growth model of Chapter 2, Predicted lives for each block are plotted in Fig. 4.1 versus the highest peak load in the block. The highest peak, which is a random variable, has a substantial influence on the predicted life for sample block type loading. The life estimates have an overall mean of 19200 cycles and a coefficient of variation (COV) of 0.13. Because the highest peak in the ASTM tabulated block is smaller than the highest peak in the average block, the predicted life (18000 cycles) is below the average predicted life.

When the AA loading is simulated continuously for the entire crack growth life, the mean life is 20400 cycles and the COV is just 0.03. This suggests that the artificial block structure, while not significantly influencing mean life in this case, is responsible for a four fold increase in the COV of the life estimate.

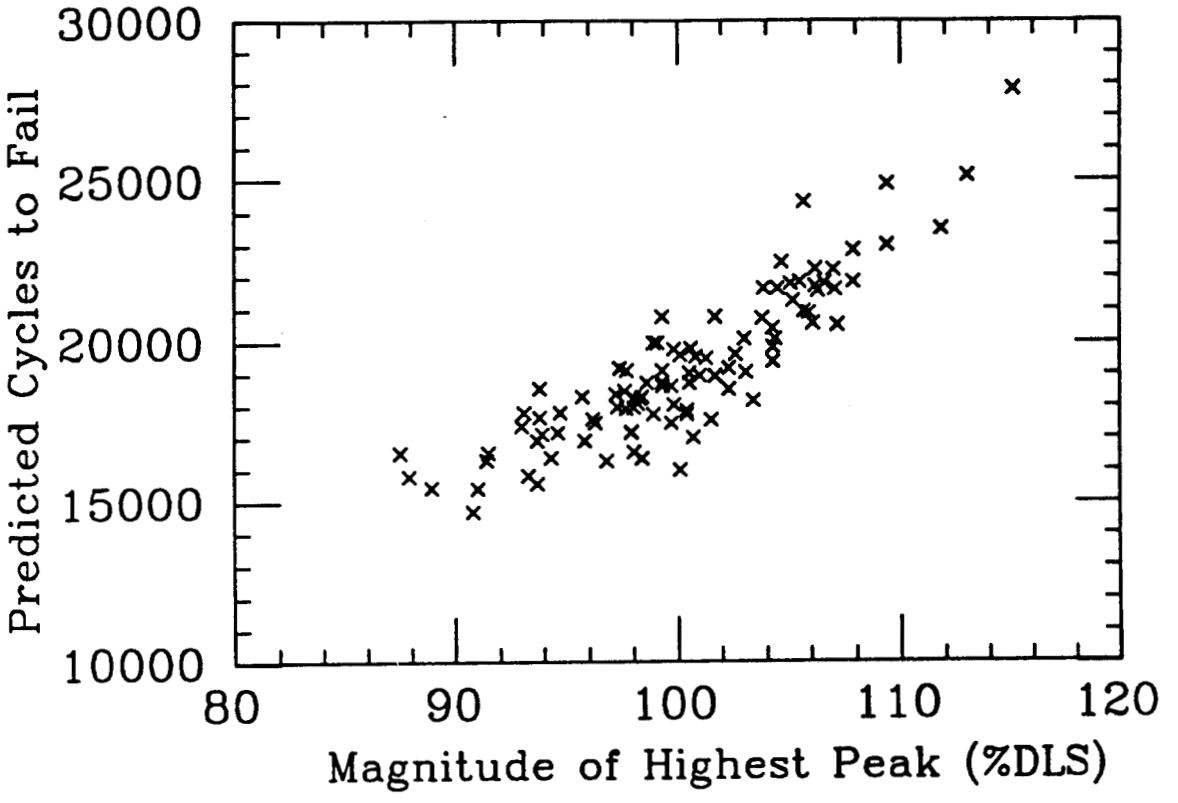

Fig. 4.1 Predicted life vs highest peak in the simulated ASTM AA load block for repeated block loading.

Simulations of the other ASTM load histories show similar results. These estimates neglect material variability, which can be much greater than load induced variability (as can be seen from Section 2.3.4 and Fig. 2.10). However, it is especially important in testing that the loading be representative of the actual environment so that the resulting test lives do not contain an important and possibly nonconservative bias due solely to the block structure.

4.3 Random Variable Models and Sequenceless Crack Growth

Random variable models have been used extensively for Palmgren-Miner fatigue analysis of narrow-band loadings [Miles, 1954; Yang, 1974; Wirsching and Light, 1980]. In this case, each range, R_i causes damage, cR_i^b. The total damage in N cycles, D_N, may be calculated in one of two ways: (1) by summing contributions cycle by cycle, so that $D_N = c\sum R_i^b$; or (2) by summing average contributions to D_N from each possible range level R. In the latter case, in N cycles one expects $N \cdot p(R)dR$ ranges between R and $R+dR$ so that

$$D_N = c\sum_{i=1}^{N} R_i^b \approx \int_{R=0}^{\infty} cR^b [N \cdot p(R)dR] = cN(2\sqrt{2}\sigma_X)^b (b/2)! \qquad (4.2)$$

Thus, D_N can be approximated by the random variable model ($p(R)$ given by Eq. 3.16 with $\alpha_2 = 1$) without the need for cycle-by-cycle summation. Actual D_N values will vary negligibly from this result in most high-cycle (large N) cases of practical interest [Crandall and Mark, 1963]. Equation 4.2 is a well known result for fatigue under random loads [Miles, 1954].

This random variable model can also be applied to crack growth if sequence effects are neglected and the crack growth equation is a separable function of stress and crack size. For example, the crack growth rate can generally be described in terms of an equation in the following form:

$$\frac{da}{dN} = C\Delta K_{eff}^b \qquad (4.3)$$

where $\Delta K_{eff} = \sqrt{\pi a}\, Y(a)\Delta S_{eff}$, as in Chapter 2. Whether the crack growth analysis contains sequence effects or not depends on the definition of ΔS_{eff}. In Chapter 2, a crack growth model with sequence effects is created by relating the effective stress range to a *reset stress* that depends on past loading. A sequenceless crack growth model is formed by defining the effective stress range in terms of the maximum, $S_{\max}$, and the minimum, $S_{\min}$, of the current stress cycle only [Nelson and Fuchs, 1976]:

$$\Delta S_{eff} = \begin{cases} S_{\max} - q_o S_{\max} & S_{\min} < q_o S_{\max};\ S_{\max} > 0 \\ S_{\max} - S_{\min} & S_{\min} > q_o S_{\max};\ S_{\max} > 0 \\ 0 & S_{\max} < 0 \end{cases} \tag{4.4}$$

Eq. 4.3 can then be integrated after separating stress and crack length terms:

$$\int_{a_o}^{a_f} \frac{da}{C(Y(a)\sqrt{\pi a})^b} = \sum_{i=1}^{N} \Delta S_{eff}^b \tag{4.5}$$

in which N is the number of cycles needed for crack growth from a_o to a_f.

4.3.1 Narrow-band Model

To use the narrow-band random variable model ($\alpha_2 = 1$), $S_{\max}$ and $S_{\min}$ are replaced in Eq. 4.4 with $m_X \pm A$, where m_X is the mean stress and A is the stress amplitude of Eq. 3.15. ΔS_{eff} thus becomes a function of amplitude and mean stress, $\Delta S_{eff}(A, m_X)$. The sum in Eq. 4.5 is then approximated as in the Palmgren-Miner case,

$$\int_{a_o}^{a_f} \frac{da}{C(Y(a)\sqrt{\pi a})^b} \approx N \int_{A=0}^{\infty} [\Delta S_{eff}(A, m_X)]^b \; p(A)\, dA \tag{4.6}$$

and solved for N. For certain forms of $Y(a)$ and large values of m_X (so that $S_{\min}$ is always greater than $q_o S_{\max}$), the integrations can be done analytically. While numerical integration is generally required, this integration is considerably faster (e.g., using quadrature points) than cycle-by-cycle crack growth calculation.

For loads with arbitrary bandwidths, the narrow-band model in Eq. 4.6 remains useful when a rough (and generally conservative) estimate of life is required. For example, analytical life estimates using the Rayleigh PDF are compared to test results for the ASTM test series (which are not narrow-band) in Fig. 4.2. Also shown are sequenceless predictions based on the tabulated load histories. The narrow-band life estimates are conservative with respect to the predictions using the actual test loads, under predicting life by less than a factor of two.

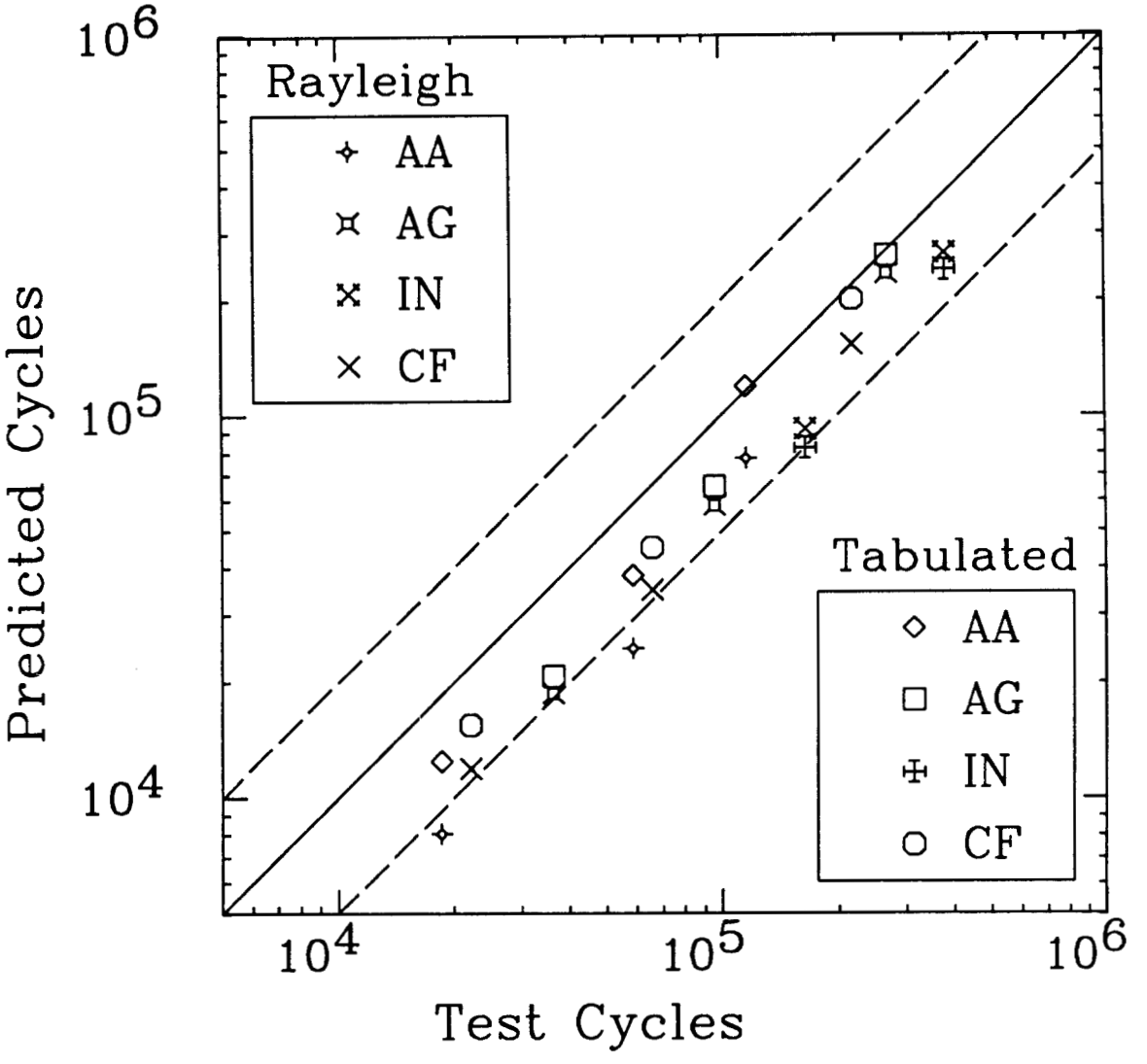

Fig. 4.2 Comparison of test life to predicted life for the ASTM test series. Predictions are made using the sequenceless crack growth model and both the actual (Tabulated) loading and the narrow-band (Rayleigh) approximation.

4.3.2 Wide-band Model

Less conservative estimates of wide-band crack growth life are available by including a measure of load bandwidth, such as $\hat{\alpha}_2$. As shown in Chapter 3, good estimates of the distributions of peaks and ranges are obtained with the theoretical distributions if the parameters are adjusted for racetrack filtering. To accomplish these adjustments, a racetrack filtering level, R_{th}, should be selected based on the crack growth exponent ($R_{th} \approx 1.0\sigma_X$ when $b=2$ and $R_{th} \approx 1.5\sigma_X$ when $b=4$). Next, α_1 can be calculated from the load PSD, and $\hat{\alpha}_2$ can be estimated using Eqs. 3.20-3.22. The reduced rate of peaks can be estimated using Eq. 3.24 with the original f_p and z_1 both calculated from the PSD.

The effective stress range, ΔS_{eff}, is written as a function of the cycle mean, X_0, and amplitude, A, by letting $S_{\min} = X_0 - A$ and $S_{\max} = X_0 + A$ in Eq. 4.4. The value of N is calculated as in the narrow-band case, except that the joint distribution of cycle mean and amplitude is required and integration is over both mean and amplitude:

$$\int_{a_o}^{a_f} \frac{da}{C(Y(a)\sqrt{\pi a})^b} \approx N \int_{X_0=-\infty}^{\infty} \int_{A=0}^{\infty} [\Delta S_{eff}(A, X_0)]^b \, p(A) \, p(X_0) dA dX_0 \quad (4.7)$$

where $p(X_0)$ and $p(A)$ are taken from Eqs. 3.14 and 3.15, respectively.

When this random variable model is applied to the sequenceless crack growth analysis of the ASTM test series (using the post-filtered regularity, $\hat{\alpha}_2$ and solving for N in Eq. 4.7) the results are almost identical to the cycle-by-cycle sequenceless summation of crack growth due to the tabulated loadings. The difference in predicted life is less than 10% for the AA loadings, less than 1% for the AG loadings, and less than 25% for the IN loadings, as shown in Table 4.1. Because the tabulated loadings are a single sample of the loading process, it may be argued that the random variable results are more representative of the actual service loading than the tabulated blocks, especially for the IN loading, which is a sample of only 300 cycles with an added *overload* in each load block.

This random variable approach to crack growth calculations, however, contains no information on load sequences. If load sequences are important, the random variable definition will be insufficient and the loading must be described as a random process. Methods of simulating loadings for cycle-by-cycle analysis

Table 4.1
Test life and sequenceless predictions, using both the tabulated loadings and the wide-band random variable model, for the ASTM test series.

Load Type	Scale Factor	Test Cycles	Predictions	
			Tabulated	Random Variable
AA	0.2	115700	119171	108225
AA	0.3	58585	38080	34383
AA	0.4	18612	12470	11341
AG	0.2	268908	260841	259546
AG	0.3	95642	65000	64352
AG	0.4	36397	20730	20763
IN	0.3	380443	240000	294030
IN	0.4	164738	82370	101970

with sequence effects are outlined in Chapter 3. Simulated loadings are used to calculate crack growth lives, with and without sequence effects, in the following sections to provide guidance in determining when sequence effects must be included in the analysis.

4.4 Simulation Study of Sequence Effects

Some advantages of the simulation approach over testing are that several parameters can be easily varied (and material property values assigned at will) and the calculations can be repeated with different samples of the random loading until the average life is determined (to within prespecified accuracy). It would be extremely expensive to duplicate such an extensive parameter study with test data. However, since this study is based on simulations instead of test data, the results can only be trusted to indicate relative sequence effects in *predicted* crack growth lives.

Stationary Gaussian random loadings were simulated and subsequent crack growth was calculated with and without sequence effects to determine the number of cycles to failure in each case. Selected loading, material, and modeling parameters were varied about two baseline cases: the ASTM AA and SAE BR loading histories and test specimens. The baseline parameters are listed in Table 4.2. Simulation results are plotted in Figs. 4.3-4.7. The *Ratios* shown are the sequenceless predictions divided by predictions that included sequence effects (prediction ratios). The prediction ratio is 0.68 for the ASTM base case and 0.48

Table 4.2 - Baseline case parameters for the sequence effect simulations.

Parameter	q_o	m_X/σ_X	C_o^*	b	$S_y/(m_X+3\sigma_X)$
ASTM	0.30	2.3	$8.4\text{x}10^{-10}$	3.64	1.45
SAE	0.35	0.0	$1.5\text{x}10^{-10}$	3.25	4.96
Parameter	R_{th}/σ_X	α_2	a_o	a_f	γ
ASTM	0.6	0.8	0.1in	1.0in	0.23
SAE	1.0	1.0	$0.35\,W^{**}$	$0.7\,W^{**}$	0.20

* Recall that $C = C_o(1-q_o)^{-b}$.
** W is the width of the test specimen.

for the SAE base case. The solid lines in the figures are for variations about the ASTM base case and the dashed lines are for variations about the SAE base case.

Plus and minus one standard deviation *error bars* are included to show the relative variability in time to failure due to different realizations of the random loading. Predictions without sequence effects have negligible variability so the deviations about the mean ratio are a result of the variability in the prediction that includes sequence effects. In general, the greater the influence of sequence effects, the greater the variability in the time to fail, because when sequence effects are significant, the time to fail depends heavily on relatively rare, high peaks.

The loading parameters that were varied include the ratio of the mean stress to the RMS stress (m_X/σ_X), regularity (α_2), and the normalized racetrack threshold (R_{th}/σ_X). Of these, only the mean stress, in Fig. 4.3, had a significant impact on the ratio of life predictions with and without sequence effects. The maximum difference (minimum ratio) occurs at mean stresses between zero and three times the RMS. A very high mean stress keeps the crack from closing, so the effective stress range is unaffected by crack closure. Sequence effects are likely to be minimal when the mean stress is greater than about $3\sigma_X(1+q_o)/(1-q_o)$, which keeps over 95% of the stress valleys in a Gaussian loading above the crack opening stress. At zero or negative mean stresses, acceleration and retardation effects begin to balance, resulting in a reduction in the difference between the two prediction methods (the ratio approaches unity).

The material parameters that were varied include q_o, C_o, and $S_y/(m_X+3\sigma_X)$ (yield stress divided by the mean plus three times the RMS, a crude estimate of maximum applied stress). Variations in each of these

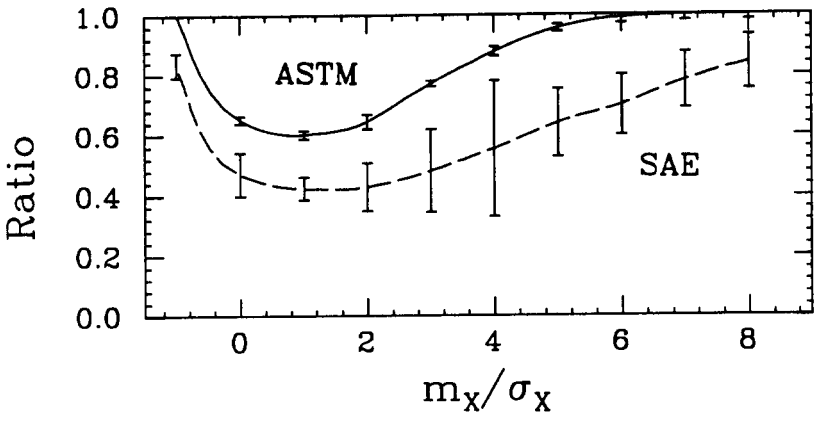

Fig. 4.3 Ratio of crack growth life predictions without sequence effects to predictions with sequence effects vs mean stress.

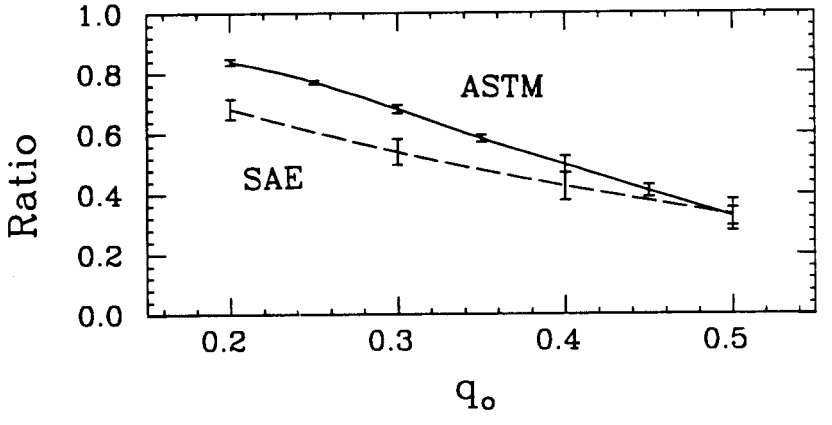

Fig. 4.4 Ratio of crack growth life predictions without sequence effects to predictions with sequence effects vs crack opening stress ratio.

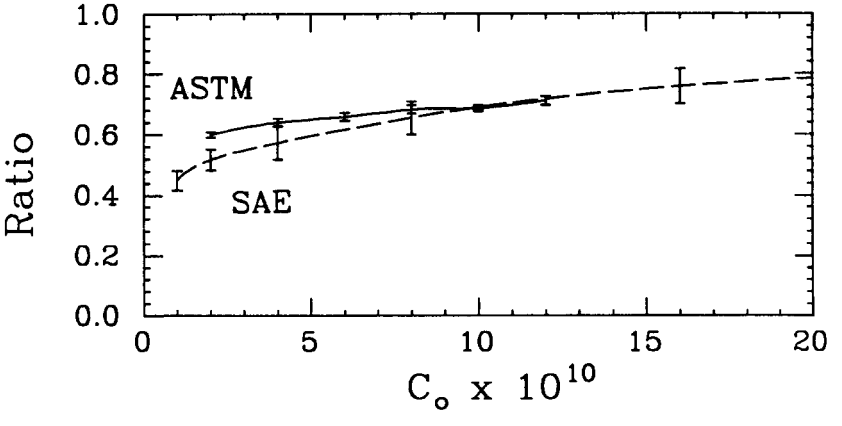

Fig. 4.5 Ratio of crack growth life predictions without sequence effects to predictions with sequence effects vs crack growth rate coefficient.

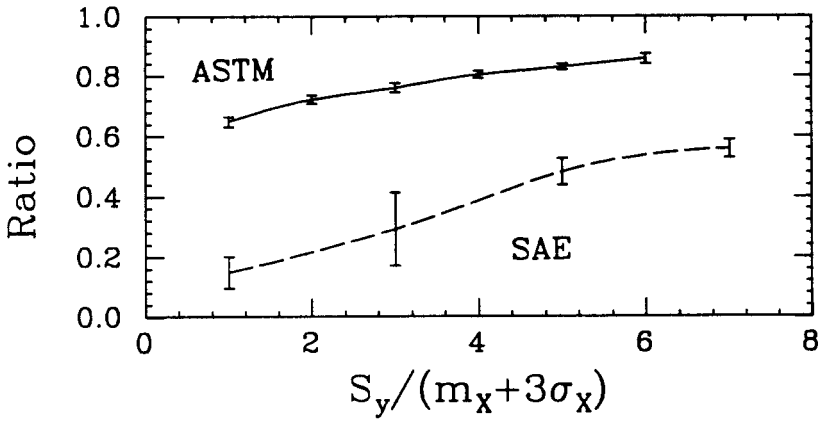

Fig. 4.6 Ratio of crack growth life predictions without sequence effects to predictions with sequence effects vs yield stress.

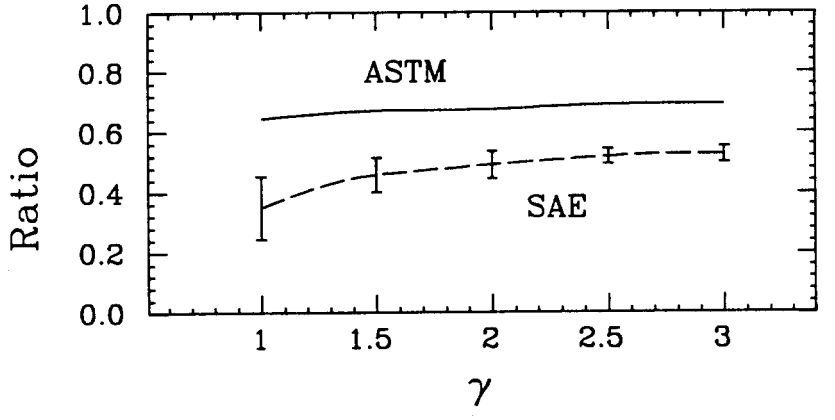

Fig. 4.7 Ratio of crack growth life predictions without sequence effects to predictions with sequence effects vs plane strain constraint factor. (The $\pm\sigma$ bounds for the ASTM case are small and have been omitted.)

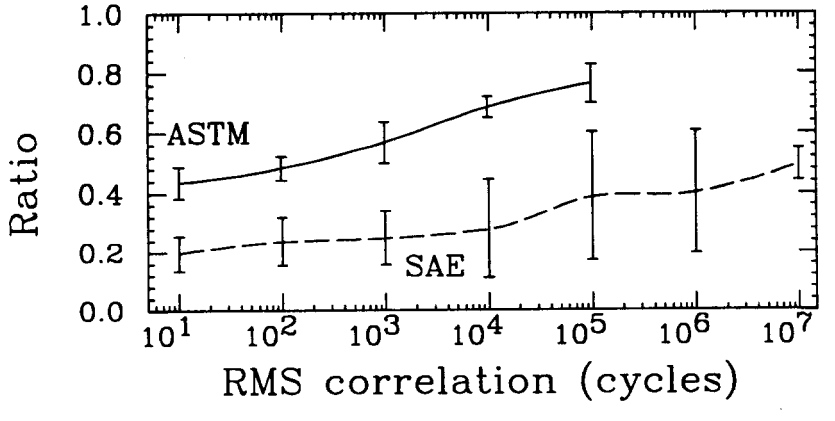

Fig. 4.8 Ratio of crack growth life predictions without sequence effects to predictions with sequence effects vs correlation time in RMS variations for nonstationary loading.

parameters showed some influence on sequence effects, as can be seen in Figs. 4.4-4.6. Sequence effects become more important as C_o and S_y decrease and as q_o increases. In general, the greatest sensitivity appears to be to the crack opening stress ratio, q_o, except for the SAE base case which is very sensitive to reductions in yield stress.

Variations in the plane strain constraint factor, γ, result in a small increase in sequence effects as γ is decreased, as shown in Fig. 4.7.

The SAE base case shows more sensitivity to sequence effects than the ASTM case in most instances. The parameter with the largest difference between the SAE and ASTM base cases is the crack growth rate coefficient, C_o, which is 5.6 times greater for the ASTM material. The higher crack growth rate allows the crack to grow through the overload induced crack-tip plastic zone much faster, reducing the duration of the effect of each overload. When the SAE crack growth rate coefficient is increased to that of the ASTM base case, the prediction ratios, shown in Fig. 4.5, are about the same (although the reverse is not true; reducing the ASTM crack growth rate coefficient does not lower the prediction ratio as far as the SAE base case level).

Variations that increase the size of the crack-tip plastic zone (decreasing S_y and γ) also cause greater differences between life predictions with and without sequence effects.

The above sensitivity to C_o, S_y, and γ point to a common effect. The greater the number of cycles required to grow the crack through the crack tip plastic zone, the greater the influence of sequence effects.

These simulation results indicate that sequence effects will not produce a significant difference in crack growth life estimates when the mean stress is sufficiently high, m_X greater than about $3\sigma_X(1+q_o)/(1-q_o)$, independent of the other parameters. This is consistent with a reported lack of sequence effects in high tensile mean stress tests [Fleck and Smith, 1984]. When the mean stress is low enough that sequence effects are more important, the magnitude of the prediction ratio depends on the material parameters that act together to determine the duration of the effect of an overload, which is governed by the size of the crack-tip yield zone and the rate of crack growth through it. In addition, the higher the crack opening stress ratio, q_o, the greater the differences between life predictions with and without sequence effects.

The standard deviation of the time to fail is consistently greater (compared to the mean) for the SAE simulations, which also show the greatest influence of sequence effects. The COV (standard deviation divided by the mean) almost always increases as the prediction ratio decreases, reflecting the greater sensitivity to relatively rare, high peaks. The increasing variability acts to negate some of benefit of the additional crack growth life that results from the retardation effect of the highest peaks.

4.5 Nonstationary Loading

A random loading is called stationary if the statistics of the loading (mean, RMS, etc...) do not change in time, i.e., a sample of the loading taken at one time will have identical statistical properties to samples taken from any other time. Although loadings are often nonstationary, they can usually be divided into segments with stationary behavior in each segment. Sequenceless crack growth predictions can then be done by calculating the crack growth rate in each segment and summing over the relative amount of time spent in each type of segment. It is highly probable, however, that the transition from one *stationary* segment to another can introduce crack growth sequence effects, especially if the transition involves a change in the overall magnitude of the load peaks.

Simulations of loadings with time varying RMS levels are used in this section to illustrate the influence of such nonstationarity on crack growth. This type of variation in the loading intensity is prevalent for structures exposed to wind and wave excitation, as well as for automotive and aircraft components that are exposed to variable road and runway roughness, or changes from normal roughness to maneuver loads. No single model will represent the wide variety of possible variations in loading intensity (RMS); as a simple approximation, it is assumed here that the RMS is a random process with a Rayleigh marginal distribution (PDF) and a duration of significant correlation given by θ_{RMS}.

This loading is simulated in the same way as the stationary loading, with the sequential simulation technique, except that the RMS, σ_X, is also simulated each cycle. Because the RMS must be non-negative, the Weibull family of distributions (of which the Rayleigh is a special case) will often be a good approximation to the real RMS distribution. A correlated sequence of Rayleigh distributed RMS values can be simulated just as the load amplitudes (A's) were simulated in Section 3.5. The general case of a Weibull distributed sequence is simulated in a similar fashion [Winterstein, 1984]. The standard deviation of the RMS is

denoted by σ_{RMS} and the correlation time is θ_{RMS}.

Because the correlation time for RMS fluctuations is usually much greater than the period of the cycles, the RMS can be simulated at relatively few points (about twice per θ_{RMS}) and linearly interpolated between them.

Simulations were conducted about the two base cases of the previous section, with $\sigma_{RMS} = 0.75\sigma_X$ (see Table 4.2 for parameter values). The prediction ratios (ratios of predicted life without sequence effects to predicted life with sequence effects) are shown in Fig. 4.8 as functions of the correlation time of RMS fluctuations, θ_{RMS}. The two extremes are: (1) a very long correlation time for which the RMS remains nearly constant at some randomly chosen value throughout the crack growth life and (2) a very short correlation time that makes the loading appear to be stationary, but no longer Gaussian, so that the peaks and ranges are no longer Rayleigh distributed.

The first extreme, long correlation time, asymptotically approaches the stationary Gaussian case. The starting value of the RMS is different for each sample (which makes the asymptotic limits differ from the baseline values of 0.48 for the SAE case and 0.68 for the ASTM case), but because of the high correlation, the RMS remains virtually constant for the duration of the crack growth life. This is an example of nonergodic behavior, where one sample is not representative of the entire random process. In both the SAE and ASTM cases, the stationary Gaussian loading shows less sensitivity to sequence effects than loadings with variations in RMS level.

The other extreme, rapidly varying RMS level, shows the most sensitivity to sequence effects in this study. Because RMS variations are so rapid, this case can be thought of as a stationary loading with non-Gaussian behavior. For a narrow-band loading, the distribution of peaks can be calculated from the joint PDF of peaks and RMS, $p(P,\sigma_X)$, which, equals the product of the PDF of RMS, $p(\sigma_X)$, and the conditional PDF of peaks given RMS, $p(P\,|\sigma_X)$:

$$p(P,\sigma_X) = p(\sigma_X)\; p(P\,|\sigma_X) \tag{4.8}$$

The marginal PDF of peaks is the integral of the joint PDF over all possible RMS values. In this example, $p(\sigma_X)$ is taken to be Rayleigh with parameter σ_{RMS} and the conditional distribution of peaks is Rayleigh with parameter σ_X (narrow-band loading). The resulting marginal PDF of peaks is;

$$p(P) = \int_{\sigma_X=0}^{\infty} p(P,\sigma_X)\; d\sigma_X = \frac{P}{\sigma_{RMS}^2}\, K_0\left(\frac{P}{\sigma_{RMS}}\right) \tag{4.9}$$

where $K_0(\cdot)$ is the zero order modified Bessel function [Abramowitz and Stegun, 1964]. (The more general case of non-Rayleigh, Weibull distributed RMS variations does not have a closed form solution for the distribution of peaks.)

The values of θ_{RMS} that are between the above two extremes have sequence effects that are bounded by these two cases. In general, the more rapid the fluctuations in RMS, the greater the influence of sequence effects on fatigue crack growth.

The mean life can be greatly under estimated by neglecting sequence effects when the RMS level fluctuates, as shown in Fig. 4.8 by the factor of five difference (ratio of 0.2) between the two prediction methods for the SAE case when the RMS correlation time is short. The equivalence of this case to a stationary, but non-Gaussian, loading indicates that similar errors are possible due to significantly non-Gaussian behavior. In addition, the COV of the time to failure is greatest when the correlation time is in the midrange of the two extremes (see the SAE results in Fig. 4.8 with $10^4 < \theta_{RMS} < 10^6$). The ASTM case, which showed relative insensitivity to sequence effects under stationary Gaussian loading, has a maximum difference, in the mean, of a factor of two, and retains relatively low COV over the entire range of RMS correlation times. Although neglecting sequence effects can under estimate life, a crack growth estimate that includes sequence effects must also consider the variability in the time to fail, because the COV can be quite large.

4.6 Distinct Overloads

The above simulations represent a general class of loadings where the maximum stresses are caused by the same source as the rest of the cyclic loading. If the overloads are caused by some other source or are due to very brief periods of increased load intensity, their magnitude may be much greater than that of the loading responsible for most of the crack growth. This case of exogenous overloads is the one that has been used most often in laboratory tests to demonstrate sequence effects in crack growth.

As an example of the way that variations in the size and spacing of overloads affect crack growth life, consider a loading that is constant amplitude between a minimum of zero and a maximum of S, with occasional tensile overloads equal to S_{ol}, as shown schematically in Fig. 4.9. This is the simplest and most often investigated situation in which retardation effects are evident. Also, for simplicity, assume that the reset stress, S_r, remains equal to S_{ol} until one of

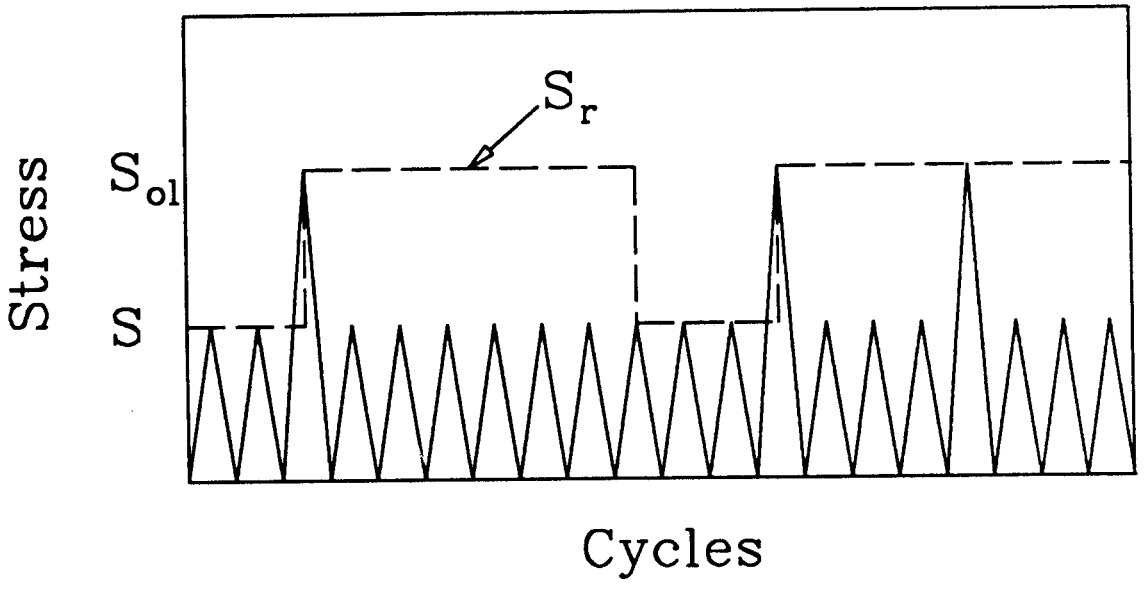

Fig. 4.9 Schematic of background stress peaks, S, overloads, S_{ol}, and reset stress, S_r, for distinct overloads simulation.

the background stress peaks extends the crack tip plastic zone, at which time the reset stress drops to S. This revision of the crack growth model of Chapter 2 retains the qualitative retardation effect and helps to visualize the state of the crack opening stress ($S_{op} = qS_r$) because there are now only two possible states: high crack opening stress following an overload, and low crack opening stress after the crack has grown through the overload affected zone. This simplified model is not, however, recommended for quantitative life estimates.

If both the number of cycles between overloads and overload magnitudes are constant, there is no variation in the predicted number of cycles to failure, and an increase in crack growth life is always predicted due to retardation effects. If, however, the number of cycles between overloads is random, the effect of one overload can sometimes overlap another, and the number of cycles to failure becomes random as well.

Simulations were done for a few values of both mean and COV of overload interarrival cycles. Evenly spaced overloads have an interarrival COV of zero. As the interarrival COV increases, the number of cycles between overloads can vary increasingly from the mean. A COV of unity is consistent with overloads with equal probability of arrival in every time interval, independent of past overloads (the Poisson model of *memoryless* random arrivals). COV values in excess of unity suggest that the overloads may *cluster;* e.g., several closely spaced overloads followed by a large number of cycles without an overload.

The results of this simulation study are presented in terms of the life extension due to the overloads; i.e., ratio of life with overloads to life without overloads. Fig. 4.10 shows the mean and COV of this ratio as a function of the average number of cycles between overloads. The average increase in life due to overloads is reduced as the interarrival COV, and hence the clustering, increases. Even spacing between overloads allows each to have maximum effect, while irregularly spaced overloads allow more gaps between periods of retarded growth. It takes more frequent overloads, on average, to achieve a given state of retardation when overloads cluster.

In addition, the COV of the time to failure increases as the number of interarrival cycles becomes more irregular. In general, it is not the mean life that is of interest but rather some percentile confidence level that is important. The combination of decreased mean life and increased COV of life due to increasing variability in overload interarrival cycles makes it much more likely that the crack growth life will be significantly lower than for evenly spaced

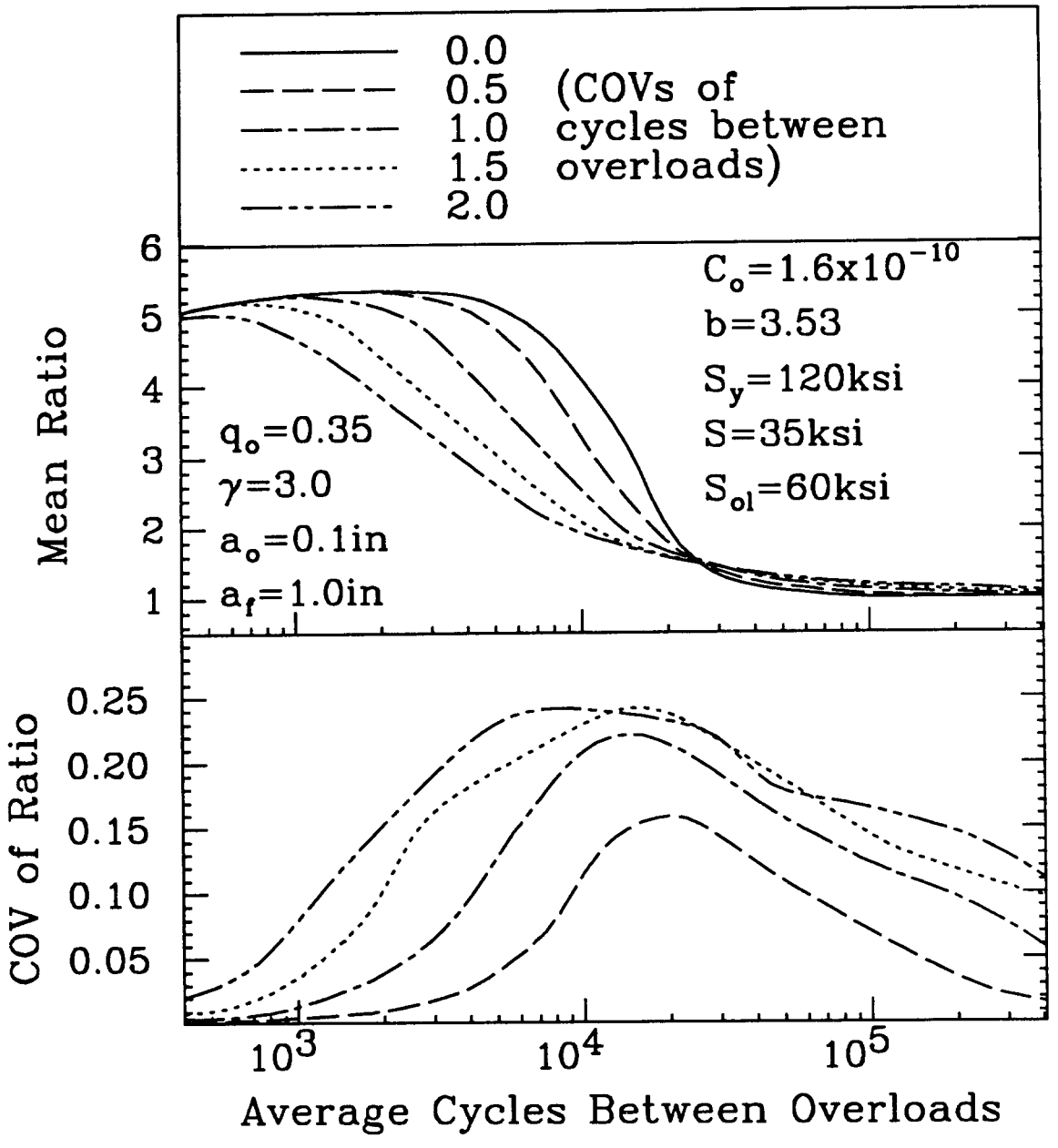

Fig. 4.10 Mean and coefficient of variation (COV) of the predicted increase in crack growth life (ratio of life with retardation to life without retardation) due to tensile overloads.

overloads. Assuming a constant number of cycles between overloads is therefore almost always nonconservative.

If a random loading has such distinct overloads, the distribution of load peaks (relative number of overloads to background loads) is insufficient information to accurately estimate crack growth life. The stochastic dynamics of the overload arrivals must also be modeled when sequences matter.

Analytical solutions for the mean and variance of time to fail due to loading with distinct overloads are possible using *diffusion models* when the overload interarrival time is memoryless, as is the case when the interarrival COV equals one. Diffusion modeling of fatigue crack growth is explored in the next chapter.

4.7 Summary

When a random loading is specified by tabulating a series of load peaks and valleys for the purpose of correctly representing sequence effects, the resulting crack growth can have an artificial sequence effect due solely to the block structure. The predicted crack growth life is highly sensitive to the highest peak in the tabulated block and may be nonconservative if this highest peak is larger than on average. This difficulty can be avoided by representing the loading as a continuous random process without the block structure. The crack growth life can then be calculated in one of two ways: (1) by integrating the random variable descriptions of the effective stress range when sequence effects are negligible, and (2) by sequentially simulating peaks and valleys and calculating crack growth cycle-by-cycle when sequence effects must be included.

Sequenceless crack growth analysis is accomplished without cycle-by-cycle summation by using the random variable models introduced in Chapter 3 (Eqs. 3.14-3.16) with parameters adjusted for racetrack filtering (Eqs. 3.21-3.25). The crack growth equation is separated into crack length and stress variables and integrated as in Eq. 4.6 for narrow-band loadings and as in Eq. 4.7 for wide band loadings. Assuming a Gaussian loading of arbitrary bandwidth to be narrow-band results in a rough (within a factor of two) and generally conservative life estimate compared to sequenceless life predictions that use the actual loading.

Simulations of crack growth life calculated cycle-by-cycle both with and without sequence effects indicate that in many Gaussian loading cases the difference between the two life predictions is less than a factor of two. This will be the case when the mean stress is higher than about $3\sigma_X(1+q_o)/(1-q_o)$,

independent of other factors. When the mean stress is lower than this, sequenceless life predictions may still be relatively accurate when the yield stress, crack growth rate coefficient, and plane strain constraint factor are all sufficiently large that the crack grows through the overload induced crack-tip plastic zone relatively quickly. The difference between sequenceless and sequence predictions is small when the crack opening stress ratio, q_o, is in the lower half of the usual range ($0.2 < q_o < 0.5$). These results were shown for variations about two base cases and may not be universally applicable.

When the loading intensity (RMS) varies with time, sequence effects are shown to be more important than for stationary Gaussian loadings. Neglecting sequence effects can lead to errors in life estimation of up to (and perhaps greater than) a factor of five when RMS fluctuations are rapid (compared to the total lifetime). Similar errors are possible for significantly non-Gaussian, stationary loading. The variability in crack growth life increases due to fluctuations in the RMS level, and must therefore also be estimated when calculating crack growth by including sequence effects. The possibility of lives much shorter than the mean removes some of the benefit of the increase in life (retardation) caused by RMS fluctuations.

Sequence effects have been repeatedly demonstrated for exogenous tensile overloads. Because of the sequence effect, a load model that includes only overload magnitude and frequency of occurrence is insufficient for crack growth estimation. The regularity of the spacing between the overloads must also be included. The assumption of regularly spaced tensile overloads is usually nonconservative.

CHAPTER 5

MODELING CRACK GROWTH AS A DIFFUSION PROCESS

5.1 Introduction

A random process can be completely described if the joint probability distributions between values of the process at all different times are known. This, of course, requires more information than can be verified for any real process, including crack growth due to random loading. Analyses of random processes therefore usually model only certain aspects of the process exactly. Traditional random vibration analysis uses an exact description of the correlation of the process at any two times through the autocorrelation function or the power spectral density (PSD). This is sufficient information to provide the exact solution for all statistics of the response of a linear system to Gaussian input. A diffusion process model, on the other hand, can reproduce nonlinear, non-Gaussian behavior, but at the expense of the exact description of the joint statistics of the process. The diffusion model restricts probabilistic *memory* to one step, in the discrete case, and to the current time, in the continuous case.

This *one-step memory,* (also called the *Markov* property) of a diffusion process means that the probability of a value of the process in the future depends only on the value of the process at the present and not on how the process arrived at the present value. A discrete example is the *random walk* in which a step is taken either to the right or to the left at each discrete time. The probability of stepping to the right or left may be a function of current position, but it is independent of the direction of past steps.

A continuous diffusion process results from the limiting case of the random walk as the time increment between steps goes to zero (the size of the steps being reduced as the square root of the time increment). When the size of each step has zero mean and has variance proportional to the time step (RMS proportional to $\sqrt{\Delta t}$), one-dimensional Brownian motion (a special case of a scalar diffusion process) results. Originally, the term *Brownian motion* was used to describe the physical motion of a pollen grain suspended in a fluid. The mathematical idealization of this motion as a diffusion process is only accurate up to a certain point.

A diffusion process is so irregular that even though it is continuous, it is never differentiable. No physical process is capable of such irregular motion with a finite amount of energy. Even the pollen grain would be seen to have some differentiable displacements if the time resolution of the observations were fine enough.

The usefulness of the diffusion model lies in the fact that in many practical applications we are not interested in the small, micro-scale behavior of the process, but are only interested in time increments large enough that the increment truly does depend on only the current value of the process and is conditionally independent of past increments [Lin, 1986]. This *Markov* property, that the change in the process can be predicted by the current value of the process alone, is the one that makes a diffusion model tractable. The long term behavior of the physical process can be identical to the idealized mathematical diffusion model even though the process is not ideally diffusive within each time increment.

This random process is called a diffusion process because the time variation of the distribution of probability obeys the *diffusion* equation, which governs both diffusive heat transfer and diffusion of contaminant. The connection between these physical processes and the diffusion of probability may be illustrated with an example. Suppose a quantity of contaminant is injected into an originally homogeneous medium. Particles of contaminant are transported by two mechanisms, drift of the medium and diffusion of contaminant through the medium. Some time after the initial injection, the contaminant will be spread throughout the medium and the concentration will be a function of position depending on the drift and diffusivity.

The path of each particle injected into the medium is one possible path for any single particle injected at the same time and place. Injecting millions of particles at one time and observing the concentration at some future time is equivalent to running millions of experiments with a single particle injected each time and observing the destination of that particle at the same time lag. The probability that a single particle ends up in any designated zone of the material after a given time lag is equal to the relative frequency that lone particles in millions of repeated experiments end up in that zone, which is in turn proportional to the concentration of contaminant in the zone after millions of particles have been injected all at once. Just as the total amount of contaminant summed over the entire medium must remain equal to what was initially injected, the total probability of the destination of a single particle must sum to unity.

Concentration of contaminant is therefore analogous to the probability density of the destination of a single particle. A more extensive, non-mathematical description of diffusion processes is presented in the February, 1985 issue of *Scientific American* [Lavenda, 1985].

The diffusion equation for the probability density at *location* X at *time* t, $p(X,t)$, is

$$\frac{\partial}{\partial t} p(X,t) = -\frac{\partial}{\partial X}(\eta(X,t)\, p(X,t)) + \frac{1}{2}\frac{\partial^2}{\partial X^2}(d(X,t)\, p(X,t)) \qquad (5.1)$$

where $\eta(X,t)$ is the drift and $d(X,t)$ is the diffusivity. (Eq. 5.1 is known as the Fokker-Plank equation, or Kolmogorov's forward equation.) If $X(0)= 0$ and the drift and diffusivity remain constant, the solution, $p(X,t)$, is the Gaussian PDF, where the mean is $(\eta\, t)$ and the variance is $(d\ t)$.

Diffusion models are possible for many physical processes, including those that can be described by a differential equation of the form

$$\frac{dX(t)}{dt} = g(X) + h(X)F(t) \qquad (5.2)$$

in which $g(X)$ and $h(X)$ are functions of state and $F(t)$ is the (random) external excitation. The form of the solution will depend on $g(X)$, $h(X)$, statistics of $F(t)$, and the boundary conditions. From here on, $g(X)$ and $h(X)$ (and hence η and d) are assumed to be *homogeneous,* i.e., they do not depend explicitly on time.

The crack growth equation fits the form of Eq. 5.2 and is therefore amenable to diffusion modeling. The basic form of the crack growth equation is

$$\frac{da(t)}{dt} = C(\sqrt{\pi a}\, Y(a)\Delta S_{eff}(t))^b \qquad (5.3)$$

The change from da/dN to da/dt is merely notational because *time* can be measured in cycles; time and cycles will be used interchangeably throughout this chapter. Each possible sample of crack length as a function of number of loading cycles (time) is like each of the possible paths of a particle of contaminant. The probability of reaching the critical crack length within a given number of cycles is analogous to the fraction of the total contaminant which has passed some barrier at a given time.

Defining an equivalent random forcing function for the diffusion model of the crack growth equation (Eq. 5.3) will depend on what random aspect of the crack growth problem is to be modeled. Lin and Yang [1983] model randomness

in material properties by defining the crack growth as a Poisson pulse process that produces a mean drift (which is a function of crack length) and a diffusive effect due to material variability. Oh [1980] models both random material properties and random loading to solve the (sequenceless) crack growth problem. Dolinski [1986] estimates crack growth with sequence effects using a Wheeler retardation model. No comparisons of Dolinski's results with either tests or simulations are available.

In this chapter solutions for the time to grow a crack from initial to final lengths are investigated with diffusion models that include load sequence effects. The case of constant amplitude loading with random overloads is analyzed using the backward equation, which is the adjoint to Eq. 5.1. The steady-state distribution of the reset stress (defined in Chapter 2) is approximated for stationary random loading using the forward equation (Eq. 5.1). Vector diffusion models of crack growth due to random loading, with sequence effects, are also discussed.

5.2 Drift and Diffusivity

Solutions for the possible outcomes of a diffusion process depend on the specification of the drift, $\eta(X)$, and diffusivity, $d(X)$. In the contaminant example, the drift is analogous to the flow of the medium into which the contaminant has been injected and the diffusivity is analogous to the diffusion of the contaminant through the medium. Each may be a function of position if, for example, the medium is a fluid flowing in a nonuniform channel (which varies the drift) while the temperature is changing (varying the diffusivity). In terms of the flow of probability, the drift represents the average increment in the process while the diffusivity represents the variance in the increment in the process.

For physical processes that can be described by differential equations with the form of Eq. 5.2, an equivalent diffusion process is obtained by defining $\eta(X)\Delta t$ to be the average value of $\Delta X = X(t+\Delta t) - X(t)$ given the current value of X, and $d(X)\Delta t$ to be the expected value of ΔX^2 given X:

$$\eta(X) = \lim_{\Delta t \to 0} \frac{E[\Delta X \mid X]}{\Delta t} \tag{5.4}$$

$$d(X) = \lim_{\Delta t \to 0} \frac{E[\Delta X^2 \mid X]}{\Delta t} = \lim_{\Delta t \to 0} \frac{Var[\Delta X \mid X]}{\Delta t} \tag{5.5}$$

The expected value of ΔX^2 is equal to the variance of ΔX (which is of order Δt) plus the squared mean of ΔX (which is of order Δt^2). In the limit, the mean square contribution goes to zero and $d(X)\Delta t$ is equal to the variance of ΔX

given the current value of X.

A random process has the Markov property, and is therefore a *diffusion* process, only if the external excitation is uncorrelated in time, i.e., a *white noise* excitation. White noise is a mathematical abstraction that does not exist in nature. Any real excitation will have to be represented by an equivalent white noise process model which can be obtained from the true process by Stratonavitch's method of stochastic averaging [Stratonavitch, 1963; Lin, 1986]. The equivalent white excitation must have the same *intensity* as the real forcing function, whose intensity, I_F, is defined to be the integral of the autocorrelation function, $R_F(\tau)$:

$$I_F = \int_{-\infty}^{\infty} R_F(\tau) d\tau = \sigma_F^2 \, \theta_F = S_F(0) \tag{5.6}$$

where σ_F^2 is the variance of $F(t)$, θ_F is (as defined in Chapter 3) the correlation time of the real $F(t)$, and $S_F(0)$ is the PSD of $F(t)$ at zero frequency. Thus, the *equivalent* white noise model for $F(t)$ preserves its intensity and, therefore, preserves the product $\sigma_F^2 \theta_F$ although σ_F^2 and θ_F go to infinity and zero respectively for white noise. By matching the actual intensity of the excitation, the white noise model preserves its low frequency content, which governs the long run behavior of Eq. 5.2. The exact description of $R_F(\tau)$ is not required, only the variance and the correlation time of the excitation are needed. This approximation restricts the validity of the diffusion model to time intervals greater than θ_F.

The *equivalent* diffusivity, $d(X)$, is given by the variance of the right hand side of Eq. 5.2 with the *equivalent* white excitation,

$$d(X) = h^2(X) \, I_F \tag{5.7}$$

The *equivalent* drift is given by the expected value of the right hand side of Eq. 5.2

$$\eta(X) = g(X) + h(X) \, E[F(t)] + \frac{1}{4} d'(X) \tag{5.8}$$

where the prime denotes differentiation with respect to the argument of the function. The last term in Eq. 5.8 is a correction for *feedback* due to diffusive changes in the process within Δt, called *parametric excitation* by Lin [1986].

Armed with the appropriate drift and diffusivity, it is possible to solve the forward equation (Eq. 5.1) for the distribution, $p(X,t)$, as will be shown in

section 5.4. In the next section, the adjoint to the forward equation, known as the backward equation, will be used to determine statistics of first passage times, such as the first passage of crack length beyond the critical length.

5.3 First Passage Statistics and the Backward Equation

The adjoint to the forward equation is the backward equation, which is given by

$$-\frac{\partial}{\partial t_o} p(X,t \mid X_o,t_o) = \eta(X_o)\frac{\partial}{\partial X_o} p(X,t \mid X_o,t_o) + \frac{d(X_o)}{2}\frac{\partial^2}{\partial X_o^2} p(X,t \mid X_o,t_o) \tag{5.9}$$

where $p(X,t \mid X_o,t_o)$ is the PDF of the value of the process at time t given that the value of the process was X_o at time t_o. The integral of $p(X,t \mid X_o,t_o)$ over all X inside the boundary yields the probability that the process has not passed out of the boundary before t, (assuming X_o is inside the boundary and the boundary is *absorbing,* i.e., the process does not leave the boundary once it reaches it). Upon integrating Eq. 5.9 with respect to X, the CDF, $P(t \mid X_o,t_o)$ and complimentary CDF, $G(t \mid X_o,t_o)= 1-P(t \mid X_o,t_o)$, of the first passage time, t, given the initial state, X_o, at time ,t_o, are shown to be solutions to the backward equation as well (with appropriate adjustments to the boundary conditions). Integrating again with respect to the first passage time, t, and applying the boundary condition that the time to the boundary is zero if the process starts on the boundary, yields [Sahay and Lennox, 1974]

$$-n\,\mu_{n-1}(X_o) = \eta(X_o)\,\mu_n{}'(X_o) + \frac{1}{2}\,d(X_o)\,\mu_n{}''(X_o) \qquad n=1,2,3,\cdots \tag{5.10}$$

where $\mu_n(X_o)$ is the n^{th} moment of the time to first passage starting from X_o given by

$$\mu_n = \int_0^\infty t^n\, p(t)dt = \int_0^\infty t^{n-1} G(t)dt \tag{5.11}$$

(The latter form is obtained through integration by parts.) Since $\mu_0= 1$ by definition, the average time to first passage, μ_1, can be found first from Eq. 5.10. The higher moments of the first passage time can then be calculated recursively from the lower moments.

A differential equation for the variance, $V = \mu_2 - \mu_1^2$, is produced by multiplying Eq. 5.10 with $n = 1$ by $2\mu_1$ and subtracting it from Eq. 5.10 with $n = 2$. The result is (dropping the explicit statements of functional dependence on X_o for brevity)

$$0 = \eta(\mu_2' - 2\mu_1\mu_1') + \frac{d}{2}(\mu_2'' - 2\mu_1\mu_1'') \tag{5.12}$$

Substituting $V' = (\mu_2' - 2\mu_1\mu_1')$ and $V'' = \mu_2'' - 2(\mu_1'^2 + \mu_1\mu_1'')$ into Eq. 5.12 yields

$$-d(\mu_1')^2 = \eta V' + \frac{d}{2} V'' \tag{5.13}$$

which has the same form as Eq. 5.10. Eqs. 5.10 and 5.13 (for mean and variance) will therefore often have very similar solutions.

The nature of the first passage problem will determine the type of boundary conditions on the differential equations. All moments of the time to reach a boundary are zero if the process starts at a boundary. In many first passage problems, there are boundaries to the left and to the right, which provide the two boundary conditions necessary to define the solution to the second order differential equation (Eq. 5.10). For the crack growth problem, there is only one boundary at the final crack length, $a = a_f$. The other boundary ($a = 0$) is physically *inaccessible,* i.e., even though the diffusion model allows small increments of negative crack growth, the time required to grow to negative crack lengths is infinite [Karlin and Taylor, 1981]. These two boundary conditions are

$$\mu_n(a_f) = 0 \qquad \text{and} \qquad \lim_{a \to 0} \mu_n'(a) e^{U(a)} = 0 \qquad n = 1,2, \cdots \tag{5.14}$$

in which $e^{U(a)}$ is the integrating factor for Eq. 5.10 and $U(a) = \int_a^{\cdot} (2\eta(u)/d(u))du$. The limit is necessary because while the integrating factor will be zero at $a = 0$, the derivative of the time to first passage may be infinite, as it is in this case. The limit of the product of the two as a approaches the boundary will determine the boundary behavior.

In first passage problems (like crack growth) where the time to the boundary is highly sensitive to the starting value (initial crack length) and much less sensitive to the boundary value (final crack length), some useful approximations can be made. The mean and variance of the time to first passage are approximated by

$$\mu_1(a_o) \approx \int_{a_o}^{a_f} \frac{da}{\eta_o(a)} \tag{5.15}$$

$$V(a_o) \approx \int_{a_o}^{a_f} \frac{d(a)}{\eta_o^3(a)}\, da \tag{5.16}$$

where η_o is the drift without the parametric excitation term; $\eta = \eta_o + (d'/4)$. These approximations are especially useful when closed form solutions to the first passage moments are not possible and numerical methods must be employed. Also, Eqs. 5.15 and 5.16 are exact when the $g(X)$ term in the drift (Eq. 5.8) is zero.

Sequenceless Crack Growth Example: As an example of the diffusion modeling approach for calculating the statistics of the time to fail due to fatigue crack growth under random loading, consider sequenceless crack growth due to narrow-band random loading with zero mean stress. A sequenceless crack growth equation is given by Eq. 5.3 with $\Delta S_{eff} = (1-q)S$, where $S = S_{\max}$ is the stress peak (see also Eq. 4.4) [Nelson, 1978]. For simplicity, let $Y(a) = 1$ and define $\tilde{C} = C(\sqrt{\pi}(1-q))^b$. The mean time to failure for this case can be obtained from previous results; the sequenceless random variable model of Chapter 4 yields a closed form solution by integrating Eq. 4.6:

$$\mu_1(a_o) = \frac{a_o^{-p} - a_f^{-p}}{p\tilde{C}E[S^b]} \tag{5.17}$$

where $p = (b/2) - 1$ is a commonly occurring term in the solution of the crack growth equation.

The crack growth equation that fits the form of Eq. 5.2 for this case is

$$\frac{da}{dt} = \tilde{C}a^{b/2}S^b \tag{5.18}$$

The coefficients in Eq. 5.2 in this case become

$$g(a) = 0 \tag{5.19a}$$

$$h(a) = \tilde{C}a^{b/2} \tag{5.19b}$$

$$F(t) = S^b(t) \tag{5.19c}$$

The drift and diffusivity are determined by substituting Eqs. 5.19 into Eqs. 5.7 and 5.8:

$$\eta_o(a) = \tilde{C}E[S^b]a^{b/2} \tag{5.20a}$$

$$d(a) = \tilde{C}^2 I_{S^b} a^b \tag{5.20b}$$

$$\eta(a) = \eta_o(a) + \frac{1}{4} d'(a) \tag{5.20c}$$

The intensity of the forcing function in Eq. 5.19c is calculated from the Rayleigh distributed stress peaks raised to the b^{th} power, $I_{S^b} = Var[S^b]\theta_{S^b}$. For crack growth applications, b is typically between 2 and 4. When $b = 2$, the intensity is the same as that of the *energy* envelope discussed in Chapter 3, which has an exponential marginal distribution. The correlation time is then $\theta_{S^2} = \theta_E$. For the exponentially distributed S^2, the COV equals one and the variance is equal to the squared mean, $Var[S^2] = E[S^2]^2$. When b is not equal to 2, the correlation and variance can be estimated by a modal expansion of $S^b(t)$ [Winterstein, 1984]. Retaining the first two modes, the intensity is approximated by

$$I_{S^b} \approx \theta_E E[S^b]^2 \left(\frac{b}{2}\right)^2 \left[1 + \frac{1}{8}\left(\frac{b}{2} - 1\right)^2\right] \tag{5.21}$$

Eq. 5.21 is exact for $b = 2$ and $b = 4$ and underestimates the exact intensity by less than 10% for $b \leq 8$. The expected value of S^b is

$$E[S^b] = (\sqrt{2}\sigma_X)^b (b/2)! \tag{5.22}$$

which is the same as was stated in Chapters 3 and 4 except for a factor of 2^b because S is a stress peak here while the earlier results were for stress ranges.

Substituting the drifts and diffusivities into Eq. 5.10 yields the differential equation for the mean first passage time. The independent variable is the initial crack length, a_o.

$$-1 = (\tilde{C}E[S^b]a_o^{b/2} + \frac{b}{4}\tilde{C}^2 I_{S^b} a_o^{b-1})\mu_1'(a_o) + \frac{1}{2}\tilde{C}^2 I_{S^b} a_o^b \mu_1''(a_o) \tag{5.23}$$

The previously obtained solution (Eq. 5.17) satisfies the boundary conditions (Eq. 5.14) and can be shown by direct substitution to satisfy the differential equation (Eq. 5.23) for the mean first passage time of the diffusion model. The diffusion model therefore gives the same result as the random variable model for the average time to failure. Because $g(a) = 0$ in this case, Eq. 5.15 could alternatively have been used (with η_o from Eq. 5.20a) to obtain the exact result, i.e., Eq. 5.17.

The variance of the time to reach the final crack length, $V(a_o)$, is governed by Eq. 5.13. After substituting the appropriate terms into Eq. 5.13, the

differential equation for the variance is

$$-\tilde{C}^2 a_o^b I_{S^b}\left(\frac{-a_o^{-p-1}}{\tilde{C}E[S^b]}\right)^2 = (\tilde{C}E[S^b]a_o^{b/2} + \frac{b}{4}\tilde{C}^2 I_{S^b} a_o^{b-1})\,V'(a_o) + \frac{1}{2}\tilde{C}^2 I_{S^b} a_o^b\,V''(a_o) \qquad (5.24)$$

which is identical to Eq. 5.23 except for the left hand side, which reduces to $-I_{S^b}/E[S^b]^2$. The boundary conditions on the variance are the same as for the mean time to fail.

The solution of Eq. 5.24 for the variance has the same form as the solution for the mean (Eq. 5.17) and can be written in terms of μ_1:

$$V(a_o) = \mu_1(a_o)\frac{I_{S^b}}{E[S^b]^2} = \mu_1(a_o)\theta_E\left(\frac{b}{2}\right)^2\left[1 + \frac{1}{8}\left(\frac{b}{2}-1\right)^2\right] \qquad (5.25)$$

Once more, because $g(a)=0$, Eq. 5.16 also gives an exact solution.

The variance of the time to fail increases linearly with the mean time to fail which makes the COV (ratio of standard deviation to mean) decrease as the square root of the time to fail. The relative variability in the time to fail due to the randomness in the loading goes to zero as the mean life increases when sequenceless crack growth analysis is employed. The same phenomenon occurs in Palmgren-Miner fatigue damage [Crandall and Mark, 1973].

5.4 Crack Growth with Distinct Overloads

The most clearly identified and often investigated situation in which retardation effects in fatigue crack growth are evident is the case where there is a single overload, or a cluster of overloads, in the presence of smaller amplitude loading. Examples include aircraft that experience overloads during landings after random flight lengths, or off-shore structures that experience brief periods of intense loading during hurricanes or other storms. This is the case of *distinct overloads,* which was the basis of the simulation study in Section 4.6. In this section, a scalar diffusion model is used to determine the mean and variance of the time to failure for the distinct overloads case.

As in Chapter 4, suppose that the background stress is a constant amplitude loading between zero and S and that overloads with a tensile magnitude of S_{ol} arrive at an average rate λ, as shown in Fig 5.1. The probability of an overload arriving in any small time interval is constant and independent of the time

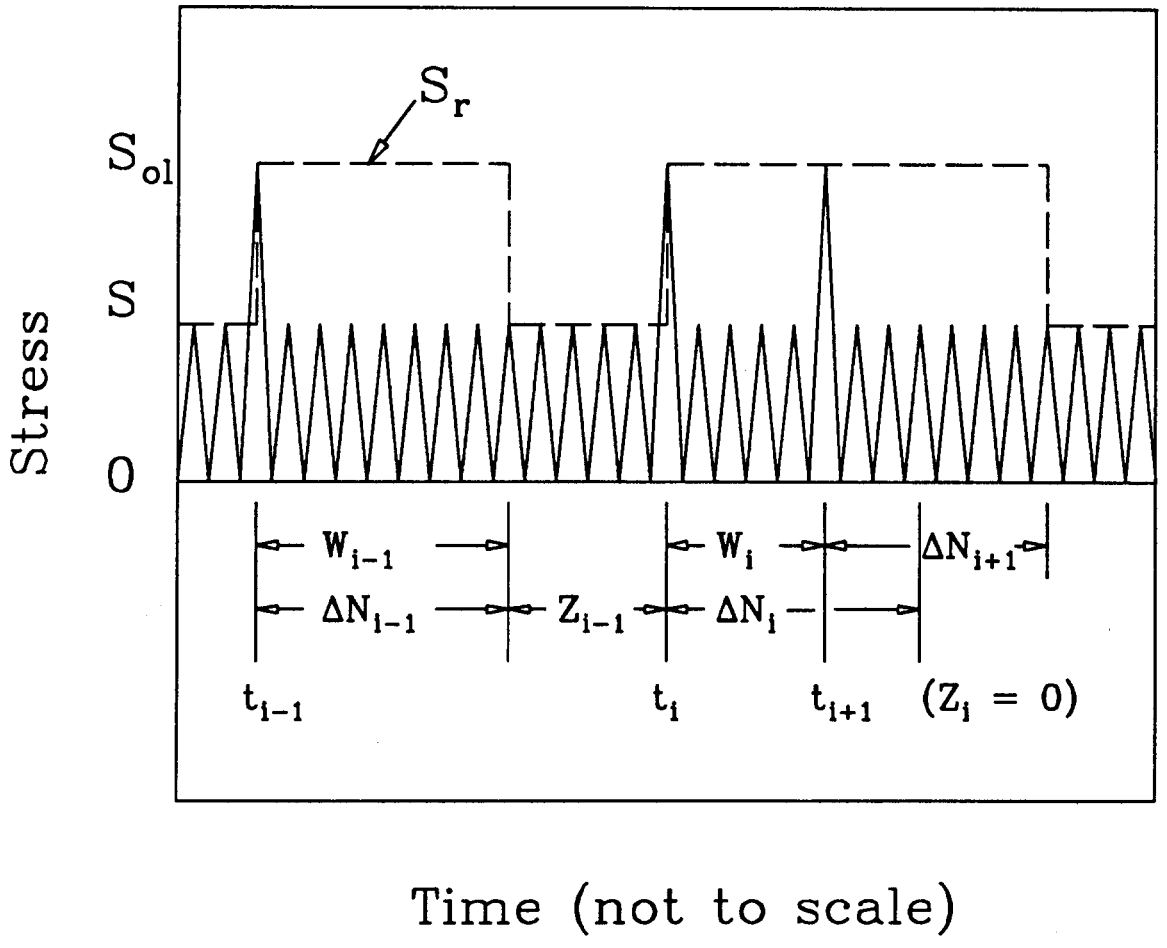

Fig. 5.1 The time between overload arrivals is split into retarded ($S_r = S_{ol}$) and unretarded ($S_r = S$) parts. The duration of the retarded part is W and the duration of the unretarded part is Z. (Actual numbers of cycles between overloads would be much greater than illustrated.)

since the last arrival, which implies that the times between arrivals will be independent and exponentially distributed (i.e., the overload arrivals follow a Poisson process with a COV of overload interarrival times equal to 1.0). The reset stress in the absence of overloads equals the maximum stress, S. At the time of an overload, the reset stress increases to S_{ol} and is assumed to remain there until the background loading causes the crack tip plastic zone to extend beyond the overload induced crack tip plastic zone (see Fig. 2.1). The distance the crack must grow between the time and the time the reset stress increases to S_{ol} and returns to S equals the difference in the sizes of the crack tip plastic zones created by stress peaks S_{ol} and S. This distance, (shown in Fig 5.2) is defined as Δa_{eff};

$$\Delta a_{eff} = d_{ol} - d_p = aY^2(a)\frac{S_{ol}^2 - S^2}{\gamma S_y^2} \tag{5.26}$$

where S_y is the yield stress, γ is the plane strain constraint factor, and $Y(a)$ is the geometric correction to the stress intensity factor.

After an overload occurs, the crack growth rate, given by Eq. 5.3, is *retarded* and $\Delta S_{eff} = S - qS_{ol}$. In the absence of overloads, the crack growth rate is *unretarded* and $\Delta S_{eff} = S - qS$. This simplification to the more general crack growth model of Chapter 2 allows the crack growth rate to be expressed as in one of two states; retarded when $(da/dt) = C_r Y^b(a) a^{b/2}$ or unretarded when $(da/dt) = C_u Y^b(a) a^{b/2}$, where

$$C_u = C\pi^{b/2}(S - qS)^b \tag{5.27a}$$

$$C_r = C\pi^{b/2}(S - qS_{ol})^b \tag{5.27b}$$

It is assumed here that $qS_{ol} < S$, i.e., the crack opening stress is less than the background stress peaks (no crack arrest).

The duration of the retarded crack growth is $N(a)$ cycles of background loading (see Figs. 5.1 and 5.2), which is a function of current crack length. If a second overload arrives before $N(a)$ cycles of background loading, the reset stress remains at S_{ol} for $N(a)$ cycles following the second overload. $N(a)$ is approximated by dividing Δa_{eff} (Eq. 5.26) by the retarded crack growth rate:

$$N(a) \approx \frac{\Delta a_{eff}}{(da/dt)} = a^{-p} Y^{2-b}(a)\frac{(S_{ol}^2 - S^2)}{\gamma S_y^2 C_r} \tag{5.28}$$

where, as before, $p = (b/2) - 1$.

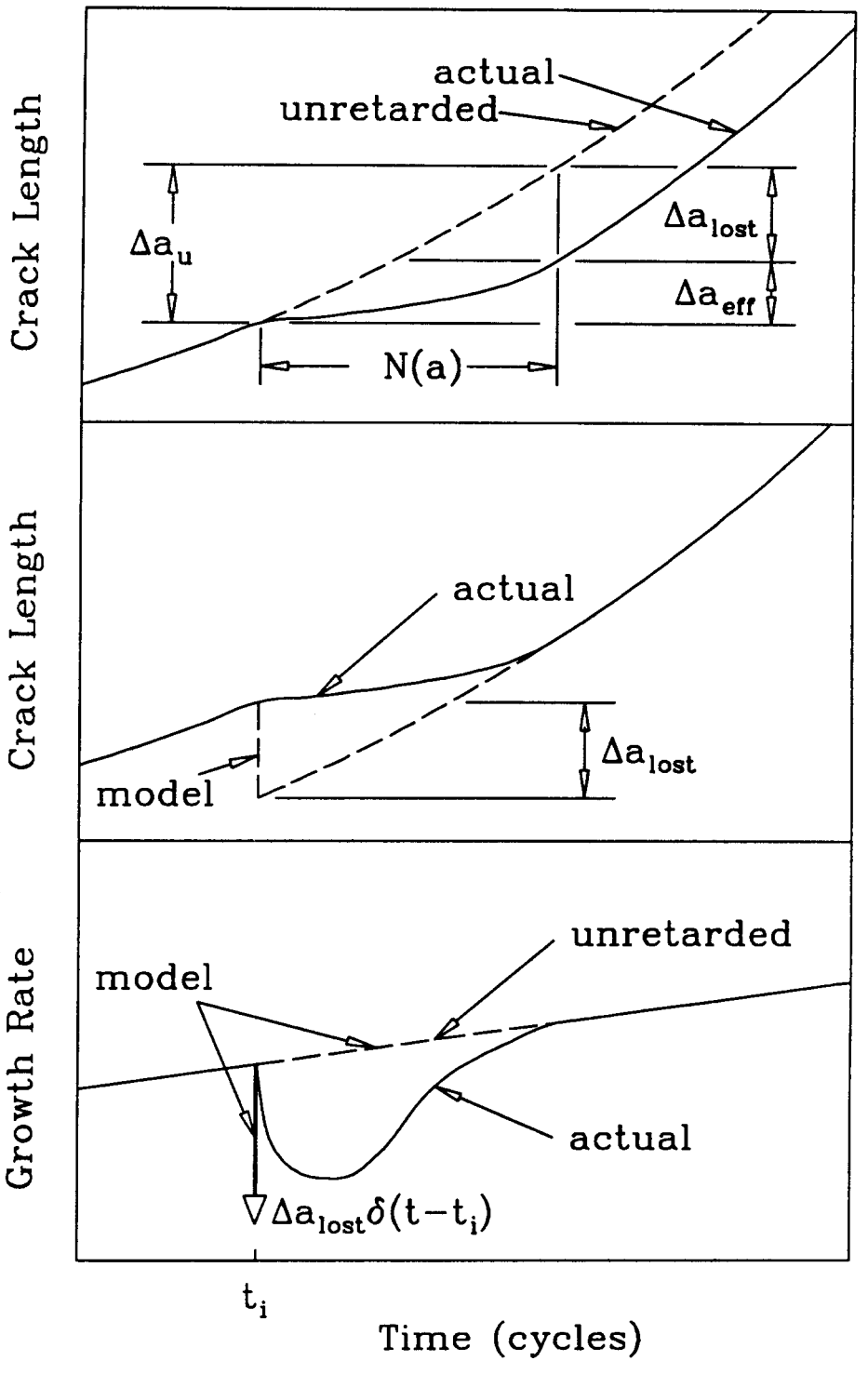

Fig. 5.2 Schematic of modeling assumption that lumps the entire retardation effect of an overload at the time of application, t_i. Top: actual and unretarded crack length vs time. Center: crack length vs time showing the modeling assumption of subtracting the retardation effect at the time of application. Bottom: indication of how the crack growth rate is modeled by a Dirac delta function corresponding to the step change in crack length.

The distance that the crack would have grown in $N(a)$ cycles at the unretarded rate is approximately

$$\Delta a_u = N(a)\, C_u\, Y^b(a)\, a^{b/2} \tag{5.29}$$

The difference between the distance the crack would have grown, Δa_u and the actual distance the crack grew, Δa_{eff}, is the crack growth which is lost due to retardation effects, as shown in Fig 5.2;

$$\Delta a_{lost} = \Delta a_u - \Delta a_{eff} = a\, Y^2(a) \frac{S_{ol}^2 - S^2}{\gamma S_y^2} \left[\frac{C_u}{C_r} - 1\right] \tag{5.30}$$

$$= N(a)(C_u - C_r) Y^b(a)\, a^{b/2}$$

If overload affected zones rarely overlap ($\lambda N(a) >> 1$), the crack growth process can be modeled by lumping the full effect of each overload at the time the overload arrives. The modeling assumption is that the crack always grows at the unretarded rate except at the arrival of each overload when there is a step change equal to $-\Delta a_{lost}$. The crack growth rate is expressed mathematically by inserting a delta function (infinite rate) with a magnitude equal to the length of the step at the arrival of each overload;

$$\frac{da}{dt} = C(\pi a)^{b/2}(S - qS)^b - \sum_i \Delta a_{lost_i}\, \delta(t - t_i) \tag{5.31}$$

where $\delta(t - t_i)$ is the Dirac delta function and t_i is the time (cycle) at which the i^{th} overload occurs (see Fig. 5.2). This equation neglects the contribution of the overloads to crack growth, which is negligible in most cases of interest, as will be shown below.

The restriction that the overload affected zones not overlap is an important one because overload effects are not additive. When the overload affected zones do overlap, the net retardation is less than would be predicted by simply subtracting Δa_{lost} when each overload arrives. Therefore, the amount of crack length subtracted at the arrival of each overload must be adjusted to reflect the actual crack growth until the next overload.

There are two limiting cases that will be investigated here. The first case, which builds on the above discussion, assumes that the crack growth rate is usually unretarded and that the overloads are relatively rare. The other case assumes the crack growth rate is usually equal to the retarded rate. In this case, overlapping is taken to be the standard event and the delta functions are used to

add crack growth to account for the time between overload affected zones when the crack growth rate is unretarded.

5.4.1 Case I - Rare Overloads.

In this case it is assumed that the background crack growth rate is unretarded. The retardation due to overloads is accomplished by subtracting increments of crack length at the arrival of each overload. The simple subtraction of an increment of crack length equal to Δa_{lost} will be correct if the durations of overload effects do not overlap, but it will overpredict retardation if overlaps do occur. This is corrected by introducing a random variable, W, which is the number of background cycles of retarded crack growth before the arrival of the next overload, as shown in Fig. 5.1. W will equal T if the overload arrives before the effect of the previous overload has died out and will equal the duration of the overload effect, $N(a)$, if there is no overlap:

$$W = min(T, N(a)) = \begin{cases} T & T < N(a) \\ N(a) & T \geq N(a) \end{cases} \tag{5.32}$$

For Poisson overload arrivals, the PDF of interarrival times is exponential with mean equal to $1/\lambda$;

$$p(T) = \lambda e^{-\lambda T} \qquad (T \geq 0) \tag{5.33}$$

The PDF of the random variable, W, is the same as for T except for a probability mass at $W = N(a)$ and zero probability of $W > N(a)$. The probability of $W = N(a)$ equals the probability that $T > N(a)$;

$$Prob[T > N(a)] = \int_{N(a)}^{\infty} \lambda e^{-\lambda T} dT = e^{-\lambda N(a)} \tag{5.34}$$

The PDF of W is therefore

$$p(W) = \begin{cases} 0 & W > N(a) \\ \lambda e^{-\lambda W} + e^{-\lambda N(a)} \delta(W - N(a)) & 0 \leq W \leq N(a) \end{cases} \tag{5.35}$$

The size of the crack growth increment associated with the arrival of an overload for Case I (Δa^I) is equal to the difference in the unretarded background crack growth and the retarded crack growth during the W cycles that the overload has an effect. The (negative) crack growth increment is therefore

$$\Delta a^I = W(C_r - C_u) Y^b(a) \, a^{b/2} \tag{5.36}$$

The crack growth rate equation which accounts for overlaps is

$$\left(\frac{da}{dt}\right)^I = C_r Y^b(a)\, a^{b/2} - (C_u - C_r) Y^b(a)\, a^{b/2} \sum_i W_i \delta(t - t_i) \qquad (5.37)$$

The overlapping of overload affected zones is modeled here by associating the retardation effect of each overload with its actual duration W_i, the minimum of the time to grow through the overload affected zone, $N(a)$, and the time to the next overload, T.

5.4.2 Case II - Frequent Overloads.

In this limiting case, the overloads are assumed to be frequent enough that the usual, or standard, crack growth rate is the retarded crack growth rate. Discrete increments of crack growth are added to account for the time between overload affected zones when the crack growth rate returns to the unretarded rate.

It is useful to define a random variable, Z, equal to the time between the end of one overload effect and the arrival of the next overload;

$$Z = max(T - N(a), 0) = \begin{cases} T - N(a) & T \geq N(a) \\ 0 & T < N(a) \end{cases} \qquad (5.38)$$

Z is related to W from Case I by $T = W + Z$. Like W, Z has the same PDF as the interarrival time, T, except that there is a probability mass at $Z = 0$ which accounts for the times when $T < N(a)$.

$$Prob[T < N(a)] = 1 - Prob[T \geq N(a)] = 1 - e^{-\lambda N(a)} \qquad (5.39)$$

The PDF of Z is therefore

$$p(Z) = \lambda e^{-\lambda(Z + N(a))} + (1 - e^{-\lambda N(a)})\delta(Z) \qquad (Z \geq 0) \qquad (5.40)$$

The added increment in crack growth, Δa^{II}, is equal to the difference between the retarded crack growth (which is the norm in this case) and the actual unretarded growth during the time, Z, when the retardation is not in effect.

$$\Delta a^{II} = Z(C_u - C_r) Y^b(a)\, a^{b/2} \qquad (5.41)$$

The crack growth rate is again given by the sum of a continuous function of crack length and delta functions in crack growth rate associated with each step change in crack length.

$$\left(\frac{da}{dt}\right)^{II} = C_r\, Y^b(a)\, a^{b/2} + (C_u - C_r) Y^b(a)\, a^{b/2} \sum_i Z_i \delta(t - t_i) \qquad (5.42)$$

No overlaps need to be considered in this case because the overlap is the standard event. It is only the spaces between overload affected zones that lead to incremental perturbations to the standard crack growth.

5.4.3 Diffusion Model of Discrete Overloads.

By lumping the entire retardation effect at the time of the overload, the model of the crack growth process is independent of the past, allowing the crack growth to be approximated as a diffusion process. Both of the above limiting cases result in crack growth equations that are in the form of Eq. 5.2. The drifts and diffusivities depend on the non-constant coefficients of this equation, which are given for each of the limiting cases as follows (recall that $C_u > C_r$ because the unretarded growth rate is greater than the retarded growth rate):

Case I -

$$g^I(a) = a^{b/2} Y^b(a) C_u \qquad (5.43a)$$

$$h^I(a) = -a^{b/2} Y^b(a)(C_u - C_r) \qquad (5.43b)$$

$$F^I(t) = \sum_i W_i \delta(t - t_i) \qquad (5.43c)$$

Case II -

$$g^{II}(a) = a^{b/2} Y^b(a) C_r \qquad (5.44a)$$

$$h^{II}(a) = a^{b/2} Y^b(a)(C_u - C_r) \qquad (5.44b)$$

$$F^{II}(t) = \sum_i Z_i \delta(t - t_i) \qquad (5.44c)$$

The delta function representations of the forcing functions are similar to *shot noise* [Lin, 1967], which is the type of impulsive random loading that results from the continual impacting of *shot* on a structure. The mean effect of shot noise is equal to the product of the mean rate of arrivals and the average effect of each arrival:

$$E[F^I(t)] = \lambda E[W] = \lambda \int_0^\infty W\, p(W) dW = 1 - e^{-\lambda N(a)} \qquad (5.45a)$$

$$E[F^{II}(t)] = \lambda E[Z] = \lambda \int_0^\infty Z\, p(Z) dZ = e^{-\lambda N(a)} \qquad (5.45b)$$

The intensity of shot noise is equal to the product of the mean rate of arrivals and the mean square of the effect of each arrival:

$$I_{F^I} = \lambda E[W^2] = \frac{2}{\lambda}\,[1-(1+\lambda N(a))e^{-\lambda N(a)}] \tag{5.46a}$$

$$I_{F^{II}} = \lambda E[Z^2] = \frac{2}{\lambda}\,e^{-\lambda N(a)} \tag{5.46b}$$

In accordance with conventional stochastic averaging procedures [Stratonavitch, 1963], the expected values and intensities of $F(t)$ are evaluated conditional on the current state, a.

The non-parametric drifts and diffusivities for Cases I and II are

$$\eta_o^I(a) = a^{b/2}Y^b(a)[C_u - (C_u-C_r)(1-e^{-\lambda N(a)})] \tag{5.47a}$$

$$\eta_o^{II}(a) = a^{b/2}Y^b(a)[C_r + (C_u-C_r)e^{-\lambda N(a)}] \tag{5.47b}$$

$$d^I(a) = a^b\,Y^{2b}(a)(C_r-C_u)^2\frac{2}{\lambda}\,[1-(1+\lambda N(a))e^{-\lambda N(a)}] \tag{5.48a}$$

$$d^{II}(a) = a^b\,Y^{2b}(a)(C_u-C_r)^2\frac{2}{\lambda}\,e^{-\lambda N(a)} \tag{5.48b}$$

(Only the non-parametric drift is included here because it is the only part that is needed to use the approximations for the mean and variance of the first passage time given by Eqs. 5.15 and 5.16., which are applicable here because the solution depends most heavily on the initial crack length.)

The above drifts are exactly the same for each of the two formulations. In both cases, the drift reflects the relative amount of time that the crack growth rate is retarded or unretarded. Since that has been consistently formulated in both approaches, it is natural for the drifts to be equivalent. The different diffusivities reflect alternative ways of modeling the random contribution of increments in *retardation*, for Case I, or increments in *growth*, for Case II.

The mean and variance of the time required for a crack to grow from initial to final crack to lengths, a_o to a_f, are approximated by Eqs. 5.15 and 5.16, and plotted in Fig. 5.3 for a wide range of mean overload interarrival times. Also plotted are the results of the numerical simulations from Section 4.6. The Case I and Case II solutions are identical in the mean because of the equivalence of the drifts. The agreement between the diffusion model and simulation for the mean time to fail is excellent for all except very short interarrival times.

The simulations included crack growth due to the overloads while this contribution was neglected in the diffusion model. As Fig. 5.3 shows, this

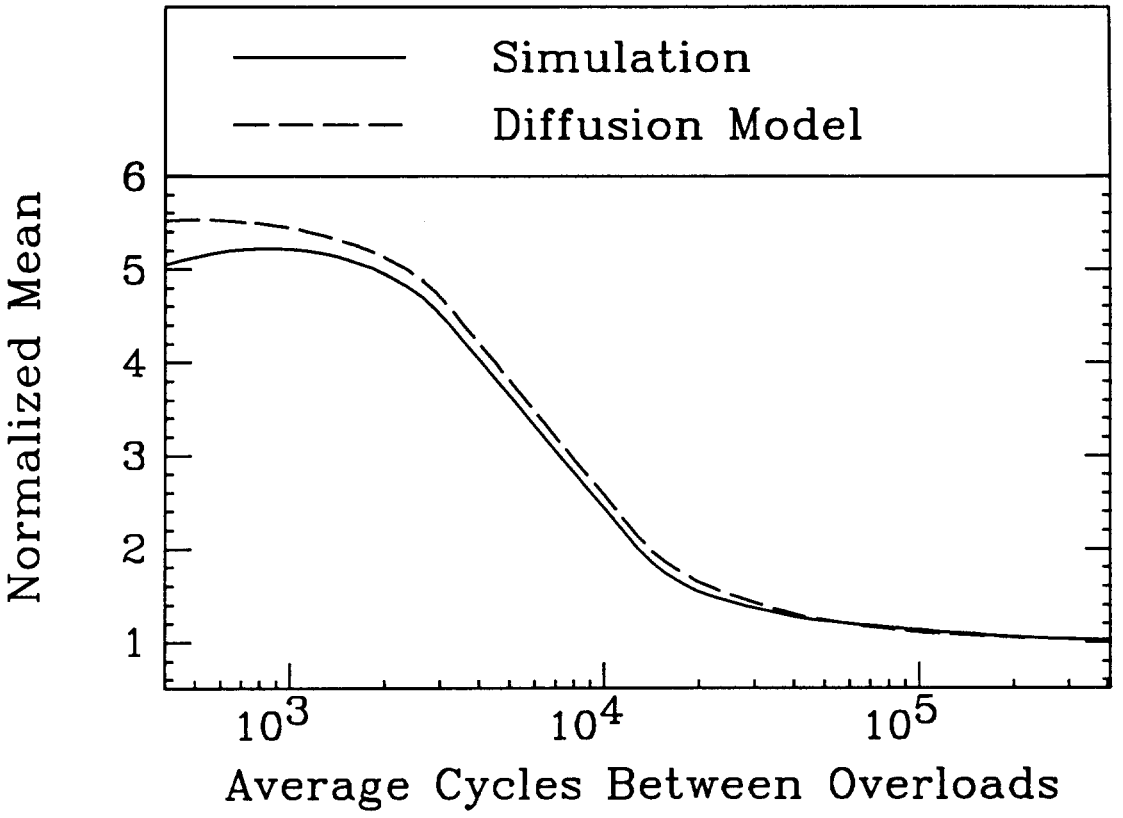

Fig. 5.3 Comparison of the mean time to failure, for constant amplitude loading with Poisson overloads, from simulation and from the scalar diffusion model.

contribution is negligible except at very frequent overloads where the crack growth rate is always retarded and the sequence effect is easily modeled. The diffusion solution can be adjusted to account for overload induced crack growth, in both cases, by adding $C(\pi a)^{b/2}Y^b(a)(S_{ol}-qS_{ol})^b\sum\delta(t-t_i)$ to both Eqs. 5.37 and 5.42.

The COVs of the first passage time, from the simulations and from both of the diffusion models, are plotted in Fig. 5.4. The two models differ in predicted variance, and hence in the predicted COV of time to fail. Each method matches the simulation COV in the region where deviations from the assumed background crack growth are not too frequent. Recall that Case I assumes unretarded crack growth with rare overloads; it matches the simulation where the mean interarrival times are long (rare overloads). Case II assumes frequent overloads with rare intervals of unretarded crack growth and matches the simulated COV in that region. Both methods overpredict the variance when the random step changes in crack length become the dominant contributor to crack growth.

The increments in crack growth in each case are carefully tailored to account for the appropriate amounts of retarded and unretarded crack growth. The Markov property of the diffusion model requires that there be no correlation between the size of one overload effect and the duration to the next overload. This condition is violated when the random variables W and Z are defined in terms of the next interarrival time, T, as shown in Fig 5.1. The results for the mean are still excellent, but the results for the variance are only good in regions where the solution is not dominated by incremental effects.

A good approximation to the COV can be obtained by combining the two cases so that each controls the COV in its own region of accuracy and a smooth transition is made in between. The combined COV, COV^{I+II}, is taken to be

$$COV^{I+II} = \left(\frac{1}{COV^{I}} + \frac{1}{COV^{II}}\right)^{-1} \tag{5.49}$$

The combined COV estimate remains accurate over the entire domain of interarrival times, as shown in Fig. 5.4.

5.4.4 Conclusions.

Based on analyses and simulations of cases with various overload sizes and material properties, a few *rules of thumb* can be stated:

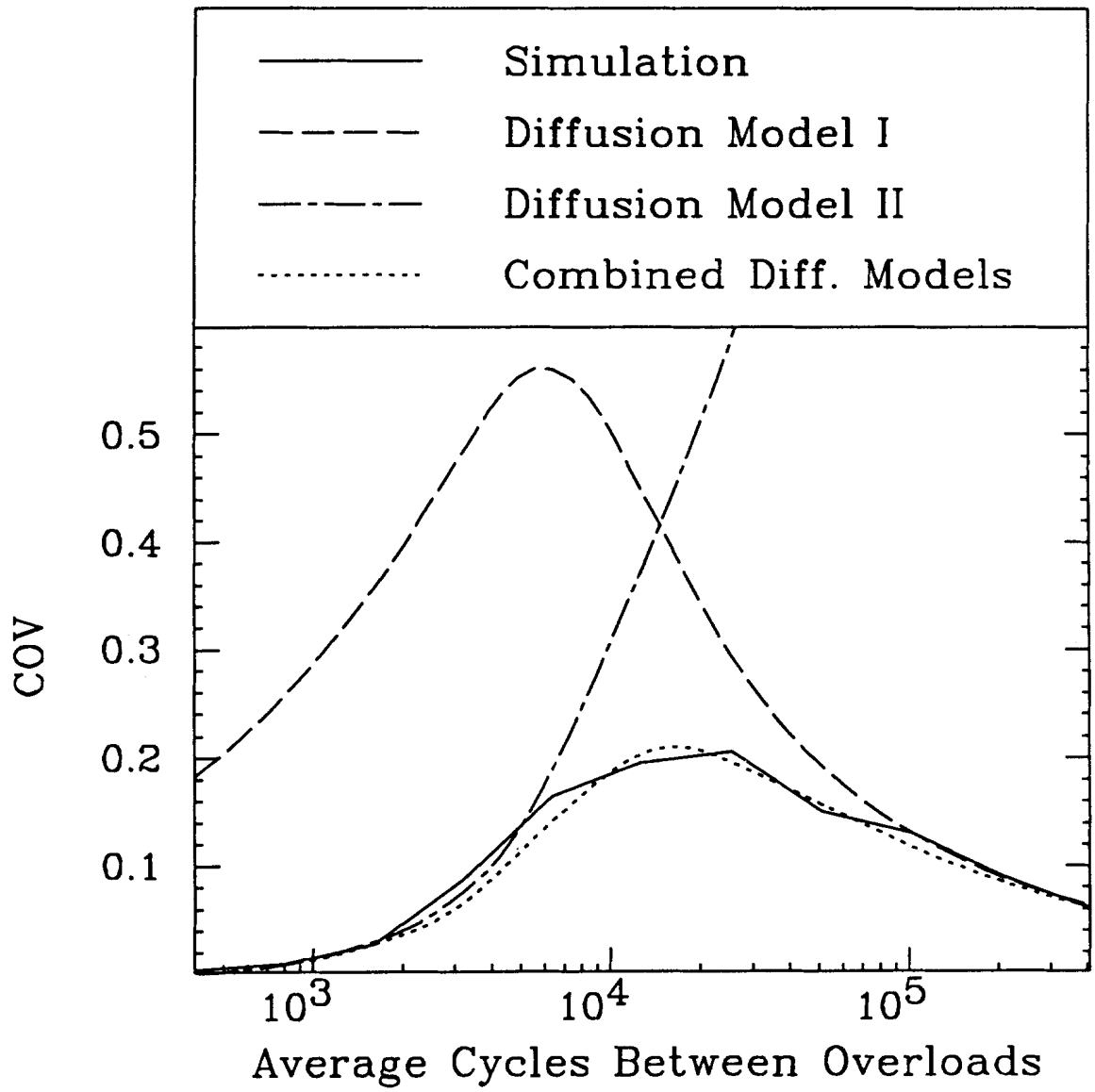

Fig. 5.4 Comparison of the COV of time to failure, for constant amplitude loading with Poisson overloads, from simulation and from each scalar diffusion model as well as a combination of the two.

(1) If $qS_{ol} < S$ (no crack arrest), the maximum life extension due to retardation effects is $(C_u / C_r) = [(S - qS)/(S - qS_{ol})]^b$.

(2) The maximum life extension occurs at a mean overload interarrival time, $1/\lambda$, between roughly $N(a_f)$ and $N(a_f)/2$. More frequent overloads do not add significant retardation, but they do begin to produce significant additional crack growth.

(3) The maximum COV of time to failure occurs at $1/\lambda$ between roughly $N(a_o)$ and $N(a_o)/2$.

By modeling the retardation effect of tensile overloads in fatigue crack growth as step changes in the crack length, a process that has an inherent memory effect can be modeled as a memoryless diffusion process. By appropriate *bookkeeping,* the equivalent drift and diffusivity are derived for use in the scalar backward equation. The statistics of the time required for the process to reach the final crack length can then be determined.

The primary assumption in this scalar model of crack growth is that the basic constant amplitude load model can be corrected by including simple *additive* corrections, namely: (I) corrections for rare overloads that cause retardation effects that rarely overlap; or (II) corrections for the rare times when there is no retardation, if overloads are frequent. Solutions for the mean first passage time are quite good even when these assumptions are not met, but solutions for the variance (and hence COV) are only accurate when the assumptions are reasonably accurate. By combining the two COV predictions, an approximate solution for the COV over the entire domain is possible.

Higher dimensional models (2D, 3D, etc...) can, in principle, model more general types of probabilistic memory and sequence effects with state variables that reflect the condition of the reset stress. In the next section, another scalar diffusion model is formulated to describe the variations in reset stress at any given crack length. Other states could include information on the loading making it possible to model more complex load processes. These *vector* diffusion models of first passage times are discussed in Section 5.7

5.5 Steady-State Distributions and the Forward Equation

In general, a crack growth prediction that includes sequence effects requires knowledge of both the current crack length and the current state of retardation as described by the *reset stress.* In the last section, a scalar diffusion model was

obtained by treating the retarded crack growth as negative increments in crack length. For the special case of Poisson (memoryless) arrivals of tensile overloads, the reset stress does not need to appear explicitly in the formulation and a scalar diffusion model is obtained.

Diffusion models can also be used to calculate statistics of steady-state processes. A random process is said to be in a *steady-state* condition when the PDF is independent of time, $p(X,t) = p(X)$. Equation 5.1 can then be reduced to a first order ordinary differential equation by integrating once with respect to X:

$$0 = \eta(X)\, p(X) - \frac{1}{2}\, \frac{d}{dX}\, (\, d(X)\, p(X)\,) \tag{5.50}$$

The general solution for the steady-state distribution, $p(X)$, of a scalar diffusion process depends on the integrating factor, $\exp[U(X)]$, introduced in Section 5.3:

$$p(X) = \frac{c}{d(X)} \exp[U(X)] \tag{5.51a}$$

where the integrating factor is the exponent of $U(X)$ given by

$$U(X) = \int^{X} \frac{2\eta(u)}{d(u)}\, du \tag{5.51b}$$

The constant of proportionality, c, is determined by the constraint that the total probability (area under $p(X)$) must sum to unity.

With the drift and diffusivity defined for all X, the steady-state distribution, $p(X)$, can be determined by Eq. 5.51. When the drift is linear in X and diffusivity is constant, $p(X)$ is Gaussian. When both drift and diffusivity are linear in X, $p(X)$ is exponential. As a practical matter, for more complicated drifts and diffusivities, numerical integration may be required to estimate the steady-state distribution.

In the next section, a scalar diffusion model of the reset stress is obtained by eliminating explicit dependence on crack length. Thus, the more general case of a stationary Gaussian random loading can be investigated by examining the process only at fixed crack lengths. By formulating the drift and diffusivity of the reset stress as it was defined in Chapter 2, a solution for the steady-state reset stress is obtained from the forward equation (Eq. 5.1). The steady-state reset stress distribution can then be calculated at integration points in crack length and the time to failure estimated by a double integration over reset stress and crack length.

5.6 Crack Growth due to Stationary Narrow-band Gaussian Loading

The reset stress is defined in Chapter 2 as the stress level necessary to produce a crack-tip plastic zone extending into material that had not previously been plastically deformed. Here, a_z is defined to be the maximum extent of the crack tip plastic zone so the reset stress plastic-zone diameter is $d_p = a_z - a$. The reset stress is given by substituting this expression for d_p into Eq. 2.2:

$$S_r = \left(\frac{(a_z - a)\gamma S_y^2}{a} \right)^{1/2} \tag{5.52}$$

(The stress intensity shape factor, $Y(a)$, has been set to unity for simplicity.) For purposes of determining the rate of decay of reset stress due to crack growth through the plastic zone, a_z can be considered constant. The reset stress is assumed to instantaneously increase to the value of the applied stress whenever a stress peak greater than the current reset stress is applied. The total rate of change of the reset stress is equal to a gradual reduction (decay) due to crack growth through the plastic zone plus positive increments (delta functions) due to large applied stress peaks.

The gradual reduction in reset stress, dS_r^-/dt, is determined by taking the derivative of Eq. 5.52 with respect to time, which gives the change in reset stress as a function of crack length, a, and the crack growth rate, da/dt (Eq. 5.3):

$$\frac{dS_r^-}{dt} = -(\gamma S_y^2)^{1/2} \left(\frac{a_z}{a} - 1 \right)^{-1/2} \left(\frac{a_z}{a^2} \right) \frac{da}{dt} \tag{5.53}$$

Substituting for a_z in terms of S_r and a yields

$$\frac{dS_r^-}{dt} = -\frac{1}{2S_r} (\gamma S_y^2 + S_r^2) \left(\frac{1}{a} \right) \frac{da}{dt} \tag{5.54}$$

The reset stress is assumed to increase instantaneously when a larger stress peak is applied. The positive rate of change of reset stress is therefore

$$\frac{dS_r^+}{dt} = \sum_i (\Delta S_r)_i \, \delta(t - t_i) \tag{5.55}$$

where t_i is the time of arrival of a stress peak greater than S_r, $\delta(\cdot)$ is the Dirac delta function, and $(\Delta S_r)_i$ is the difference between the stress peak, $S_{\max}$, and the reset stress, S_r, given that the peak is above the current reset stress; $\Delta S_r = (S_{\max} - S_r \mid S_{\max} > S_r)$.

The total rate of change of reset stress is the sum of Eqs. 5.54 and 5.55:

$$\frac{dS_r}{dt} = -\frac{1}{2S_r}(\gamma S_y^2 + S_r^2)\left(\frac{1}{a}\right)\frac{da}{dt} + \sum_i (\Delta S_r)_i \delta(t - t_i) \tag{5.56}$$

Equation 5.56 has the form of Eq. 5.2 where the first term is the $g(S_r)$ contribution and the second term is the $h(S_r)F(t)$ contribution. Because many cycles of loading with peaks less than the reset stress will grow the crack between each time the reset stress is increased, the gradual decrease in reset stress (Eq. 5.54) can be treated as deterministic, given S_r, by averaging over the applied stress

$$g(S_r) = -\frac{1}{2S_r}(\gamma S_y^2 + S_r^2)\left(\frac{1}{a}\right) E_S\left[\frac{da}{dt}\,|S_r\right] \tag{5.57a}$$

$$h(S_r) = 1 \tag{5.57b}$$

$$F(t) = \sum_i (\Delta S_r)_i \delta(t - t_i) \tag{5.57c}$$

where $E_S[\cdot]$ represents the expectation over applied stress. The drift and diffusivity are given by substituting Eqs. 5.57 into Eqs. 5.7 and 5.8.

The increases in reset stress (Eq. 5.55) can again be treated as *shot-noise* [Lin, 1967]. An estimate of the rate of arrivals is simply the probability that the next peak is greater than the current reset stress, which is (for Gaussian loadings)

$$\lambda(S_r) = Prob\,[S_{\max} > S_r] = \exp\left(\frac{-S_r^2}{2\sigma_X^2}\right) \tag{5.58}$$

When the peaks of the process are correlated, occurrences of peaks above any given level of reset stress tend to *cluster* making the average rate of arrival of clusters less than λ. Adjustments for clustering in stationary narrow-band Gaussian processes have been given [Vanmarcke, 1975; Winterstein, 1984] with non-Gaussian modifications [Winterstein, 1987].

The size of the increase, ΔS_r, can be determined by comparing the relative frequency that S_r and higher levels are crossed. Given that S_r has been exceeded, the probability that some level, $S_r + \Delta S_r$, is also crossed is equal to the fraction of times that the process also crosses $S_r + \Delta S_r$. Therefore, the rate that level $S_r + \Delta S_r$ is crossed divided by the rate that level S_r is crossed is the

probability that the reset stress increment is greater than ΔS_r:

$$Prob\,[increment > \Delta S_r] = G(\Delta S_r) = \frac{\lambda(S_r + \Delta S_r)}{\lambda(S_r)} \qquad (\Delta S_r > 0) \quad (5.59)$$

where $G(\Delta S_r)$ is the complementary CDF of ΔS_r.

The expected size of an increase in reset stress is the integral of ΔS_r times the PDF, $p(\Delta S_r)$, which, after integration by parts, becomes the integral of the complementary CDF:

$$E[\Delta S_r] = \int_0^\infty G(\Delta S_r)\, d\,\Delta S_r = \frac{1}{\lambda(S_r)} \int_{S_r}^\infty \lambda(S) dS \qquad (5.60)$$

The expected value of the squared increment in the reset stress is similarly defined in terms of the complementary CDF through integration by parts:

$$E[(\Delta S_r)^2] = \int_0^\infty 2\,\Delta S_r\; G(\Delta S_r)\, d\,\Delta S_r = \frac{1}{\lambda(S_r)} \int_{S_r}^\infty 2(S - S_r)\lambda(S) dS \qquad (5.61)$$

The upward drift and diffusivity involve the product of $\lambda(S_r)$ and either Eq. 5.60 or 5.61, which results in the cancellation of the $\lambda(S_r)$ term in both cases. Using Eq. 5.58 to model the rate of overload arrivals, the drift and diffusivity for Gaussian loadings are (defining superscripts (+) and (−) to be upward and downward contributions as in Eq. 5.54 and 5.55):

$$\eta_o^-(S_r) = g(S_r) = -\frac{1}{2S_r}(\gamma S_y^2 + S_r^2)\left(\frac{1}{a}\right) E\left[\frac{da}{dt}\,|S_r\right] \qquad (5.62a)$$

$$\eta_o^+(S_r) = \lambda(S_r) E[\Delta S_r] = \sqrt{2\pi}\sigma_X \Phi\left(\frac{-S_r}{\sigma_X}\right) \qquad (5.62b)$$

$$d(S_r) = \lambda(S_r) E[(\Delta S_r)^2] = 2\sigma_X^2 \left[\exp\left(\frac{-S_r^2}{2\sigma_X^2}\right) - \sqrt{2\pi}\frac{S_r}{\sigma_X}\,\Phi\left(\frac{-S_r}{\sigma_X}\right)\right] \qquad (5.62c)$$

$$\eta_p(S_r) = \frac{1}{4}\, d'(S_r) = -\frac{1}{2}\sqrt{2\pi}\sigma_X \Phi\left(\frac{-S_r}{\sigma_X}\right) \qquad (5.62d)$$

where $\Phi(\cdot)$ is the standard Gaussian CDF. The total drift is $\eta = \eta_o^- + \eta_o^+ + \eta_p$, which reduces to $\eta = \eta_o^- + \eta_o^+/2$ in this case.

The steady-state distribution of reset stress is determined by substituting Eqs. 5.62 into Eq. 5.51 and calculating the integral for $U(S_r)$, which, in general, must be done numerically.

Fig. 5.5 shows the predicted steady-state reset stress distribution compared with the steady-state distribution obtained by simulation (with the crack length artificially fixed). The diffusion prediction matches the mean of the distribution, but has different behavior in the tails. This may be due to the fact that the diffusion model includes the correct average rate of overload arrivals and distribution of overload amplitudes, but the non-Poisson arrival of overload clusters is not correctly represented. Results obtained using the adjustments that account for overload clustering produced PDFs with roughly the same shape as the diffusion result in Fig. 5.5 but with a slightly reduced mean reset stress.

The average rate of crack growth can be calculated, at any given crack length, by integrating over both applied stress and reset stress. The effective stress intensity range, as defined in Section 2.2.2, depends on $S_{\max}$, $S_{\min}$, and S_r. The stress maxima and minima can now be defined in terms of the random variable models of Chapter 3, because the loading dynamics have been included in the steady-state reset stress distribution. For a narrow-band Gaussian loading, $S_{\max} = m_X + A$ and $S_{\min} = m_X - A$, where A is the Rayleigh distributed cycle amplitude. The effective stress range is defined as the (positive) range from the crack opening stress, qS_r, to the maximum stress, $S_{\max}$ (as in Eq. 2.4). The expected crack growth rate is

$$E[(da/dt)\,|\,a] = C(\pi a)^{b/2} \int_{S_r=0}^{\infty} \int_{A=0}^{\infty} (\Delta S_{eff}^{b}\,|\,S_r, A)\, p(A)\, p(S_r)\, dA\, dS_r \quad (5.64)$$

An approximation to the expected crack growth rate is obtained by fixing the reset stress at the mean value, $\bar{S}_r$, and only integrating over applied stress:

$$E[(da/dt)\,|\,a] = C(\pi a)^{b/2} \int_{A=0}^{\infty} (\Delta S_{eff}^{b}\,|\,\bar{S}_r, A)\, p(A)\, dA \quad (5.65)$$

The expected time to grow to the final crack length (which is equivalent to the number of cycles because time has been measured in cycles) is estimated by integrating the reciprocal of the expected crack growth rate over all crack lengths. This integral is approximated by discretizing the crack length into n intervals with sizes Δa_i, and summing the expected number of cycles to grow through each interval at the expected growth rate associated with each interval:

$$E[N] = \sum_{i=1}^{n} \frac{\Delta a_i}{E[(da/dt)\,|\,a = a_i]} \quad (5.66)$$

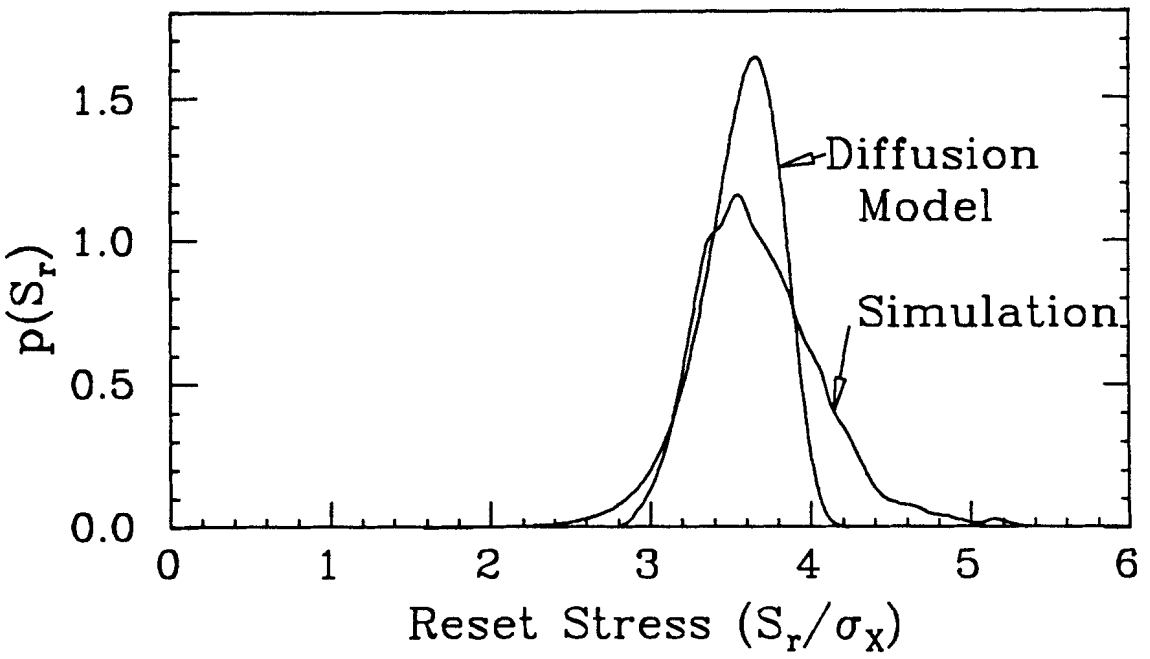

Fig. 5.5 Steady-state reset-stress distributions obtained from simulation (at a crack length of 0.1 in.) and from the scalar diffusion model.

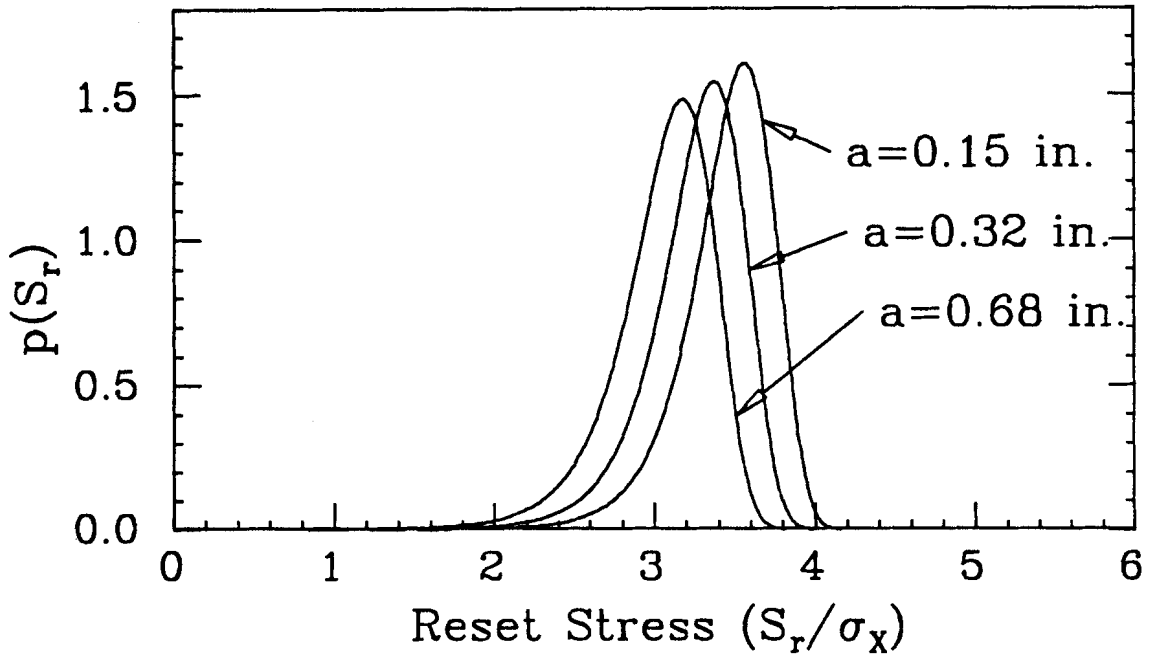

Fig. 5.6 Steady-state reset-stress distributions calculated using the diffusion model at three crack lengths associated with the three logarithmically selected integration points for crack growth from 0.1 to 1.0 in.

in which a_i is the integration point in the i^{th} interval. If the intervals are chosen logarithmically, as few as three integration points can estimate the integral to within an accuracy of a few percent (for crack growth from 0.1 inch to 1.0 inch).

Because the reset stress distribution is relatively narrow, the two methods of calculating the average crack growth rate (Eqs 5.64 and 5.65) give approximately the same result. Although Eq. 5.64 theoretically provides a better estimate of crack growth rate, the poor behavior in the tails of the predicted reset stress distribution makes that method slightly less accurate. Both methods were within 10% of the crack growth life calculated by simulating the crack growth cycle-by-cycle, using the same crack growth model, with a variety of material and loading parameters, as shown in Table 5.1.

Use of Eq. 5.58 for λ neglects bandwidth effects, and is most accurate for larger values of the damping ratio, ς (ς>2%). The adjustments that account for clustering lead to more accurate predictions for very lightly damped narrow-band loadings (ς<2%). Simulation results for fatigue crack growth life showed differences due to bandwidth to be typically less than about 20%.

Table 5.1
Simulation results for narrow-band Gaussian loading compared to diffusion model predictions; (a) by integrating over the reset stress distribution, and (b) by using the average value of S_r.

Parameter Values					Diffusion Models		Simulation
m_X	θ_E	b	C_o	q_o	(a)Integration	(b)Average S_r	
(ksi)	(cycles)	(da/dN = in./cycle)			(cycles)	(cycles)	(cycles)
0.0	3.2	3.5	$1x10^{-9}$	0.35	$1.07x10^4$	$1.12x10^4$	$1.11x10^4$
0.0	3.2	3.5	$5x10^{-10}$	0.35	$2.63x10^4$	$2.74x10^4$	$2.75x10^4$
0.0	3.2	3.5	$1x10^{-10}$	0.35	$2.04x10^5$	$2.10x10^5$	$2.21x10^5$
40.0	3.2	3.5	$1x10^{-10}$	0.35	$7.4x10^3$	$7.15x10^3$	$7.2x10^3$
40.0	8.0	3.5	$1x10^{-10}$	0.35	$7.4x10^3$	$7.15x10^3$	$7.0x10^3$
0.0	16.0	3.5	$1x10^{-10}$	0.35	$2.04x10^5$	$2.10x10^5$	$1.91x10^5$
20.0	3.2	3.0	$5x10^{-10}$	0.30	$4.30x10^4$	$4.29x10^4$	$4.35x10^4$
20.0	16.0	3.0	$5x10^{-10}$	0.30	$4.30x10^4$	$4.29x10^4$	$3.92x10^4$

Other Parameter Values
a_o = 0.1in.; a_f = 1.0in.; γ= 1.0; σ_X = 20.0ksi.

Calculating a *steady-state* reset stress distribution assumes that a steady state has been obtained. In the above derivation, the reset stress clearly depends on the crack length, which is constantly changing. The method works only because the reset stress distribution changes slowly with crack length. Figure 5.6 shows the predicted reset stress distribution $p(S_r)$ for three different crack lengths associated with three logarithmically selected integration points between $a_o = 0.1$ in. and $a_f = 1.0$ in.

Estimates of the variance of the time to fail require information on the dynamic interaction of reset stress and crack length. A vector diffusion model, which treats each quantity as a component of the state vector, could be used to calculate the variance of time to fail.

5.7 Vector Diffusion Crack Growth Models

In principle, the modeling capabilities of diffusion processes can be greatly extended by expanding their state space from a scalar quantity, such as crack length alone, to a vector of related quantities (e.g., current values of reset stress and applied stress as well as crack size). The dynamics of this set of state variables would then be defined by a vector governing equation analogous to Eq. 5.2:

$$\frac{d\mathbf{X}}{dt} = \{g(\mathbf{X})\} + \mathbf{H}(\mathbf{X})\{F(t)\} \tag{5.67}$$

where $\mathbf{X}$ is the vector state, $\{g(\mathbf{X})\}$ and $\{F(t)\}$ are both vectors, and $\mathbf{H}(\mathbf{X})$ is a square matrix. This leads to a set of drifts and diffusivities describing the rates of change of all the state variables, analogous to Eqs. 5.4 and 5.5:

$$\eta_i(\mathbf{X}) = \lim_{\Delta t \to 0} \frac{1}{\Delta t} E[\Delta X_i \mid \mathbf{X}] \tag{5.68}$$

$$d_{ij}(\mathbf{X}) = \lim_{\Delta t \to 0} \frac{1}{\Delta t} E[\Delta X_i \Delta X_j \mid \mathbf{X}] \tag{5.69}$$

where X_i and X_j are components of the state vector, $\mathbf{X}$.

These drifts and diffusivities can be used in vector analogs of the forward and backward equations to obtain various useful fatigue statistics. For example, moments of fatigue life satisfy the vector analog to Eq. 5.10 given by

$$-n\,\mu_{n-1}(\mathbf{X}_o) = \sum_i \eta_i(\mathbf{X}_o) \frac{\partial \mu_n(\mathbf{X}_o)}{\partial X_i} + \frac{1}{2} \sum_i \sum_j d_{ij}(\mathbf{X}_o) \frac{\partial^2 \mu_n(\mathbf{X}_o)}{\partial X_i \partial X_j} \tag{5.70}$$

where $\mathbf{X}_o$ is the initial state vector and μ_n is the n^{th} moment of the time to reach the final crack length boundary in state space.

A two dimensional model that accounts for load sequence effects is created by including both S_r and a in a vector diffusion process. The same drift and diffusivity in reset stress derived in Section 5.6 apply to the vector model. Applied stress is again treated in expectation because of its relatively short correlation time. The drift in crack length is the expected rate of crack growth conditional on the current state, which now includes instantaneous crack length and reset stress. The model contains no diffusive changes in crack length. Estimates of crack growth life again match the mean simulation results, but the variance is underestimated due to the same approximations that caused the scalar model to misrepresent the tails of the steady-state reset stress distribution.

The most general diffusion models of crack growth would include not only a and S_r in their state spaces, but also the applied stress. A three dimensional model is created by including the scalar stress envelope as a third vector state. Randomness in the loading is modeled as a white noise excitation on the stress envelope; there need not be any diffusive changes in crack length or reset stress. Although this formulation is more direct, inaccuracies in the mean time to fail are possible because the envelope does not follow all of the stress peaks. Also, the rate at which the reset stress should increase when the applied stress envelope is greater than S_r is somewhat arbitrary.

By modeling the stress process as the response of a linear oscillator to white noise excitation and using the traditional linear system formulation of including the response and its first derivative in the state vector, a four dimensional model is created. This provides a smoother, more realistic model of changes in applied stress (and hence reset stress and crack growth) than the lower-dimensional models afford. In particular, the increase from three to four dimensions provides an unambiguous means of defining the rate of change of the reset stress (setting it equal to the stress velocity) when a stress peak exceeds the current reset stress.

Fatigue life statistics can be estimated from these models by numerically solving Eq. 5.70. One may, for example, expand the unknown moments as weighted series of specified *trial functions* of the initial state variables, and determine the weighting coefficients by standard weighted residuals techniques (e.g., Galerkin's method). Based on limited numerical experience, it appears that for four or more dimensions the needed computational effort may be comparable to what is required for accurate estimates from simulation, particularly with the efficient sequential simulation of Section 3.5. One advantage of the analytical result is that because only the left-hand-side of Eq. 5.70 (the *load* term) changes

with the order of the moment, the extra effort required to estimate higher moments is rather small (the *stiffness* matrix relating the weighting coefficients to the *load* need not be recalculated). Of course, because the lower moments appear as their *loading* in Eq. 5.70, these higher-order moments may deteriorate in accuracy (although perhaps less rapidly than higher moments of simulated fatigue lives). If one wishes to estimate moments of state variables, such as crack size, after a given number of cycles of applied stress, the forward equation (Eq. 5.1) can be similarly generalized to include multiple state variables.

5.8 Summary

Scalar diffusion models of physical processes are possible when the process can be described by the evolution of a single variable in a way that is independent of the past behavior, but may depend on the current state. Mathematically, a diffusion process is so irregular (not differentiable anywhere) that no physical process is similar on a micro-time scale. Longer term behavior, however, can often be accurately predicted with the use of diffusion models. Solutions for moments of the time to reach a boundary are obtained through use of the backward equation (Eq. 5.9). Solutions for steady-state distributions are possible using the forward equation (Eq. 5.1).

The crack growth model introduced in Chapter 2 can be formulated in ways that lend themselves to diffusion modeling. In general, calculating crack growth due to random loading depends on three variables: crack length, applied stress, and reset stress (a variable that accounts for the history dependence of the crack opening stress). If any two of these variables can be treated separately (e.g., in expectation or held fixed) a scalar diffusion model can be created. The example of crack growth due to narrow-band loading without sequence effects eliminates reset stress dependence and absorbs the applied stress into the *white noise* forcing function, resulting in dependence on crack length only.

Constant amplitude loading with discrete tensile overloads is treated as a scalar diffusion process by modeling abrupt changes in effective stress range (from unretarded to retarded growth) as a memoryless Poisson event. The retardation effect of the overloads is included in the forcing function as a *shot noise* excitation. Solutions for both mean and variance of the time to fail are shown to match simulation results for this special loading case.

Crack growth due to narrow-band Gaussian loading is predicted by solving the forward equation for the steady-state distribution of reset stress at selected

crack lengths. The applied stress is treated in expectation (averaged) because its correlation time is much shorter than the correlation time of the reset stress. The solutions for the mean time to fail, calculated from steady-state reset stress distributions at each integration point in crack length, are within 10% of simulation results for a wide variety of material and loading parameter values. This provides a useful alternative to crack growth simulation when only the mean life is required. The variance of the time to fail due to random loading depends on the dynamic interaction between reset stress and crack length, which can not be predicted by this scalar model.

By increasing the dimension of the state space, a more refined dynamic model is obtained. Unfortunately, the amount of computational effort needed to analyze a diffusion process increases quickly with its dimension. The optimal model dimension depends on both the analyst's goal and the available computational resources, as well as on the particular problem at hand. For example, the above scalar diffusion models are appropriate for particular loading cases, or when limited statistics of time to fail are required (i.e., only the mean). Two-dimensional models accurately predict the mean life, but underestimate the variance. Higher-dimensional models, which follow reset stress changes less ambiguously, provide a means of estimating variability in crack growth life due to random loading, but can be computationally expensive (rivaling simulation computation time in many cases). The simulation results from Chapter 4, however, indicate that variability due solely to the randomness in a stationary Gaussian loading is often small (observe the $\pm$ one standard deviation error bars in Figs. 4.3-4.7) when compared to overall variability in fatigue crack growth life.

CHAPTER 6

CONCLUSIONS AND FUTURE WORK

6.1 Conclusions

Ideally, estimates of the crack growth life of a structural component should account for all known sequence effects and should predict both mean and variance of the time to fail, but there is generally insufficient information for this prediction. For particular applications, however, it is often possible to obtain useful estimates without completely describing the random loading or all of the sequence effects.

The crack growth model of Chapter 2 accounts for sequence effects by representing the crack closure phenomenon in a simplified way. Comparisons with test data show that the model is capable of relatively accurate crack growth life predictions with a minimum of input data. The loading can be specified, including probable sequences, with an efficient simulation method that generates only those events in a random loading that are significant in a fatigue sense. The significant events, described by the random variables that define cycle means and amplitudes after racetrack filtering, are sequentially simulated. Sequence effects can be modeled and crack growth calculated analytically by using scalar diffusion models to estimate the crack opening stress for stationary Gaussian loadings. For nonstationary applications, when crack growth must be calculated cycle-by-cycle, the above simulation method is shown to be easily adapted to sequentially simulate the nonstationary parameters. Sequence effects are usually important for loadings with distinct overloads, but the stochastic dynamics of the overload arrivals can diminish the effect. Diffusion models are capable of predicting mean and variance of time to failure for some special load cases of this type.

Crack growth estimates that neglect sequence effects are also shown to be a very useful alternative when the application requires a rough, and generally conservative, life estimate. These life estimates are obtained by simple integrals of the random variable load models without cycle-by-cycle calculation of crack growth. A conservative estimate is obtained by assuming a Gaussian loading to be narrow-band; more accurate estimates are available using the random

variable models of wide-band loadings after racetrack filtering. For stationary Gaussian loadings, the sequenceless estimate is often within a factor of two of the more computationally expensive prediction that includes sequence effects. When sequence effects do produce a substantial crack growth retardation, increasing the mean life, there is usually an associated increase in the variability of the time to failure. Even though the mean life may be several times longer than the sequenceless prediction, there remains a relatively high probability that the actual life will again be close to the sequenceless prediction (within a factor of two).

6.2 Suggestions for Future Work

The direction for future work in crack growth modeling depends on the discoveries, in the next few years, of the physical processes governing fatigue crack propagation. Currently, the emphasis on linking the crack opening stress ratio, q_o, to the applied stress ratio, R, is a stumbling block, because, in a random loading environment, the stress ratio is often difficult to define. It may be possible, however, to define a *reset stress* like parameter for the stress valleys (minima) which can be used in conjunction with the reset stress to continuously monitor an equivalent stress ratio. In hindsight, the crack opening stress ratio should probably have been a function of maximum stress, as well as stress ratio; it would not have been too difficult, and may be important in some applications.

The load models presented here have emphasized Gaussian loadings, while many loadings on structural components are non-Gaussian. The extension of this work to non-Gaussian loading is possible with only minor additional effort in implementing the load models. Most non-Gaussian loadings can be converted to Gaussian by a simple transformation, which may be based on moments of the distribution, or may be based on empirical estimates of the actual non-Gaussian distribution. Once the loading is transformed to Gaussian, all of the methods presented here apply. The appropriate random variable models can then be transformed back to the original loading distribution to calculate crack growth. (The ASTM loadings used here were transformed Gaussians; the ASTM life predictions presented here were obtained by this procedure.) As shown in Chapter 4, sequence effects in life estimates for non-Gaussian loadings can be substantial.

Nonstationary loadings are treated here by simulating the loading and calculating crack growth cycle-by-cycle. Analytical solutions to nonstationary

loading problems may be possible using the approach of Section 5.6, where scalar diffusion models were used on an inherently multi-dimensional problem by uncoupling the crack length dependence (long correlation time) from the reset stress (intermediate correlation time) and from the applied stress (short correlation time). The key again lies in the correlation time of the nonstationary parameter. If the correlation time is short, the loading can be treated as an equivalent stationary loading with an adjusted distribution of peaks (see Section 4.5). If the correlation time of the nonstationary parameter is long, the crack growth may be estimated independently at different parameter values and then integrated over all possible parameter values (expectation over the nonstationary parameter). Intermediate correlation times can be bounded by these two limiting cases.

Vector diffusion models should probably be pursued more vigorously as the availability of *super computers* increases. Although the additional accuracy and flexibility of a vector model is costly in terms of present computational abilities, it is possible that these costs may be minimal in the future.

REFERENCES

Abramowitz, M. and Stegun, I.A. [1964]. *Handbook of Mathematical Functions,* National Bureau of Standards, Applied Mathematics Series, No. 55, June 1964.

Barsom, J.M. [1976]. "Fatigue Crack Growth Under Variable Amplitude Loading in Various Bridge Steels," *Fatigue Crack Growth under Spectrum Loads, ASTM STP 595,* 1976, pp. 217-235.

Broek, D. [1984]. *Elementary Engineering Fracture Mechanics,* Martinus Nijhoff Publishers, The Hague, 1984.

Brown, L.M. [1981]. "Dislocations and the Fatigue Strength of Metals," *Dislocation Modeling of Physical Systems,* ed. M.F. Ashby, et. al., Pergamon Press, 1981, pp. 51-68.

Chand, S. and Garg, S.B.L. [1983]. "Crack Closure Studies under Constant Amplitude Loading," *Engineering Fracture Mechanics,* Vol. 18, No. 2, 1983, pp. 333-347.

Chang, J.B. and Hudson, C.M., Eds. [1981]. *Methods and Models for Predicting Fatigue Crack Growth Under Random Loading, ASTM STP 748,* American Society for Testing and Materials, Philadelphia, PA, 1981.

Chang, J.B. [1981]. "Round-Robin Crack Growth Predictions on Center-Cracked Tension Specimens under Random Spectrum Loading," *Methods and Models for Predicting Fatigue Crack Growth Under Random Loading, ASTM STP 748,* Eds. J.B. Chang and C.M. Hudson, 1981, pp. 3-40.

Chang, J.B., Szamossi, M., and Liu, K-W. [1981]. "Random Spectrum Fatigue Crack Life Predictions With or Without Considering Load Interactions," *Methods and Models for Predicting Fatigue Crack Growth Under Random Loading, ASTM STP 748,* Eds. J.B. Chang and C.M. Hudson, 1981, pp. 115-132.

Corten, H.T. and Dolan, T.J. [1956]. "Cumulative Fatigue Damage," *Proceedings of the International Conference on Fatigue of Metals,* The Institution of Mechanical Engineers, London, England, 1956, pp. 235-246.

Cotrell, A.H. [1969]. *Mechanical Properties of Matter,* John Wiley and Sons, New York, NY, 1969.

Crandall, S.H. and Mark, W.D. [1963]. *Random Vibration in Mechanical Systems,* Academic Press, New York, NY, 1963.

de Koning, A.U. [1980]. "A Simple Crack Closure Model for Prediction of Fatigue Crack Growth Rates under Variable Amplitude Loading," NLR MP 80006, 1980.

Dill, H.D. and Saff, C.R. [1977]. "Effect of Fighter Attack Spectrum on Crack Growth," AFFDL-TR-76-112, McDonnell Douglas Aircraft Co., St. Louis, MO, March 1977.

Dolinski, K. [1986]. "Studies on Stochastic Fatigue Crack Growth," Laboratorium für den Konstruktiven Ingenieurbau (LKI) Technische Universität München, Munich, Germany, 1986.

Elber, W. [1971]. "The Significance of Fatigue Crack Closure," *Damage Tolerance in Aircraft Structures, ASTM STP 486,* 1971, pp. 230-242.

Elber, W., [1976]. "Equivalent Constant-Amplitude Concept for Crack Growth Under Spectrum Loading," *Fatigue Crack Growth under Spectrum Loads, ASTM STP 595,* 1976, pp. 236-250.

Fine, M.E. [1980]. "Fatigue Resistance of Metals," The 1979 Campbell Memorial Lecture, *ASM Met. Trans.,* Vol. 11A, March 1980, pp. 365-379.

Fleck, N.A. and Smith, R.A. [1984]. "Fatigue Life Prediction of a Structural Steel Under Service Loading," *Int. J. Fatigue,* Vol. 6, No. 4, 1984, pp. 203-210.

Forrest, P.G. [1962] *Fatigue of Metals,* Pergammon Press, Oxford, England, 1962.

Forsyth, P.J.E. [1969]. *The Physical Basis of Metal Fatigue,* American Elsevier Publishing Co., New York, NY, 1969.

Freudenthal, A.M. and Gumbel, E.J. [1956]. "Physical and Statistical Aspects of Fatigue," *Advances in Applied Mechanics,* Vol. 4, 1956, pp. 117-158.

Freudenthal, A.M. and Heller, R.A. [1959]. "On Stress Interaction in Fatigue and a Cumulative Damage Rule," *J. Aero-Space Science,* Vol. 26, No. 7, 1959, pp. 431-442.

Fuchs, H.O., Nelson, D.V., Burke, M.A., and Toomay, T.L. [1977]. "Shortcuts in Cumulative Damage Analysis," *Fatigue under Complex Loading: Analyses and Experiments, Advances in Engineering,* Volume 6, Ed. R.M. Wetzel, SAE, Warrendale, PA, 1977, pp. 145-162.

Fuchs, H.O. and Stephens, R.I. [1980]. *Metal Fatigue in Engineering,* John Wiley and Sons, New York, NY, 1980.

Führing, H. [1981]. "Practical Application of a Model for Fatigue Damage With Irregular Cyclic Loading," *Advances in Fracture Research, Proc. 5th Int. Conf. on Fracture* Cannes, France, Ed. D. Francois, Vol. 4, 29March-3April 1981, p. 1823.

Gardner, F.H. and Stephens, R.I. [1974]. "Subcritical Crack Growth Under Single and Multiple Periodic Overloads in Cold-Rolled Steel," *Fracture Toughness and Slow-Stable Cracking, ASTM STP 559,* 1974, pp. 225-244.

Griffith, A.A. [1920]. "Phenomenon of Rupture and Flaws in Solids," *Philosophical Transactions of the Royal Society,* Series A, Vol. 221, 1920, p. 163.

Hood [1842] Institute of Civil Engineers (British), Minutes of Proceedings, Vol. 2, 1842, p. 180.

Hudson, C.M. [1981]. "A Root-Mean-Square Approach for Predicting Fatigue Crack Growth under Random Loading," *Methods and Models for Predicting Fatigue Crack Growth Under Random Loading, ASTM STP 748,* Eds. J.B. Chang and C.M. Hudson, 1981, pp. 41-52.

Johnson, W.S. [1981]. "Multi-Parameter Yield Zone Model for Predicting Spectrum Crack Growth," *Methods and Models for Predicting Fatigue Crack Growth Under Random Loading, ASTM STP 748,* Eds. J.B. Chang and C.M. Hudson, 1981, pp. 85-102.

Jono, M., Song, J., and Kikukawa, M. [1984]. "Fatigue Crack Growth and Crack Closure of Structural Materials under Random Loadings," *Advances in Fracture Research ICF-6,* Vol. 3, Pergamom Press, Oxford, England, 1984, pp. 1735-1742.

Jono, M., Song, J., and Sugeta, A. [1985]. "Prediction of Crack Growth and Crack Closure Under Non-Stationary Random Loading," *Proc., ICOSSAR '85, 4th Int. Conf. on Struct. Safety and Reliability,* Kobe, Japan, May 1985, pp. I-465—I-474.

Karlin, S. and Taylor, H. [1981]. *A Second Course in Stochastic Processes,* Academic Press, New York, NY, 1981.

Kikukawa, M., Jono, M., and Kondo, Y. [1981]. "An Estimation Method of Fatigue Crack Propagation Rate Under Varying Loading Conditions of Low Stress Intensity Level," *Advances in Fracture Research, Proc. ICF5, 5th Int. Conf. on Fracture,* Cannes, France, Ed. D. Francois, Vol. 4, 29March-3April

1981, pp. 1799-1806.

Larsen, J.M. and Annis, C.G., Jr. [1980]. "Observation of Crack Retardation Resulting from Load Sequencing Characteristic of Military Gas Turbine Operation," *Effect of Load Spectrum Variables on Fatigue Crack Initiation and Propagation, ASTM STP 714,* Eds. D.F. Bryan and J.M. Potter, 1980, pp. 91-107.

Lavenda, B.H. [1985]. "Brownian Motion," *Scientific American,* Vol. 252, No. 2, February 1985, pp.70-85.

Lin, Y.K. [1967]. *Probabilistic Theory of Structural Dynamics,* McGraw-Hill, Inc., New York, NY, 1967.

Lin, Y.K. and Yang, J.N. [1983]. "On Statistical Moments of Fatigue Crack Propagation," *Engineering Fracture Mechanics,* Vol. 18, No. 2, 1983, pp. 243-256.

Lin, Y.K. [1986]. "Some Observations on the Stochastic Averaging Method," *Probalistic Engineering Mechanics,* Vol. 1, No. 1, 1986, pp. 23-27.

Madsen, H.O. [1982]. "Deterministic and Probabilistic Models for Damage Accumulation due to Time Varying Loading," *Dialog 5-82,* Ed. G. Mohr, Danish Engineering Academy, Civil Engineering Department, Lyngby, Denmark, 1982.

Madsen, H.O., Krenk, S., and Lind, N.C. [1986]. *Methods of Structural Safety,* Prentice-Hall, Englewood Cliffs, NJ, 1986, pp. 252-284.

Manson. S.S., Freche, J.C., and Ensign, C.R. [1967]. "Application of a Double Linear Damage Rule to Cumulative Fatigue," *ASTM STP 415,* 1967, p. 384.

McNerney, G.M. and Veers, P.S. [1984]. "A Markov Method for Simulating Non-Gaussian Wind Speed Time Series," SAND84-1227, Sandia National Laboratories Report, Albuquerque, NM, October 1984.

Miles, J.W. [1954]. "On Statistical Fatigue Under Random Loading," *Journal of Aeronautical Sciences,* Vol. 21, 1954, pp. 753-762.

Miner, M.A. [1945]. "Cumulative Damage in Fatigue," *J. Appl. Mech., Trans. ASME,* Vol. 67, September 1945, p. A159.

Moore, H.F. and Kommers, J.B. [1927]. *The Fatigue of Metals,* McGraw-Hill Books Co., New York, NY, 1927.

Nelson, D.V. and Fuchs, H.O. [1976]. "Prediction of Fatigue Crack Growth under Irregular Loading," *Fatigue Crack Growth under Spectrum Loads,*

ASTM STP 595, 1976, pp. 276-291.

Nelson, D.V. and Fuchs, H.O., [1977]. "Predictions of Cumulative Fatigue Damage using Condensed Load Histories," *Fatigue under Complex Loading: Analyses and Experiments, Advances in Engineering,* Volume 6, Ed. R.M. Wetzel, SAE, Warrendale, PA, 1977, pp. 163-187.

Nelson, D.V. [1978]. "Cumulative Fatigue Damage in Metals," Stanford University PhD Dissertation, March, 1978.

Newman, J.C. Jr. [1981]. "A Crack-Closure Model for Predicting Fatigue Crack Growth under Aircraft Spectrum Loading," *Methods and Models for Predicting Fatigue Crack Growth Under Random Loading, ASTM STP 748,* Eds. J.B. Chang and C.M. Hudson, 1981, pp. 53-84.

Newman, J.C. Jr. [1982]. "Prediction of Fatigue Crack Growth under Variable-Amplitude and Spectrum Loading Using a Closure Model," *Design of Fatigue and Fracture Resistant Structures, ASTM STP 761,* Eds. P.R. Abelkis and C.M. Hudson, 1982, pp. 255-277.

Oh, K.P. [1980]. "The Prediction of Fatigue Life Under Random Loading: A Diffusion Model," *Int. J. Fatigue,* July 1980. pp. 99-104.

Orowan, E. [1950]. *Fatigue and Fracture of Metals,* MIT Press, Cambridge, 1950.

Orringer, O. [1984]. "Rapid Estimation of Spectrum Crack-Growth Life Based on the Palmgren-Miner Rule," *Computers & Structures,* Vol. 19, No. 1-2, 1984, pp. 149-153.

Paris, P.C. and Erdogan, F. [1963]. "A Critical Analysis of Crack Propagation Laws," *J. Basic Eng., Trans. ASME,* Vol. 85, 1963, p. 528.

Powell, A. [1958]. *Journal of the Acoustical Society of America,* Vol. 30, 1958, p. 1130.

Rankine, W.J.M. [1843] Institute of Civil Engineers (British), Minutes of Proceedings, Vol. 3, 1843, p. 105.

Rice, S.O. [1944; 1945]. "Mathematical Analysis of Random Noise," *Bell System Technical Journal,* Vols. 23 and 24, 1944 and 1945. Reprinted in *Selected Papers on Noise and Stochastic Processes,* Ed. N. Wax, 1954, pp. 133-294.

Rolfe, S.T. and Barsom, J.M. [1977]. *Fracture and Fatigue Control in Structures - Applications of Fracture Mechanics,* Prentice-Hall, 1977.

Sahay, B. and Lennox, W. [1974]. "Moments of the First-Passage Time for a Narrow-Band Process," *Journal of Sound and Vibration,* Vol. 32, No. 4, 1974, pp. 449-458.

Sandor, B.I. [1972]. *Fundamentals of Cyclic Stress and Strain,* University of Wisconsin Press, Madison, WI, 1972.

Schijve, J. [1960]. "Fatigue Crack Propagation in Light Alloy Sheet Material and Structures," Rep. MP 195, National Luchtvaart Laboratorium, Amsterdam, Aug. 1960.

Schijve, J., Jacobs, F.A., and Tromp, P.J. [1971]. "The Effect of Load Sequence on Fatigue Crack Propagation under Random Loading and Program Loading," NLR TR 71014 U, National Aerospace Laboratory NLR, The Netherlands, 1971.

Schijve, J. [1973]. "Effect of Load Sequences on Crack Propagation Under Random and Program Loading," *Engr. Fract. Mech.,* Vol. 5, 1973, pp. 269-280.

Schijve, J. [1981]. "Some Formulas for the Crack Opening Stress Level," *Engineering Fracture Mechanics,* Vol. 14, 1981, pp. 461-465.

Shinozuka, M. and Jan, C.-M. [1972]. "Digital Simulation of Random Processes and its Applications," *Journal of Sound and Vibration,* Vol. 25, No. 1, 1972, pp. 111-128.

Socie, D.F. [1977]. "Prediction of Fatigue Crack Growth in Notched Members under Variable Amplitude Loading Histories," *Engineering Fracture Mechanics,* Vol. 9, 1977, pp. 849-865.

Socie, D.F. and Kurath, P. [1983]. "Cycle Counting for Variable-Amplitude Crack Growth," *Fracture Mechanics: Fourteenth Symposium—Volume II: Testing and Applications, ASTM STP 791,* Eds. J.C. Lewis and G. Sines, 1983, pp. II-19—II-32.

Stephens, R.I., McBerney, G.W., and Oliphant, L.J. [1974]. "Fatigue Crack Growth with Negative R-Ratios Following Tensile Overloads," *Int. J. Frac. Mech.,* May 1974, p. 587.

Stratonovich, R.L. [1963]. *Topics in the Theory of Random Noise,* Vols. 1-2, Gordon and Breach, London, England, 1963.

Swanson, S.R. [1968]. "Random Load Fatigue Testing: A State of the Art Survey," *Materials Research & Standards,* MTRSA, Vol. 8, No. 4, April 1968, pp. 10-44.

Timoshenko, S.P. [1953]. *History of Strength of Materials,* McGraw-Hill Book Co., New York, NY, 1953.

Trebules, V.W., Roberts, R., and Hertzberg, R.W. [1973]. "Effect of Multiple Overloads on Fatigue Crack Growth in 2024-T3 Alluminum Alloy," *Progress in Flaw Growth and Fracture Toughness Testing, ASTM STP 536,* 1973, pp. 115-146.

Tucker, L. and Bussa, S. [1977]. "The SAE Cumulative Fatigue Damage Test Program," *Fatigue Under Complex Loading: Analyses and Experiments, Advances in Engineering,* Volume 6, Ed. R.M. Wetzel, SAE, Warrendale, PA, 1977, pp. 1-54.

Vanmarcke, E.H. [1975]. "On the Distribution of the First-Passage Time for Normal Stationary Random Prosesses," *J. Appl. Mech.,* Vol. 42, March 1975, pp. 215-220.

Vargas, L.G. and Stephens, R.I. [1973]. "Subcritical Crack Growth Under Overloading in Cold Rolled Steel," *Proc. Third Int. Conf. on Fracture,* Munich, Germany, April 1973.

von Euw, E.F.J., Herzberg, R.W., and Roberts, R. [1972]. "Delay Effects in Fatigue Crack Propagation," *Stress Analysis and Growth of Cracks, ASTM STP 513,* 1972, p. 230.

Watson, P., Hoddinott, D.S., and Norman, J.P. [1973]. "Periodic Overloads and Random Fatigue Behavior," *Cyclic Stress and Strain Behavor, ASTM STP 519,* 1973, p. 271.

Wetzel, R.M. Ed. [1977]. *Fatigue Under Complex Loading: Analysis and Experiments, Advances in Engineering,* Volume 6, Society of Automotive Engineers, Warrendale, PA, 1977.

Wheeler, O.E. [1972]. "Spectrum Loading and Crack Growth," *J. Basic Engr., Trans. ASME,* Vol. 94, 1972, p. 81.

Willenborg, J., Engle, R.M., and Wood, H.A. [1971]. "A Crack Growth Retardation Model Using an Effective Stress Concept," Report TM-71-1-FBR, Wright-Patterson Air Force Base, Ohio, 1971.

Winterstein, S.R. [1984]. "Diffusion Models and the Energy Fluctuation Scale: A Unified Approach to Extremes and Fatigue," Technical Report No. 64, John A. Blume Earthquake Engineering Center, Stanford University, Stanford, CA, Nov. 1984.

Winterstein, S.R., and Cornell, C.A. [1985]. "Fatigue and Fracture under Stochastic Loading," *Proceedings,* Fourth International Conference on Structural Safety and Reliability (ICOSSAR), Vol. III, Kobe, Japan, May 27-29, 1985, pp. 745-749.

Winterstein, S.R. [1987]. "Moment-Based Hermite Models of Random Vibration," Technical University of Denmark, Lyngby, Denmark, March 1987.

Wirsching, P.H. and Light, M.C. [1980]. "Fatigue under Wide Band Random Stress," *Journal of the Structural Division,* ASCE, Vol. 106, No. ST7, July 1980, pp. 1593-1607.

Wöhler, A. [1867] *Engineering,* (translated and edited anonymously) Vol. 4, 1867, p. 160.

Yang, J.N. [1974]. "Statistics of Random Loading Relevant to Fatigue," *Journal of the Engineering Mechanics Division,* ASCE, Vol. 100, No. EM3, June 1974, pp. 469-475.

DISTRIBUTION:

Battelle-Pacific Northwest Laboratory
P.O. Box 999
Richland, WA 99352
Attn: L. Wendell

DOE/ALO
Albuquerque, NM 87115
Attn: G. P. Tennyson

DOE/ALO
Energy Technology Liaison Office
NGD
Albuquerque, NM 87115
Attn: Capt. J. L. Hanson, USAF

DOE Headquarters (20)
Wind/Oceans Technologies Division
1000 Independence Avenue
Washington, DC 20585
Attn: L. J. Rogers
P. R. Goldman

FloWind Corporation (2)
1183 Quarry Lane
Pleasanton, CA 94566
Attn: L. Schienbein

A. D. Garrad
Garrad Hasson
10 Northampton Square
London EC1M 5PA
UNITED KINGDOM

Dr. I. J. Graham
Southern University
Department of Mechanical Engineering
P.O. Box 9445
Baton Rouge, LA 70813-9445

Indal Technologies, Inc. (2)
3570 Hawkestone Road
Mississauga, Ontario
CANADA L5C 2V8
Attn: D. Malcolm

Massachusetts Institute of Technology
77 Massachusetts Avenue
Cambridge, MA 02139
Attn: Professor R. M. N. Pelloux

G. M. McNerney
US Wind Power
160 Wheeler Road
Burlington, MA 01803

R. Lynette
R. Lynette and Associates
15042 N. E. 40th Street
Suite 206
Redmond, WA 98052

RANN, Inc.
260 Sheridan Ave., Suite 414
Palo Alto, CA 94306
Attn: A. J. Eggers, Jr.

Gwen Schreiner
Librarian
National Atomic Museum
Albuquerque, NM 87185

Solar Energy Research Institute
1617 Cole Boulevard
Golden, CO 80401
Attn: R. W. Thresher

Stanford University
Dept. of Aeronautics and
Astronautics Mechanical Engineering
Stanford, CA 94305
Attn: Holt Ashley

USDA, Agricultural Research Service
Southwest Great Plains Research Center
Bushland, TX 79012
Attn: Dr. R. N. Clark

Robert E. Akins
Washington and Lee University
P.O. Box 735
Lexington, VA 24450

Michael B. Anderson
Sir Robert McAlpine & Sons, LTD
P.O. Box 74
London WC1N 1LG
UNITED KINGDOM

C. Allin Cornell (5)
110 Coquito Way
Portola Valley, CA 94025

Drew V. Nelson (5)
Mechanical Engineering Design Division
Stanford University
Stanford, CA 94305

Keith Ortiz
Dept. of Aero. and Mech. Eng.
Aero Building #16
University of Arizona
Tucson, Arizona 85721

Royce G. Forman ES5
NASA Johnson Space Center
Houston, TX 77058

Steven R. Winterstein
Civil Engineering Department
Stanford University
Stanford, CA 94305

Zdenek P. Bazant
Professor of Civil Engineering
Northwestern University
Evanston, Illinois 60201

Robert Bea
PMB Systems Engineering Inc.
500 Sansome Street, Suite 400
San Francisco, CA 94111

Ove Ditlevsen
Afdelingden for Baerende
Konstruktiner, Bldg. 118
Danmarks Tekniske Hojskole
DK 2800 Lyngby, DENMARK

Mircea Grigoriu
Dept. of Civil Engineering
Cornell University
Ithica, New York 14853

Armen Der Kiureghian
Dept. of Civil Engineering
725 Davis Hall
University of California
Berkeley, California 94720

Y.K. Lin
Ctr. for Appl. Stochastic Res.
College of Engineering
Florida Atlantic University
Boca Raton, Florida 33431

S.C. Liu
National Science Foundation
1800 G Street, N.W.
Washington, D.C. 20550

Loren Lutes
Dept. of Civil Engineering
Rice University
P.O. Box 1892
Houston, Texas 77251

Henrik O. Madsen
Reliability Analysis
A.S. Veritas Research
P.O. Box 300, N-1322
Hovik, NORWAY

Rudiger Rackwitz
Technical Univ. of Munich
Lab.f.Konstrukt.Ingenieurbau
Munich 2 F.R.G. D-8000

B. F. Spencer, Jr.
Dept. of Civil Engineering
University of Notre Dame
Notre Dame, IN 46556

Paul H. Wirsching
Dept. of Aero. and Mech. Eng.
University of Arizona
Tucson, Arizona 85721

J.N. Yang
Dept of Civ., Mech. and Env. Eng
School of Eng. and Appl. Science
The George Washington University
Washington, D.C. 20052

James T.P. Yao
Dept. of Civil Engineering
Purdue University
West Lafayette, Indiana 47907

A.H. Ang
Dept. of Civil Engineering
University of Illinois
Urbana, Illinois 61801

M. Shinozuka
Department of Civil Engineering
Columbia University
632 Mudd
New York, N.Y. 10027

E. Vanmarcke
Dept. of Civil Engineering
Princeton University
Princeton, New Jersey 08544

Daniele Veneziano
Dept. of Civil Engineering
Mass. Institute of Technology
Cambridge, Massachusetts 02139

Yi-Kwei Wen
Dept. of Civil Engineering
University of Illinois
Urbana, Illinois 61801

Bela I. Sandor
Engineering Mechanics Dept.
University of Wisconsin
1415 Johnson Drive
Madison, WI 53706

Ilyoung Hong
FMC Corporation
1205 Coleman Ave Box 580
Santa Clara, CA 95052

Manohar B. Motwani
CPC Group General Motors Corp.
30001 Van Dyde Ave.
Warren, MI 48090-9060

Dr. Walter Schutz
IABG
Einsteinstrasse 20
8012 Ottobrunn F.R.G.

Norman E. Dowling
ESM Department
Virginia Tech.
Blacksburg, VA 24061

SINTEF (2)
7034 Trondheim - NTH
Norway
Attn: Oddvar Eide
Knut Engesvik

J. C. Newman
NASA Langley Research Center
Mail Stop 188E
Hampton, VA 23665

M. R. Mitchel
Rockwell International Science Center
1049 Camino Dos Rios
Thousand Oaks, CA 91360

R. I. Stephens
Mechanical Engineering Dept.
University of Iowa
Iowa City, IA 52242

Roy Watanabe
Boeing Comercial Aircraft Co.
Mail Stop 77-88, Box 3707
Seattle, WA 98124

Paul R. Abelkis
Mail Code 36-90
MacDonnel Douglas Aircraft Co.
3855 Lakewood Blvd.
Long Beach, CA 90846

John C. Ekvall
Lockheed California Co.
Dept. 76-23, Bldg. 63, Plant A-1
Burbank, CA 91520

1510	J. W. Nunziato
1520	C. W. Peterson
1521	R. D. Krieg
1522	R. C. Reuter, Jr.
1523	J. H. Biffle
1524	A. K. Miller
1524	P. S. Veers (20)
1530	L. W. Davison
1550	R. C. Maydew
1832	J. A. Van Den Avyle
3141	S. A. Landenberger
3151	W. L. Garner (3)
3154-3	C. H. Dalin (28) For DOE/OSTI (Unlimited Release)
3160	J. E. Mitchell (15)
3161	P. S. Wilson
6000	D. L. Hartley
6200	V. L. Dugan
6220	D. G. Schueler
6225	H. M. Dodd (50)
6225	T. D. Ashwill
6225	D. E. Berg
6225	P. C. Klimas
6225	D. S. Oscar
6225	L. L. Schluter
6225	H. J. Sutherland
7541	R. Rodeman
7542	T. L. Paez
8024	P. W. Dean
8316	D. A. Hughes